Master Thesis, Department of Geosciences

# Imaging reservoir quality: seismic signature of geological processes, SW Loppa High, Norwegian Barents Sea

**Shahzeb Haider**

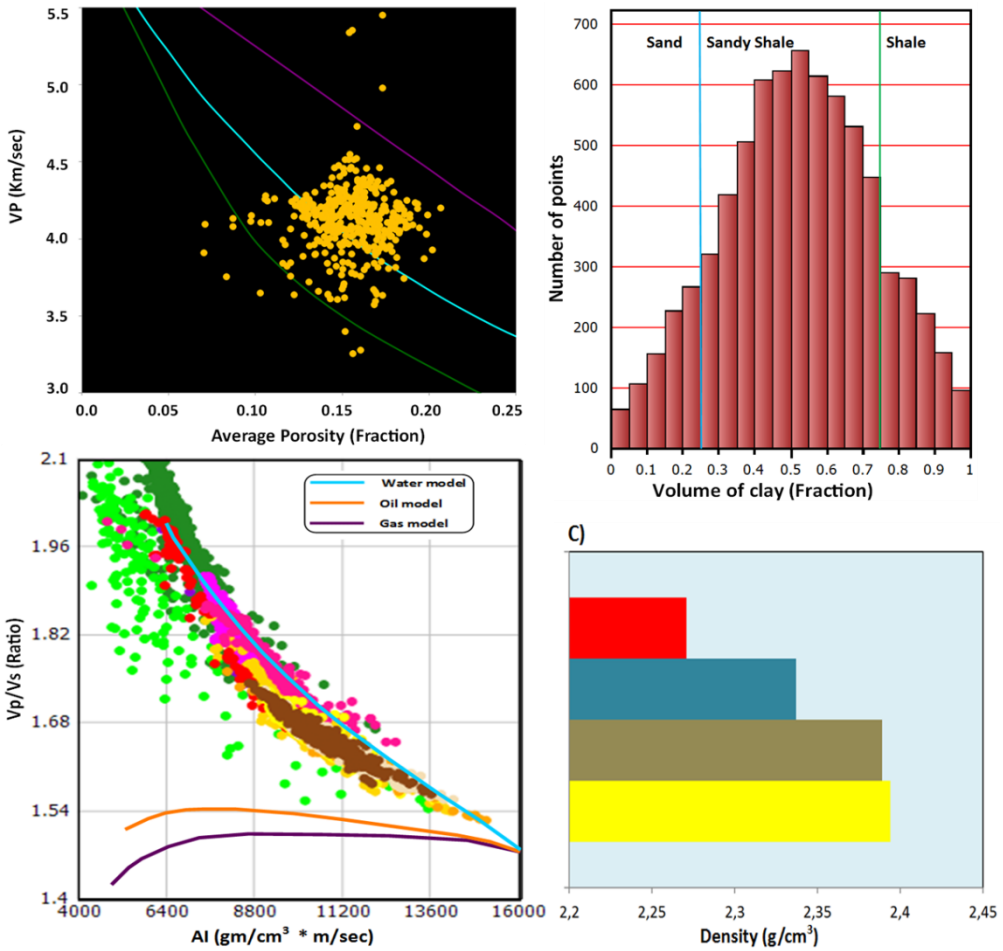


UNIVERSITY OF OSLO

FACULTY OF MATHEMATICS AND NATURAL SCIENCES

# Imaging reservoir quality: seismic signature of geological processes, SW Loppa High, Norwegian Barents Sea

**Shahzeb Haider**


Master Thesis in Geosciences

Discipline: Petroleum geology and petroleum geophysics

Department of Geosciences

Faculty of Mathematics and Natural Sciences

University of Oslo

28.05.2013

*“It is not the mountain we conquer but ourselves”*

*Edmund Hillary*

# Preface

This thesis is part of the ‘‘BarRock’’ (Barents Sea Rock Properties) project and is submitted to the Department of Geosciences, University of Oslo (UiO), in candidacy of the M.Sc. in Petroleum Geology and Petroleum Geophysics.

This research has been performed at the Department of Geosciences, University of Oslo,during the period of January 2013- May 2013 under the supervision of Nazmul Haque Mondol, Associate Professor, Department of Geosciences, University of Oslo, Norway.

# Dedication

*To the memories of my dear Mom, her many sacrifices made everything possible. And to my sisters, whose presences give me strength to strive against the odds.*

# Acknowledgment

I take this opportunity to express my gratitude to the people who have been instrumental in the successful completion of this project. I would like to show my greatest appreciation to my supervisor MD Nazmul Haque Mondol, Associate Professor, Department of Geoscience, University of Oslo. I can't say thank you enough for his tremendous support and help. I feel encouraged and motivated every time I attend his meeting. Without his backing and guidance this project would not have materialized.

I also take this opportunity to express a deep sense of gratitude to Michael Heeremans and IT staff. Department of Geosciences for their technical support and assistance in various ways during my research work whereas I am obliged to the academic and administrative members of the Department of Geosciences for their cooperation during this research work.

I am equally thankful to the people working on the BarRock project. Especially Mohammad Koochak Zadeh, his suggestions and ideas helped me achieving this goal.

I also take this opportunity to express my heartiest gratitude to Arif Naushad Butt, previous master's students and a very good friend of mine. His consistent help and motivation throughout this project made it very easy to finish.

I also place on record, my sense of gratitude to Ahsan Amin, Aftab Javed, Pyoosh, Sirikarn Narongsirikul and Samai Sanon for the time they spent to review my manuscript. Their valuable suggestions helped me to improve my writing skills.

Moreover, I am indebted to my study group mates, Fahad Ashraf, Omer Saeed who remained a consistent source of motivation for me. Their team spirit, qualitative discussion and the social life will never be snubbed.

Finally, yet importantly, I would like to express my heartfelt thanks to Almighty, my beloved sisters for their blessings, brothers my friends and classmates for their help and wishes for the successful completion of this project.

# *Abstract*

*This study focuses imaging reservoir quality of SW Loppa High using five exploration wells. The study area is located at the northern vicinity of the Hammerfest Basin, Norwegian Barents Sea. The geology of the Norwegian Barents Sea is far complex compared to other hydrocarbon provinces (North Sea, Norwegian Sea) in the offshore Norway. The geological complexity makes reservoir characterization in the Barents Sea quite difficult. Several stages of uplift and erosion influence the petroleum play and reservoir parameters. All these geological factors made reservoir rocks very complex.*

*This study considered an integrated approach of petrophysical analysis, rock physics diagnostics and AVO modeling to characterize three reservoir sandstones of L. Cretaceous Knurr Formation, M. Jurassic Stø Formation and M. Triassic Snadd Formation. The Knurr Formation possesses clastic wedge deposits developed over the footwall during exhumation whereas the Stø Formation deposited during shoreface environment. whereas The northern side of the study area holds thick shale units of the Snadd Formation which are carrying reservoir sandstones, deposited during sea level fall. The Knurr Formation in well 7120/1-2 shows very good reservoir quality whereas in well 7120/2-2 high shale volume deteriorates the reservoir quality. The Stø Formation shows the same trend from well 7120/1-2 to 7120/2-2. The Snadd Formation which comprises thick units of shale holds sandstones with fair reservoir quality. The sandstone units embedded in oil mature source rock could be a possible future prospect.*

*The petrophysical analysis revealed two types of trends; inter-formational changes from one well to the other and the intra-formational changes within a single well. The Knurr Formation which holds dominating part of the L. Cretaceous clastic wedge changes its facies from west to east. It becomes more shaly in the eastern part and the net-to-gross ratio reduces almost 50%. The porosity also decreases towards east which ultimately effects the hydrocarbon saturation which is almost negligible towards east. The Stø Formation showed no difference on net-to-gross towards east but the porosity decreased drastically. The hydrocarbon saturation towards east is also insignificant for the Stø Formation in the studied well (7120/2-2). The reduction in porosity is due to the deep burial diagenesis of high temperature which leads to chemical compaction. The reservoir quality of the Snadd Formation decreases from east to west.*

*The effect of cementation, fluid sensitivity and lithology is analyzed using rock physics templates. The Knurr Formation found to have effect of less cementation in contrast to the deeply buried Stø Formation. The effect of cementation increased from west to east where the rocks are found at higher present day burial depth. The Snadd Formation has thickness ten times higher than the Knurr and Stø Formations in the Loppa High area found at shallower present day depth with low temperature gradient. The Rock Physics Templates revealed that the Snadd Formation has gone through chemical compaction which is also supported by the phenomenon of exhumation in the study area. The Snadd Formation prior to uplift has attained the greater burial depth and so higher temperature which was necessary for chemical compaction (cementation).*

*It is clear from Rock Physics Diagnostics that the cemented reservoir sandstones are not that sensitive to fluid changes as compared to unconsolidated rocks. Combination of Rock Physics Diagnostics and AVO modeling for cemented reservoir section showed change in seismic parameters but not that robust as usually observed in the unconsolidated sandstones. Fluid replacement modeling shows gradual decrease in density of reservoir rocks with the increase in percentage of gas. The seismic velocities only shows sharp changes when the gas is introduced to the reservoir despite the amount of gas substituted to the reservoir sandstones. From above observations it can be concluded that the conventional methods of reservoir characterization are not good enough to image reservoir quality. Multi-disciplinary integration is the key to the success for hydrocarbon exploration. It minimizes the exploration risk and enhances the quality of imaging reservoir rocks.*

# NOMENCLATURE

AI: Acoustic Impedance
AVO: Amplitude Versus Offset
BHT: Bottom Hole Temperature
BSF: Below Sea Floor
E: East
EI: Elastic Impedance
Fm: Formation
FRM: Fluid Replacement Modeling
HC: Hydrocarbon
HI: Hydrocarbon Index
H-R: Hashin-Shtrikman
HR: Hampson Russell
Hz: Hertz
IGR: Gamma Ray Index
IP: Interactive Petrophysics
K: Bulk Modulus
Km: Kilometer
LH: Loppa High
LMR: Lamda-Mu-Rho
m: Meter
mD: Milli Darcy
MD: Measured Depth
MPa: Mega Pascal
ms: Millisecond
N: North
N/G: Net-To-Gross Ratio
PR: Poisson's Ratio
RPT: Rock Physics Template
RPTs: Rock Physics Templates
Rw: Resistivity of Water
S: South
$S_{hc}$: Hydrocarbon Saturation
SI: Shear Impedance
Sw: Water Saturation
TOC: Total Organic Carbon
TVD: Total Vertical Depth
Vp: P-wave Velocity
Vs: S-wave Velocity
Vsh: Volume of Shale
W: West
μ: Shear Modulus
μρ: Mu-Rho
ρ: Density
λρ: Lamda-Rho

# Table of contents

# List of figures

# List of tables

# Chapter 1: Introduction

## 1.1 General introduction

The discovery of Ekofisk in 1969 in the Norwegian sector of the North Sea has opened new horizons for petroleum exploration in the Norwegian continental shelf. Till 1980 the premier focus for petroleum exploration was the North Sea but many discoveries in the North Sea led the geoscientists to pay attention towards the two other parts of Norwegian continental shelf; the Norwegian Sea and the Barents Sea. Continental breakup resulted formation of these three hydrocarbon provinces which were part of a large epicontinetal sea standing between Fennoscandia, Greenland and Svalbard (Faleide et al. 2010). This study has main focuses on imaging reservoir quality of the SW Loppa High area in the Norwegian Barents Sea. The greater Barents Sea is surrounded by Franz Josef Land (Russia) in north, Svalbard (Norway) in northwest, Greenland Sea in west, Norwegian and Russian main land in south and the Novaya Zemlya Island in the east (Fig.1.1). The present demand and increased economic value of hydrocarbons push exploration towards deep-waters and further north to find hydrocarbons in the Arctic Circle.

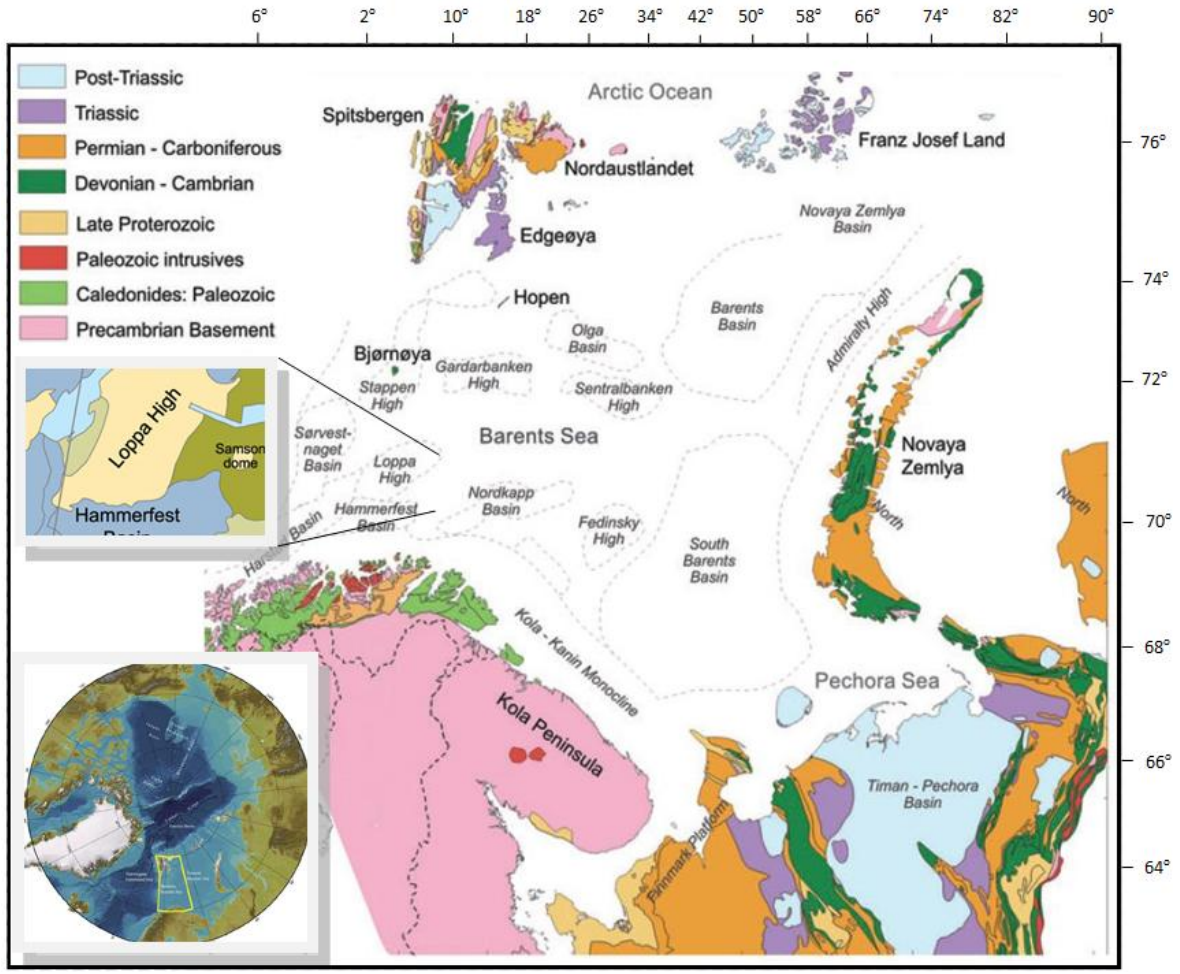


**Figure.1.1**: Location map of the Greater Barents Sea. A small zooming view of the study area is also shown (modified from Worsly 2008 ; Glørstad et al.2010; Henriksen et al. 2011).

Increase in exploration of extreme areas has also triggered oil industry to pay attention toward improving qualitative and quantitative studies of subsurface. Nowadays one of the premiere focuses is to enhance understanding of reservoir rocks by integration of seismic, well logs, electromagnetic and laboratory data of cores & cuttings. Seismic gives acoustic impedance, Vp/Vs ratio, elastic moduli and bulk density whereas well logs give porosity, permeability, temperature, fluid saturation, clay contents and texture. The data is acquired by using expansive refined tools and then processed using advanced software. There is a continuous improvement in this technology but still chances of errors and uncertainties are present. After many years of exploration experience in the Norwegian Barents Sea it has been proven that the heterogeneous reservoirs carry good hydrocarbon prospects (e.g. recent oil discoveries of Skrugard and Havis).

## 1.2 Background and motivation

Available fossil fuel reserves are decreasing day by day and energy demand is increasing so the modern world is trying to find more and more energy sources. Hydrocarbons cannot be generated synthetically for fulfilling the demand of world. There is only one way to overcome this problem which is to explore the hidden reserves. With the application of modern geophysical techniques and detailed studies of unexplored area it may not be impossible.

From the last three decades the Barents Sea is one of the foremost focused areas for hydrocarbon exploration. The Norwegian Barents Sea comprising an area of 23,000 $km^2$ which is roughly two times the area of the Norwegian North Sea (13,000 $km^2$). Exploration started in the Southwestern (SW) Barents Sea in 1980's. The success rate in the Norwegian Barents Sea is high; one out of three wells drilled in the area. But the discoveries are mostly of gas and have relatively low economic values due to a large distance from the gas market. Presence of several source rocks and good reservoir sands makes the Barents Sea area more attractive for exploration. So far there are several discoveries but not that prolific as expected. It is generally believed that the Barents Sea area is not an easy task to explore due to several stages of uplift and erosion. It strongly affected maturation of source rock and the reservoir properties like porosity, permeability driven by both mechanical and chemical compaction and also hydrocarbon leakage. Uplift also affects the traps/caps rocks specifically the study area where so far only few technical discoveries have been found. A recent gas discovery in the well 7120/2-3S make the study area more exciting to research as it was considered earlier as barren in terms of possibility to find commercial hydrocarbons. The challenges associated to find hydrocarbon and to enhance understanding of reservoirs quality motivate the research to take it further.

## 1.3 Research objectives

The main objective of the study is to image reservoir quality of the Snadd Formation of M. Triassic age, the Stø Formations of M. Jurassic age and the Knur Formation of L. Cretaceous age encountered in five exploration wells (7120/1-1, 7120/1-2, 7120/2-1, 7120/2-2, and 7121/1-1) in the SW Loppa High (Fig.1.2; Table.1.1), Norwegian Barents Sea. The main objective explains further to divide work packages in following categories:

- To calculate net-to-gross (shale volume), porosity, permeability and hydrocarbon saturation of reservoir sandstones using pertophysical well log analyses.

- To correlate different reservoir horizons to investigate their lateral variations and thickness encountered in the five studied wells.

- To investigate reservoir rock properties using different rock physics templates.

- To perform AVO modeling of reservoir units and to compare of modeling results to investigate sensitivity of fluid in shallow unconsolidated reservoir to deep cemented reservoirs.

## 1.4 Study area

Outline of the Loppa High is diamond shaped and is located between 71°50'N, 20°E and 71°55'N, 22°40'E and 72°55'N, 24°10'E and 73°20'N, 23°E (Fig.1.2) (Gabrielsen 1990). Loppa High is joined by the Lolhem Platform, bounded by Hammerfest Basin towards its south and Bjørnøya basin towards its North-West (Sayago et al. 2012). Asterias Fault Complex separates the Loppa High from the Hammerfest Basin and Bjarmeland Platform is situated towards the east. Towards the west it has Ringvassøya-Loppa and Bjørnøyrenna fault complex. The Salvis Dome, a major salt structure in the area, and the Maud Basin which is a syncline, are located at north-eastern limit of the Loppa High (Gabrielsen et al. 1990). The average water depth is about 336 m.

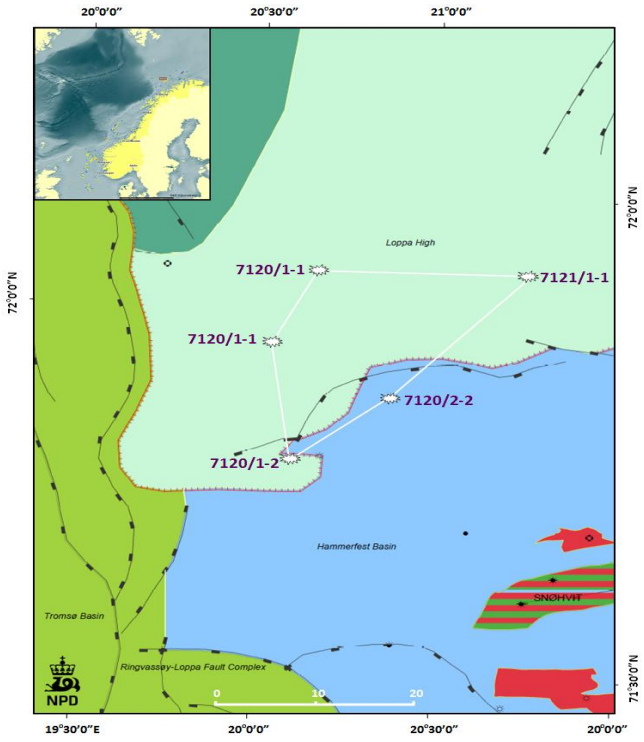


**Figure.1.2:** Location of the study area shown in the inset map (shaded zone). A zooming view of the study area is also shown with locations of all studied wells (modified from NPD 2013).

The first wildcat well 7120/2-1 drilled in the area in May, 1985 by Norsk Hydro Produksjon AS. Several exploration wells drilled afterwards by different companies; five of them are included in the study (Table 1.1). The estimated recoverable reserves in the area are ranging from negligible to 200 x $10^6$ $m^3$ oil equivalents (Sund et al. 1986).

**Table.1.1:** Key information of five studied wells in the SW Loppa High area.

| Well Name | Water Depth (m) | Total Depth (m) | Fluid Content | Operators | Drilling Year |
|---|---|---|---|---|---|
| **7120/2-1** | 387 | 3484 (TVD) | Oil Shows | Norsk Hydro Produksjon AS | 1985 |
| **7121/1-1R** | 369 | 5000 (MD) | Water | Esso Exploration and Production Norway | 1986 |
| **7120/1-1R2** | 342 | 3978 (TVD) | Oil/Gas Shows | A/S Norske Shell | 1986 |
| **7120/1-2** | 304.5 | 2613 (TVD) | Oil | A/S Norske Shell | 1989 |
| **7120/2-2** | 336.5 | 2794 (MD) | Oil Shows | Norsk Hydro Produksjon AS | 1991 |

## 1.5 Chapter's description

The whole thesis is divided into six different chapters. The first chapter includes a general introduction of the greater Barents Sea and more specifically the study area. It also describes research motivation, objectives, limitations and future implication of the research.

Geological background of the study area is given in chapter 2. It includes regional tectonic history and geological evolution of the grater Barents Sea and its impacts on the study area, stratigraphy of different sequences and correlation of the source and reservoir rocks in the area of interest in this study. Petroleum system (Source rocks, reservoir rocks and traps) and geometry of reservoir units are also described here in detail.

Chapter 3 describes methodologies and theoretical background of the thesis work. Theoretical background for petrophysical analysis, rock physics diagnostics and AVO modeling is given more in detail. It also includes the explanation of dataset used and methodology involved in this study.

Petrophysical analysis has been described in chapter 4. It includes shale volume calculation, net-to-gross estimation, porosity prediction and determination of water and hydrocarbon saturations.

A brief description of rock physics analysis is given in chapter 5. Detailed analysis of main reservoir rocks (Knurr , Stø and Snadd Formations) is carried out using rock physics diagnostics.

Chapter 6 focuses the AVO modeling. A general summary and conclusions of the study are given in chapter 7.

## 1.6 Limitations and future implications

This thesis is time limited (only 18 weeks), time limitation remained the main hurdle during this study, which did not allowed to integrate the well logs study with the thin section study. The shear wave velocity (Vs) is not available in the studied well logs, which is an important factor for rock physics diagnostics. Shear wave velocity (Vs) is calculated from the Vp using different empirical relationships. This Vs value then used for rock physics analysis, which may not reflect the absolute behavior of Vs and could give ambiguity in results. Permian carbonates have good reservoir potential but due to time limitation carbonates reservoirs are not studied in this work.

This study is based only on five wells drilled much earlier in the area. The data from a recent discovery well 7120/2-3S is not included as it is not released yet for public. Due to unavailability of thin section and time constrained, petrographical studies are not carried out. In future one could do petrography by using different methods i.e. optical microscopy, SEM and XRD. With the integration of this study results with the petrographical studies one could make a better reservoir image with fewer chances of uncertainty and ambiguities.

The compaction study of the reservoir section is not carried out. One could also study the effect of mechanical and chemical compaction on the reservoir rocks. Compaction study can better help to distinguish the sharp changes in velocity and porosity. Ultimately it can be used to predict reservoir quality.

# Chapter 2: Geology of the study area

Understanding the petroleum geology of any area is very important to start petroleum exploration in the area. It includes the study of regional and local tectonics, structural elements and stratigraphy. The depositional pattern and environment of source and reservoir rocks, their burial depth and temperature, hydrocarbon expulsion from source rock and its migration to the reservoirs and capacity of cap rocks/seals. Several tectonic events made the Geology of the Greater Barents Sea and the study area very complex. The following section will focus on the geology of the Greater Barents Sea with the special emphasis on the study area; the SW Loppa High.

## 2.1 Tectonic history and geological evolution

The Greater Barents Sea is extended over the north-western rim of the Eurasian Continental Shelf. The Cenozoic opening of the Norwegian Greenland Sea followed by Eurasia Basin, has delimited the Barents Sea with a young passive margin towards the north and west (Fig.2.1). It has gone through several tectonic events, but the most prominent among these are the Post Caledonian rift phases, Late Devonian?-Carboniferous, Middle Jurassic Early-Cretaceous and Early Tertiary (Faleide et al. 2010). The major part of the Barents Sea was affected by crustal extension during Late Paleozoic times. The significant effects of this extension are; lateral migration of rifting generally towards the West, pronounced development of pull-apart and rift basins in the south-west and the formation of strike-slip belt in the north (Faleide et al. 2010). During Mesozoic and Cenozoic, halo-kinesis also affected the structure of the region. Reactivation of faults also took place, where old fracture system was reactivated instead of forming new fractures, although the 'new' stress regime was different from the old 'one' (Gabrielsen 1984). A short description of tectonic history, geologic evolution and depositional environments of the Greater Barents Sea including the study area is given bellow.

### 2.1.1 Paleozoic

The Loppa High has very complex evolution history, which at least starts from Late Carboniferous. It has gone through fault reactivation and several stages of uplift and erosion. In Early Carboniferous terrigenous sediments deposited which were later onlaped by Late Carboniferous and Permian carbonates. The general dip of these sediments was towards the east (Wood et al. 1989). The Loppa High and other structural highs of the area were eroded and transgressed during Early Permian. The Loppa High tilted towards east and also thinned during Late Permian (Berglund et al. 1988).

During Lower to Upper- Carboniferous time mostly clastic sediments were deposited in the extensional basin. Fan shaped northeasterly trending rift system was developed during Middle Carboniferous, which had half graben geometry. This rift system developed several interconnected extensional basins; deposition of syn-rift sediments was also taken place at the same time. During Late Carboniferous the movement of rotated fault blocks ceased and the basin was filled by Late Carboniferous and Early Permian cyclical dolomites, massive limestone and evaporates. The carbonates deposition was ceased in the whole region in Early Permian and platform clasts started to deposit. The basin kept on subsiding till Late Permian but the deposition changed from clastic sediments to shales and cherty limestones (Faleide et al. 2010).

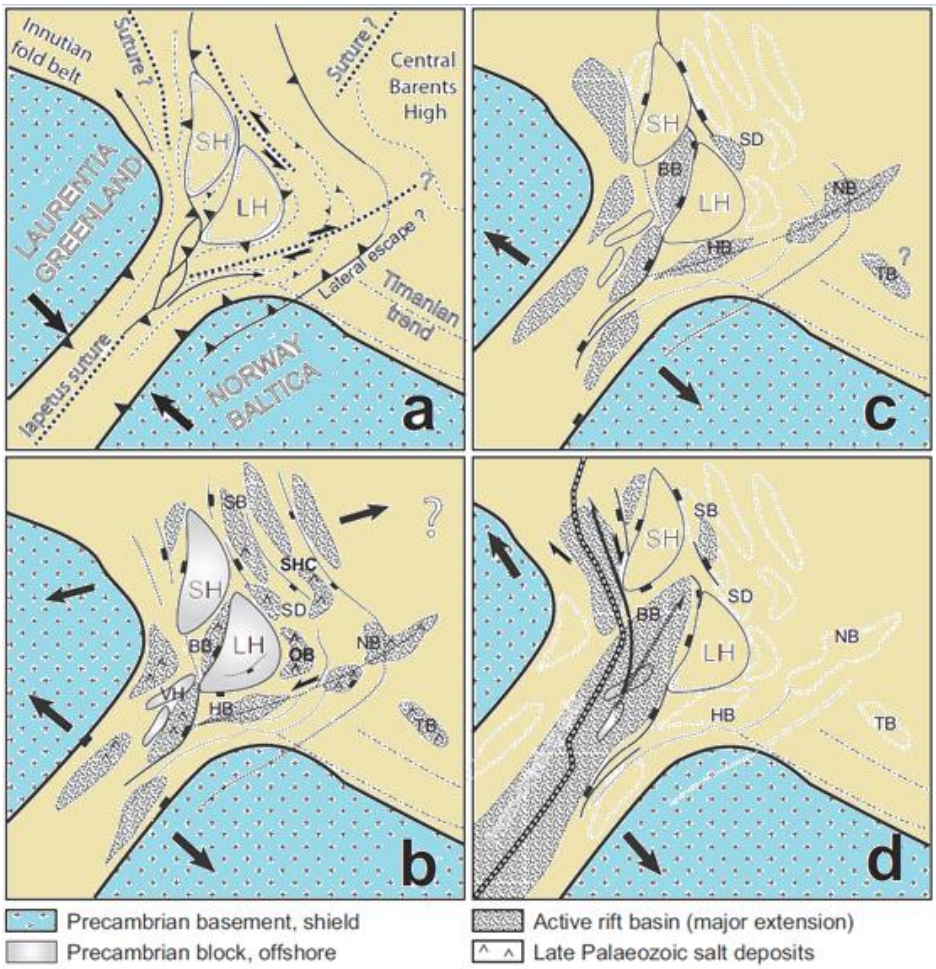


**Figure 2.1:** The Tectonic evolution of the Barents Sea. (a) During Devonian time lateral escape between Laurentia and Baltic took place; (b) During Latest Devonian-Carboniferous reactivation of shear zone and graben development took place; (c) Salt tectonic and Main stages of graben development took place due to rifting in Early to Mid-Mesozoic; (d) Increment in crustal thinning during Late Mesozoic and lateral shear migration and ultimately breakup between Baltic and Laurentia in Early Cenozoic time (Modified from Gernigon and Bronner 2012).

## 2.1.2 Mesozoic

During Early Triassic, pre-Triassic sediments on the Loppa High were eroded and clastic sediments of Lower Triassic and Middle Triassic onlaped over the eroded surface. Figure 2.2 (d) shows no structural expression of the Loppa High during Late Triassic-Middle Jurassic (Wood et al. 1989). Deep marine conditions prevailed during Early Triassic with the deposition of shales whereas at the basin edges towards east and south more clastic sediments were found (Faleide et al. 2010). The main source areas were the Baltic Shield and Uralain Highland. Northward and westward prograding delta was formed in Middle Triassic when the Barents Sea was under continental environment. In central and northern part of the Barents Sea, deep marine conditions remained throughout the Middle Jurassic time with the deposition of a very good source rock. Regression and erosion took place in Late Triassic. Early to middle Jurassic was the time of deposition of reservoir sandstones in the SW Barents Sea. These sediments also covered the Finnmark Platform, Loppa High and

Hammerfest Basin but the area has gone through partial erosion of these sediments during uplift.

The Middle Jurassic rifting phase in SW Barents Sea is marked by sequence boundary (Faleide et al. 2010). This rifting phase led to the formation of high angle normal faults and sea level changes resulted in to deposition of Stø Formation (Berglund et al. 1986). Rifting continued in the Cretaceous and resulted formation of deep basin (16-17 km) in the Barents Sea (Faleide et al. 2010). The rifting of the Western Barents Sea has reactivated the faulting in the Loppa High during Late Jurassic to Early Cretaceous. The uplift and erosion associated with this event sourced the adjacent basins towards the south and west, with Triassic and Jurassic sediments. The Loppa High remained growing until Early Tertiary.

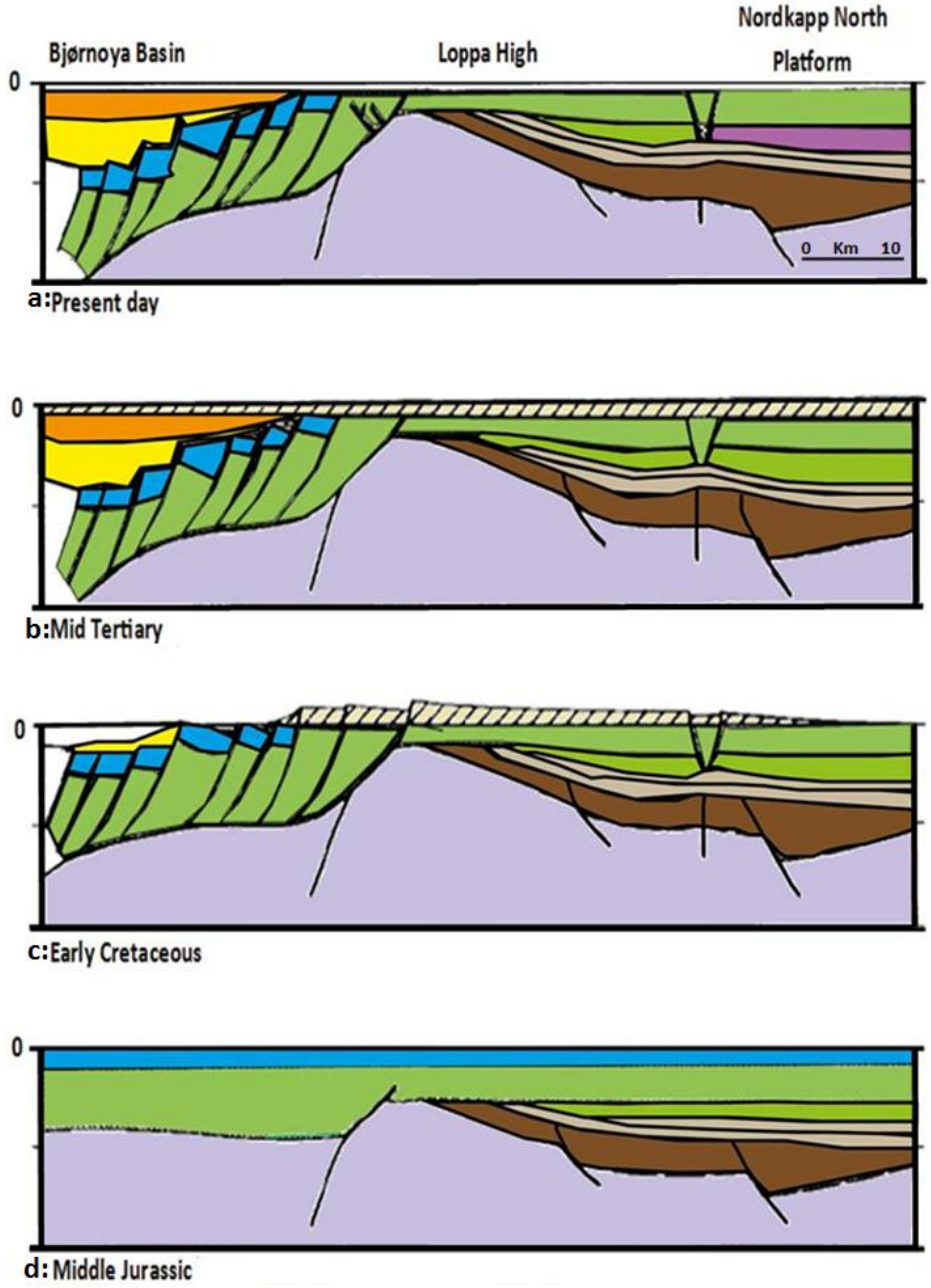


**Figure 2.2:** Schematic diagram of major evolution stages of the Loppa High (modified from Wood et al. 1989).

### 2.1.3 Cenozoic

The two-stage opening of the Norwegian-Greenland Sea was the main phenomena behind Cenozoic evolution of the predominantly sheared western Barents Sea. Continental breakup gave rise to sea floor spreading in Paleocene which is followed by rapid subsidence in the Late Paleocene (Faleide et al. 2010). The entire area was blanketed by sediments towards the end of Paleocene and the Loppa High became provenance which supplied sediments to the Trømsø Basin. Along the western margin of the Senja Ridge some local faults also developed. The sea floor spreading gave rise to the formation of a regional shear zone between Norwegian Sea and Eurasia which triggered the formation of the Svalbard and Barents Sea during Eocene. Sea floor spreading lead to the development of oceanic crust during Oligocene and the uplifted area sourced the Neogene and Quaternary sediments (Faleide et al. 1993a). The Loppa High continued emerging until Early Tertiary. Most of the Cenozoic strata are missing in the Loppa High area due to erosion (Fig.2.2c,d) (Henriksen et al. 2011). According to Wood et al. (1989) more than 1000 m of sediments were deposited during Early Tertiary but due to the Late Tertiary uplift there was significant erosion of about 500-1000 m. The present day expression of the Loppa High is shown in EW and NW-SE transect in the Figure 2.3.

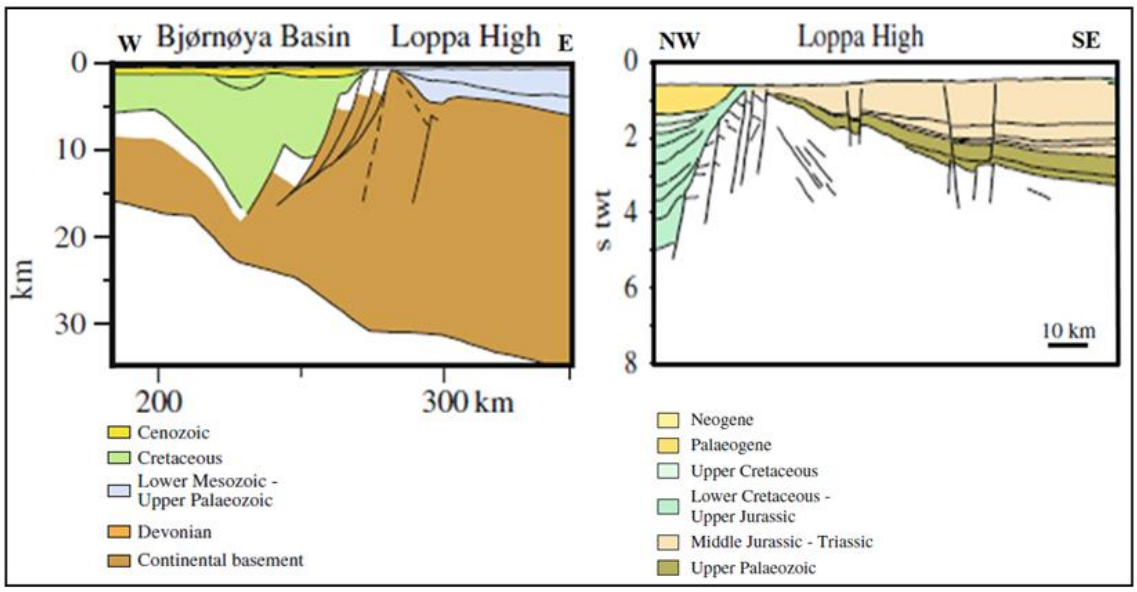


**Figure 2.3:** Two cross-sections a) from W to E and b) from NW to SE, showing present expression of the Loppa High (modified from Faleide et al. 2010).

## 2.2 Structural elements

As discussed earlier, the Barents Sea has gone through various phases of tectonic activity during different geological times. The Greater Barents Sea is divided into two major parts, the eastern and north-eastern parts which are considered as stable platforms and the western Barents Sea which remained tectonically most active during Mesozoic and Cenozoic times (Gabrielsen et al. 1990). The Western Barents Sea has huge thickness of Upper Paleozoic and Mesozoic rocks divided into three different geological zones (Fig.2.4) which are; 1) the Svalbard Platform has upper Paleozoic to Mesozoic sediments; 2) A basin between the Norwegian coast and Svalbard Platform divided further into sub basins and highs of Tromsø, Bjørnøya, Sørvestsnaget and Harstad Basins; and 3) the Norwegian continental margin

further divided into sub-basins and highs of the Finnmark Platform, Loppa High, Hammerfest Basin and the Fingerdjupet sub-basin (Faleide et al. 1993 a, b).

The Loppa High was formed due to late Jurassic to Early Cretaceous and Late Cretaceous-Tertiary tectonic activity bounded on the east and south by a monocline towards the Bjarmeland Platform and the Hammerfest Basin. The Southern Loppa High Fault Complex is marking its boundary with the Hammerfest Basin towards south. It comprising two large normal faults dipping towards the south (Hammerfest Basin) and some complex faults which are dipping towards the north often cut apart each other. It is considered that these faults were of strike slip nature during Jurassic but later on changed into normal faults due to extension taken place in Cretaceous time (Berglund et al. 1988). The Bjørnøyrenna and Rigvassøy-Loppa Fault Complexes are situated towards the western boundary of the Loppa High.

The Bjørnørenna Fault Complex is an extensional feature bordered between the Loppa High and Bjøonøya Basin. The complex nature of this fault zone is characterized by multiple phases of deformation with two to three phases of inversion. The Ringvassøy-Loppa Fault Complex comprise numerous normal faults which were reactivated a number of times (Berglund et al. 1988; Gabrielsen et al. 1993). The Maud basin and Salvis Dome which is a salt structure are located towards the northern margin of the Loppa High. The salt was deposited in the Pre-Permian time (Fig.2.4) (Gudlaugsson et al. 1998).

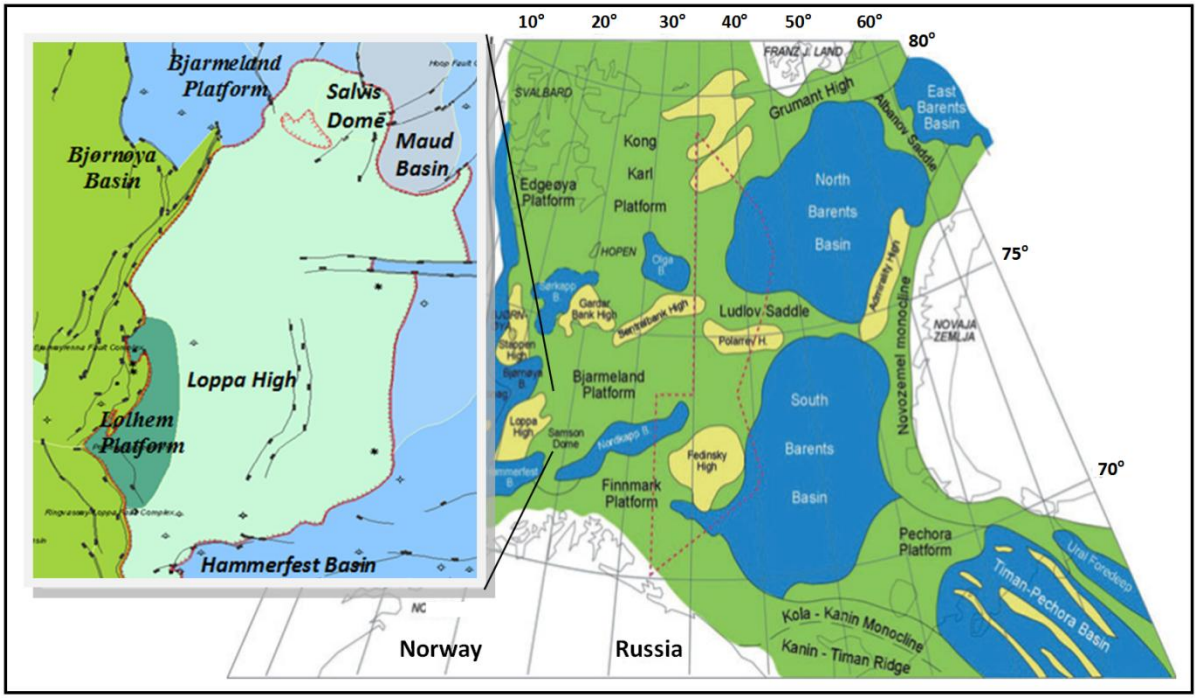


**Figure 2.4:** Structural elements of the Barents Sea (Modified from Worsly 2008; NPD 2013).

## 2.3 Stratigraphy

The prominent feature of the Barents Sea stratigraphy is the Palaeogene-Recent uplift and erosion which is shown by a main unconformity at the base of the Quaternary. During Paleozoic time four major stratigraphic groups deposited. They show significant shift in

facies on onshore to offshore boundary due to the changes in the drainage pattern, basin configuration, palaeoclimate, tectonic activity and the relative sea level changes (Henriksen et al. 2011). The seismic section of the Loppa High area shows a distinctive feature of these groups where fault controlled sedimentation resulted into thin sedimentation which progressively thickens towards east (Fig.2.5) (Larssen et al. 2002).

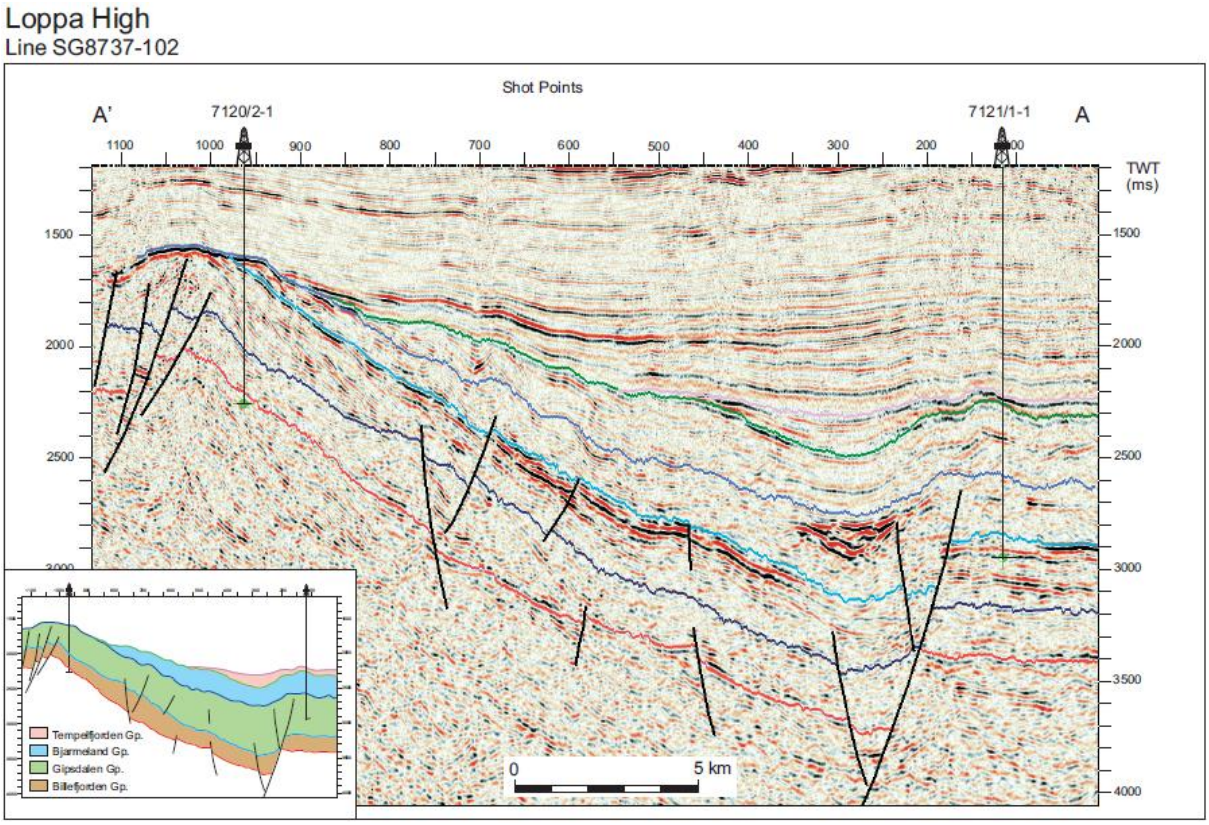


**Figure 2.5:** Seismic section SG8737-102 showing stratigraphic correlation between the wells 7120/2-1 and 7121/1-1. Here the Paleozoic sediments thickness progressively decreases from East to West (A to A') (Larssen et al. 2002).

Basin subsidence during Mesozoic gave rise to the deposition of deep marine shales and later events of rifting also deepen the sea which is the reason of good quality source rocks deposited during Mesozoic specifically in the Jurassic time. Rifting also developed high angle normal faults which resulted into erosion and deposition of reservoir rocks. Main reservoir rocks of the Barents Sea are sandstones which were mostly deposited during Jurassic (Faleide et al. 1993). The marine mudrocks deposited in Eocene time overlying of Cretaceous strata by a regional unconformity. In the Loppa High area most of the Cenozoic Strata are missing due to the effect of erosion which can be clearly seen in Figure 2.6 (Henriksen et al. 2011). The detail description of some important stratigraphic groups and formations are given in the following sections.

## 2.3.1 Billefjorden Group

In the Loppa High area about 847 m thick arkosic breccia, conglomerates and other types of volcanoclastic sediments have been penetrated by the well 7120/2-1 (Fig. 2.3). Brownish siltstones and mudstones are present in the basal part. They have average thickness of 115 m. The sediments of the Mid-Carboniferous Gipsdalen Group which are overlying the

Billefjorden Group show close resemblance to them. The sediments are deposited in alluvial fans and proximal braided stream systems, and the volcanoclatic sediments found in well 7120/2-1 showing a local volcanic activity at that time. Palynomorph studies show Early Carboniferous age (Viséan to early Serpukhovian) of this group (Larsen et al. 2002).

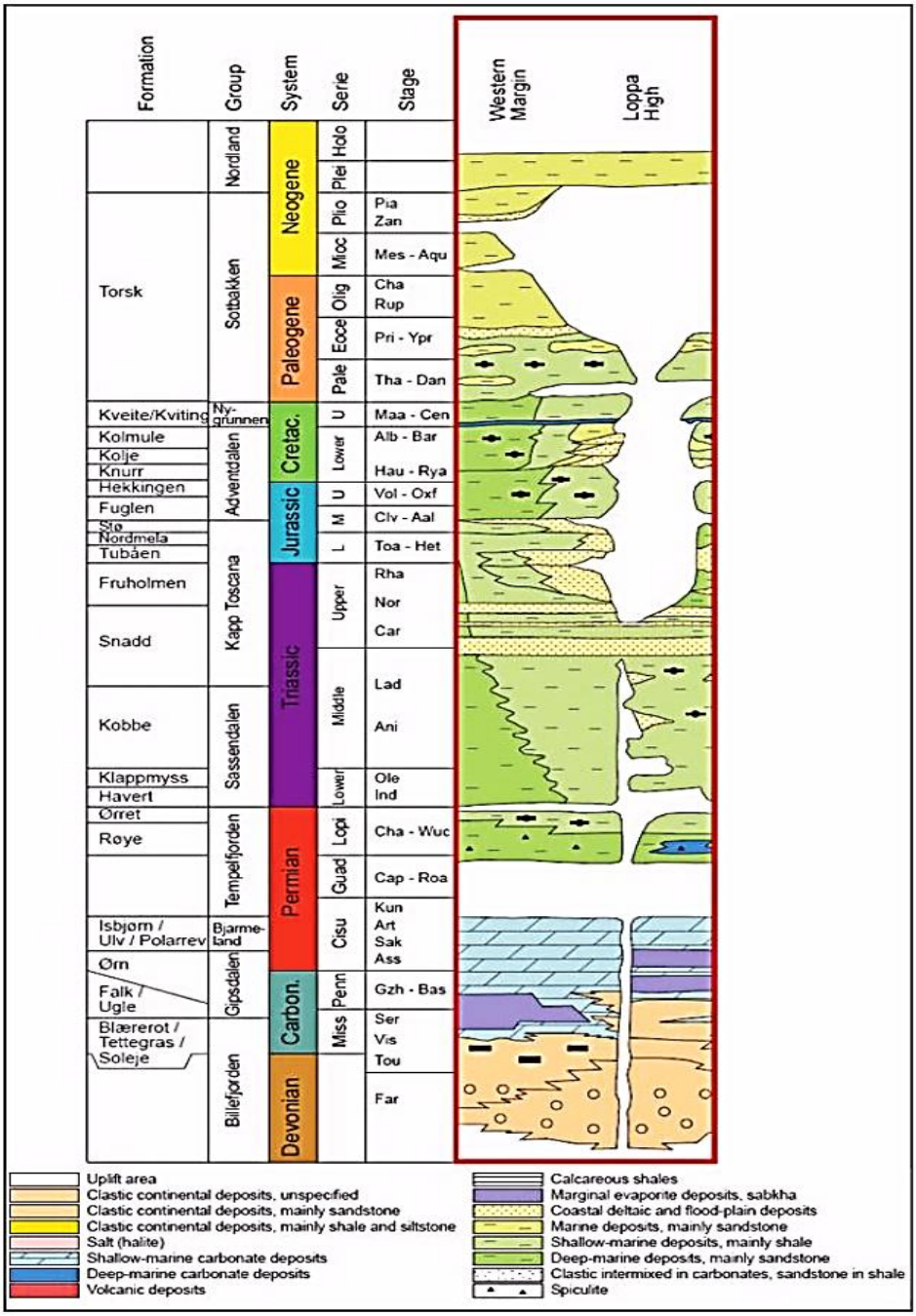


**Figure 2.6:** Stratigraphic succession of the Loppa High (Elvebekk 2008, Cited by Hassan 2012).

## 2.3.2 Gipsdalen Group

The Loppa High is considered as good reference section for the Gipsdalen Group, where it is penetrated by different wells (7120/1-1, 7120/2-1 and 7121/1-1) and also clearly identifiable

in 3D seismic. Continental red bed sandstones, siltstones and conglomerates show finning upward sequence which is found in the lower part. The middle part containing the mixture of grey colored siliciclastics marine sandstones and marine carbonates. The upper part consists of alternating beds of dolomites and limestones with occasional patches of phylloid algal-Palaeoaplysina buildups and some evaporites. The Loppa High and Finnmark Platform consists the thickest carbonate deposits. Middle Carboniferous (Serpukhovian to Bashkirian) is the age of the Gipsdalen Group (Larsen et al. 2002).

### 2.3.3 Bjarmeland Group

Fine grained sliciclastics, marls and thinly bedded limestones are dominated in the area. In well 7120/1-1 siliciclastic shales are interbeded with limestones. Well 7120/1-1 holds maximum thickness of this group. The deposition of this group took place in cool water environment. This group is comprised of the Ulv Formation, Polarrev Formation and the Isbjørn Formation of Early Permian (mid-Sakmarian to late Artinskian) age (Larsen et al. 2002).

### 2.3.4 Tempelfjorden Group

The thickly developed tempelfjorden group in the study area is comprised of dark grey speculates, silicified skeletal limestones, fine grained siliciclastics with marl, speculitic cherts, shales, silt/sandstones and claystones. The formations assigned to this group are the Røye Formation and Ørret Formation of Mid-Late Permian (late Artinskian to? Tatarian) age (Larsen et al. 2002).

- **Røye Formation**

In the Loppa High area Røye Formation is comprised of interbedded silicified marls, silty carbonate mudstone and calcareous claystone with thin interbedded cherts. The lower part was deposited in low relief platform environment whereas middle and upper parts were deposited during distal marine, moderate to deep shelf condition with the influence of seasonal high energy storm episodes. Core data suggests mid Permian (Kungurian to? Kazanian) age (Larsen et al. 2002).

- **Ørret Formation**

This formation is comprised of sandstones, siltstones and shales. Organic shales are mature in study area for hydrocarbon generation. In well 7120/1-1 the formation is 173 m thick. The environment of deposition ranges from deltaic and lower coastal plain environment but in the study area it shows more influence of deep marine anoxic environment. The formation is deposited in Permian age (Larsen et al. 2002); (Ohm et al. 2008).

### 2.3.5 Sassendalen Group

Shales of grey to black color and claystones are common in this group but grey siltstones and sandstones can also be found. In the study area these sediments are deposited in marine environment during Early-Middle Triassic (Anisian/Ladinian). The formations assigned to this group are the Havert Formation, Klappmyss Formation and the Kobbe Formation (Dalland et al. 1998; Worsley, 2008).

- **Havert Formation**

It is shale of medium to dark grey color with minor interbedded pale grey siltstones and sandstones. The Havert Formation was deposited in marginal marine to open marine environment. The thickness of this formation in well 7120/1-1 is 58 m. Early Triassic (Griesbachian-Dienerian) age is suggested by palynomorphs (Dalland et al. 1988).

- **Klayppmyss Formation**

The lower part of the Klayppmyss Formation is medium to dark shale whereas the upper part is interbedded shales, siltstones and sandstones. It was deposited during open marine environment palynofacies suggest Middle Triassic age (Dalland et al. 1988).

- **Kobbe Formation**

The organic rich Kobbe Formation deposited during Middle Triassic (Anisian/Ladian) age is a good hydrocarbon source rock (Worsley 2008). It is deposited during marine transgression associated with anoxia during the times of maximum flooding (Henriksen et al. 2011).

### 2.3.6 Kapp Toscana Group

Pale grey sandstone units are common in this group, which are considered as good hydrocarbon reservoir rocks with minor amount of coal and shale. The formations assigned to this group are the Snadd Formation, Fruholmen Formation, Tubåen Formation, Nordmela Formation and the Stø Formation (Dalland et al. 1988). Figure 2.7, shows cores of the Stø Formation and Fruholmen Formation with their respective gamma ray curves.

- **Snadd Formation**

Grey shale in the lower part which becomes coarser into shale with interlayering of siltstone and sandstones. In the middle part Calcareous interlayering and limestone is present. The upper part consists of thin coaly lenses. The Snadd Formation was deposited during Triassic (Dalland et al. 1988).

- **Fruholmen Formation**

The basal part of this formation is blackish mudrock formed during marine anoxia gradually changes marine sandstones in the middle part and the upper part is terrestrial sandstone. The upper part is mostly coarse grained strata deposited by braided streams. This formation was deposited in Late Triassic (Early Noranian) times (Fig.2.7b) (Henriksen et al. 2011).

- **Nordmela Formation**

This formation consists of siltstone, claystones and shales with some coals in the lower and middle part whereas upper part consists of sandstones. The age of the formation is Early Jurassic (Sinemirian- Pliensbachian). The major part of this formation is deposited in flood plain to tidal flat environment whereas the sandstones bodies were deposited by tidal channels and estuaries (Dalland et al. 1988).

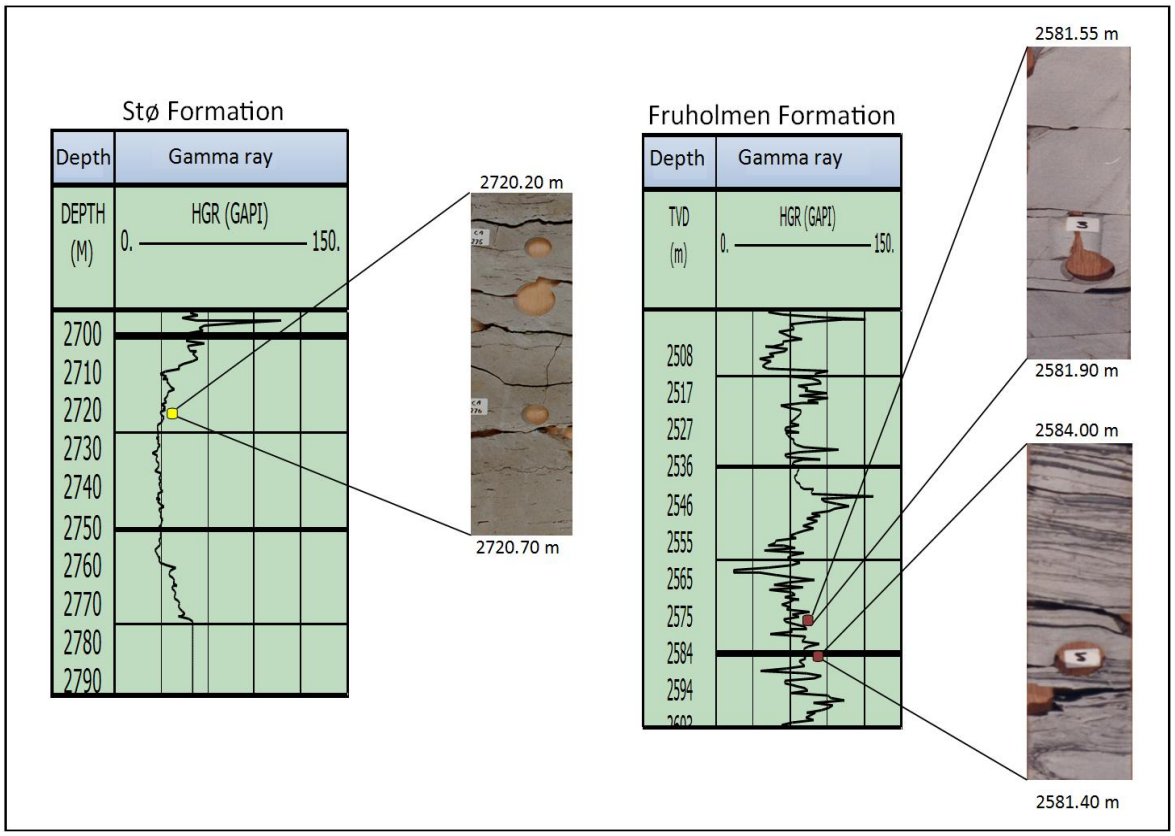


**Figure 2.7:** a) Grey sandstone of the Stø Formation with low gamma ray value from well 7120/2-2, b) The sandy portion of the Fruholmen Formation penetrated by well 7120/1-2.

- **Stø Formation**

This formation consists of well sorted sandstones with thin layers of siltstone and shale. Coastal progradation deposited sand bodies whereas siltstone and shale bodies are represented by regional transgression. This formation was deposited in Middle Jurassic (Pliensbachian-Bajocian) time (Fig 2.7 a) (Dalland et al. 1988).

- **Tubåen Formation**

The Tubåen Formation has sandstone as a major lithology with subsidiary amount of shale and minor coals. The sandstone is deposited in deltaic environment whereas the coaly and shaly portion belongs to protected back barrier lagoonal environment. The age designated to this Formation is Late Triassic to Early Jurassic (Late Rhaetia- Early Hattangian) (Dalland et al. 1988; Henriksen et al. 2011).

## 2.3.7 Adventdalen Group

This group mainly consists of claystones and shales with patches of dolomitic limestone. Deep and calm marine environment prevailed during the deposition of this group (Dalland et al. 1988). But at the Jurassic-Cretaceous boundary we can see the sudden change in depositional environment from deep marine to open marine due to the fall of sea level (Worsley 2008). Basically this group consists of dark grey to brownish grey shale and claystone with interlayering of greyish brown siltstones, dolomite and limestone but in the

Loppa High area clastic fan facies can be found. The formations assigned to this group are the Fuglen Formation, Hekkingen Formation, Knurr Formation, Kolje Formation and the Kolmule Formation (Dalland et al. 1988).

**Fuglen Formation**

The Fuglen Formation comprises pyritic mudstone interbedded with thin limestone and dark shales and white limestone. It was deposited during deep marine conditions in condensed section. The age assigned to this formation is Middle to Late Jurassic (Callovian-Oxfordian) (Henriksen et al. 2011; Dalland et al. 1988).

- **Hekkingen Formation**

This formation consists of brownish to dark grey shale which is divided into two members, the lower Alge Member and the upper Krill Member. The formation was deposited in deep marine anoxic environment. The age assigned to this formation is Late Jurassic (Kimmeridgian to Early Ryazanian) (Henriksen et al. 2011).

- **Knurr Formation**

Claystone of grayish brown to dark grey color with interbedded dolomite and limestone deposited during open marine to distal marine conditions. Footwall upliftment also deposited clastic sediments in the study area. The palynofacies data suggests Early Cretaceous (Ryazanian to Early Barremian) age (Fig.2.8) (Dalland et al. 1988).

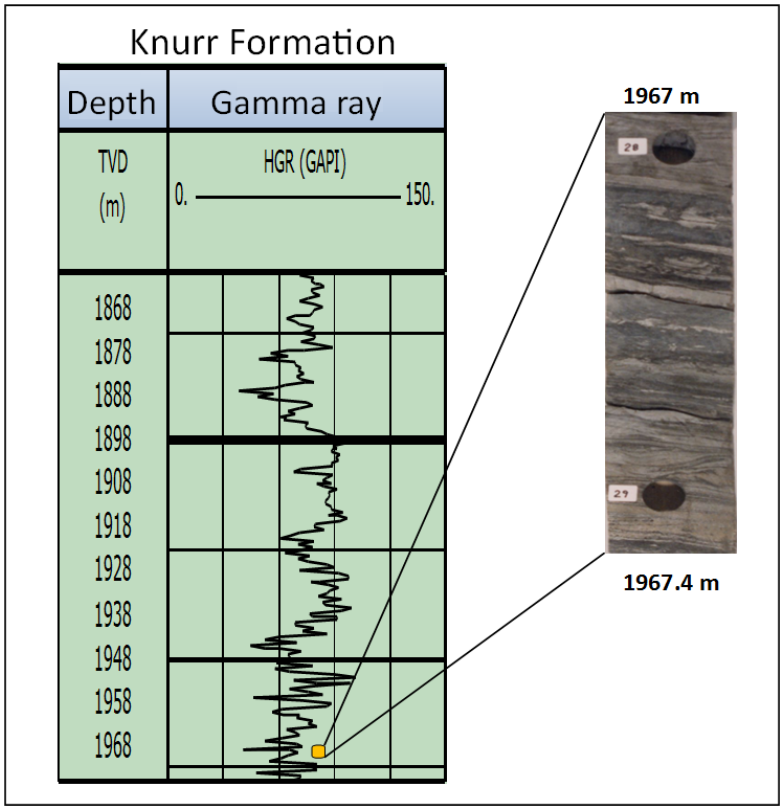


**Figure 2.8:** Core shows the thin grey sandstone of the Lower Cretaceous Knurr Formation holds average porosity of 17%, penetrated by well 7120/1-2.

- **Kolje Formation**

Claystone of grayish brown to dark grey color with interbeds of dolomite and pale limestone deposited during open to distal marine condition with the influence of good water circulation. Middle Cretaceous (Barremian to Early Aptian) age is designated to this formation (Henriksen et al. 2011).

- **Kolmule Formation**

The Kolmule Formation is dark grey to green claystone and shale with limestone and dolomite stringers. It was deposited during open marine condition. The age assigned to this formation is Mid Cretaceous (Aptian to Mid-Cenomanian) (Dalland et al. 1988).

### 2.3.8 Nygrunnen Group

It comprises greenish grey to grey claystones with thin limestone intervals. The formations assigned to this group are the Kveite Formation and Kviting Formation. This group is mostly eroded in the study area. The Kviting Formation is only penetrated by well 7120/2-2 whereas the Kveite Formation is only penetrated by well 7120/1-2. This group was deposited in open marine and deep shelf environment.

### 2.3.9 Sotbakken Group

This group is dominated by claystones with minor inclusion of siltstones, volcanic tuffs and carbonates. Claystones were deposited in sub-littoral to deep shelf environment during Late Paleocene to Early-Middle Eocene. The Torsk Formation is the only representative rock unit of this group (Dalland et al. 1988).

### 2.3.10 Nordland Group

Sandstones and claystones are dominant in this group, where sand contents increasing upward. No formation yet been assigned to this group which is deposited during bathyal to glacial marine environment. Late Pliocene and Pleistocene is its age (Dalland et al. 1988).

## 2.4 Petroleum System

The petroleum system is a combination of different processes and elements of petroleum geology. It is an important factor which has vast application in exploration, research and resource evaluation. So petroleum system can be defined as, "a set of crucial elements that in combination create a hydrocarbon bearing basin, composed of source rock, reservoir rock, seal/trap, migration and synchronization between hydrocarbon generation and formation of traps". A basin can have one or more effective petroleum systems (Magoon and Beaumont 2003).

Three main petroleum systems occur in the Grater Barents Sea area (Fig.2.9).

- Paleozoic system positioned in eastern part of the Barents Sea.
- Early to Middle Triassic system situated in south-western and southern part of the Barents Sea.

- Late Jurassic petroleum system situated in western part of Barents Sea

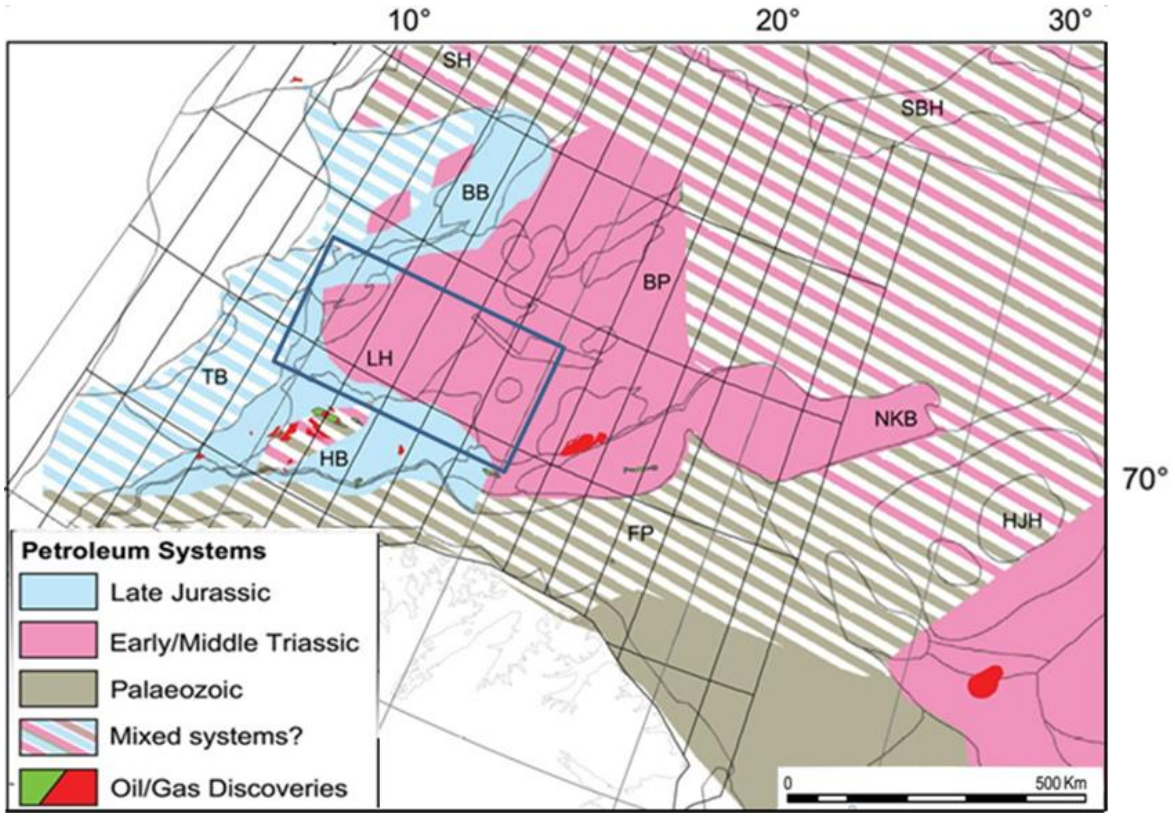


**Figure 2.9:** Map of three main petroleum systems of greater Barents Sea. The study area comprises Early-Middle Triassic system as well as Late Jurassic petroleum system, shown by blue block (Henriksen et al. 2011).

In the Loppa High area Triassic petroleum system is most operative. The isotopic values of oil samples taken from the Snadd Formation (Loppa High) are quite similar to geochemical appearances of classic Triassic system. This oil is generated from type II kerogen which shows marine anoxic origin. Correlation of oil samples from the Loppa High (Landian reservoir) and Hammerfest Basin also proved different ages of their source rocks (Henriksen et al. 2011).

## 2.4.1 Source rocks

The sedimentary rock that is capable of generating or has generated petroleum is called as source rock. The rocks which are generating and expelling petroleum at any time is called "active source" rocks whereas the source rock which has stopped generation and expulsion of petroleum is called as "inactive source rock" (Peter et al. 1994).

According to Henriksen et al. (2011), source rocks of different potential have been proven in the Greater Barents Sea, ranging in age from Silurian to Cretaceous. The peak time for oil generation in the Barents Sea was Landinian with a transformation ratio of 0.4-0.6. The structurally complex Loppa High has a good maturity value for source rocks of Triassic age (Ohm et al. 2008). A schematic chart of the major source rocks penetrated by wells in the Loppa High area is given in Table 2.1.

**Table 2.1:** The major source rocks of the study area (Modified from Henriksen et al. 2011).

| Age | Formation | Common Thickness | Kerogen type | TOC (%) | HI (mg $g^{-1}$ TOC) | Data Source |
|---|---|---|---|---|---|---|
| **Barremian** | Kolje | <30 | II–II/III | 1–7 | 130 | Ohm et al. (2008); Statoil |
| **Kimmeridgian** | Hekkingen | 10–250 | II/III | 20 | 300 | Ohm et al. (2008); Statoil |
| **Carnian-Norian** | Snadd | | III–I | <5 | <600 | Statoil |
| **Ladinian** | Snadd | 1-15 | II | 6 | 300-500 | Statoil |
| **Anisian** | Kobbe | 5-20 | II–II/III | 2-8 | 200-590 | Isaksen & Bohacs |
| **Late Permian** | Ørret | 80-350 | II/III | <3.5 | 200-330 | Ohm et al. (2008); Statoil |

The Ørret Formation of Permian age is oil mature in the Loppa High and Finnmark Platform but it is over-mature in most of mapped areas in the Barents Sea (Ohm et al. 2008). The Kobbe Formation formed in marine anoxia deposited during Middle Triassic (Anisian) (Henriksen et al. 2011). The lower part of the Snadd Formation was deposited in marine anoxic environment during maximum flooding of sea with good source rock potential. The vertical thickness of this source rock is very low but it has a fair gas/oil potential, hydrocarbon index value raging 400-500 mg/g TOC. Isotopic values of the oil from well 7120/1-2 recommend Pre-Jurassic zones to be oil mature. The Hekkingen Formation of Late Jurassic (Kimmeridgian), deposited in marine anoxic environment, has shown heavy isotope values for oil (Ohm et al. 2008). The Kolje Formation of Early Cretaceous (Barremian), formed during marine transgression in anoxic environment is organic rich and has good potential for oil generation. (Henriksen et al. 2011).

**Source rock Correlation**

The Hekkingen Formation considered as the main source rock of the Barents Sea which is holds 20% average TOC value and 300 mg $g^{-1}$ TOC hydrogen index value. The Kolje Formation is also possess good source rock qualities is present directly above the Knurr Formation in wells 7120/1-2 and 7120/2-2. The thickness of the Hekkingen Formation and Kolje Fromation decreases from the Hammerfest Basin towards the Loppa High, they are absent in wells 7120/1-1, 7120/2-1 and 7121/1-1. The Snadd Formation is has maximum average thickness of 1300 m in this area is not penetrated by well 7120/1-2 and 7120/2-2 (Fig. 2.10).

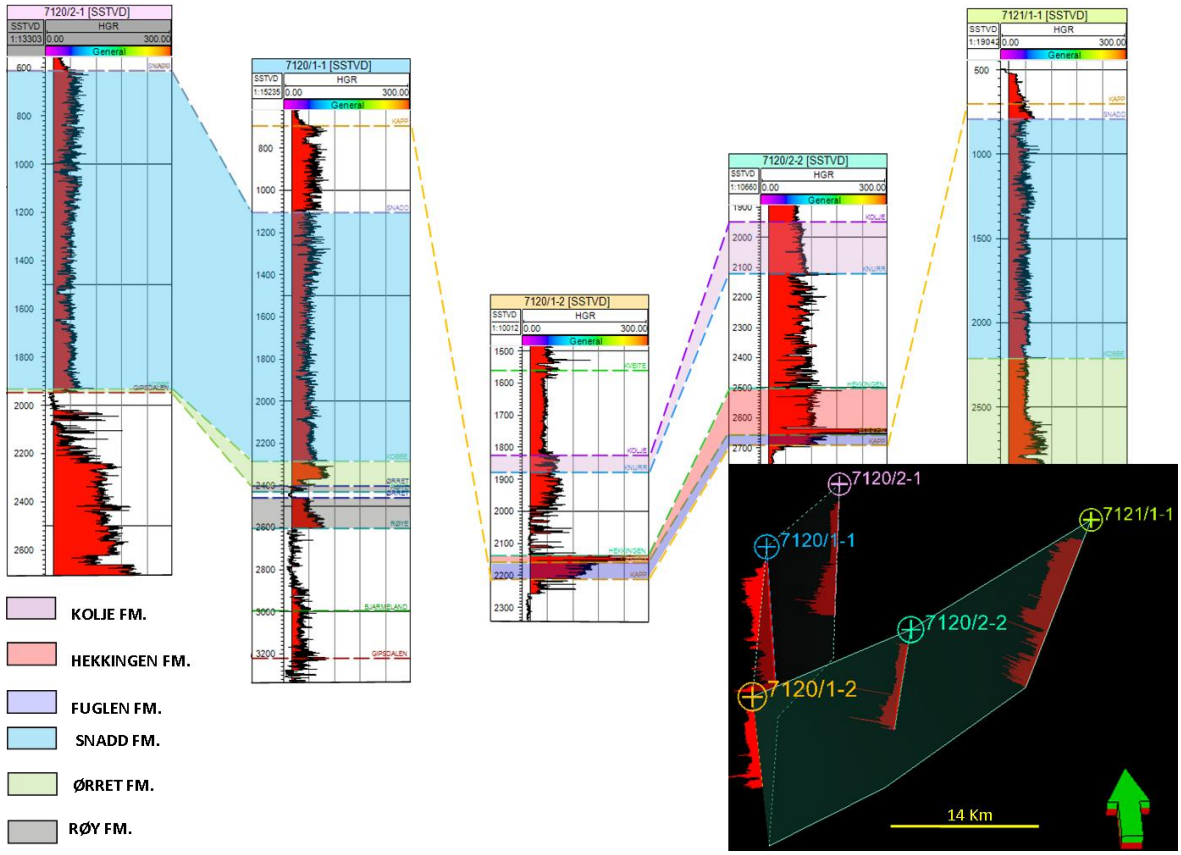


**Figure 2.10:** Correlation of source rocks (Hekkingen FM) penetrated in five wells in the SW Loppa High area.

## 2.4.2 Reservoirs rocks

Moving oils from source to the reservoir rocks requires porosity higher than 10-12% and permeability above 15-20 mD (Knutsen et el. 2010). The Barents Sea is considered to be crowded by different reservoir types which are ranging from Paleozoic carbonates to Paleozoic deep marine sandstones. The Kapp Toscana Group (ranging Late Triassic to Middle Jurassic age) is considered to hold the most prolific reservoirs in the Norwegian Barents Sea. The Kapp Toscana Group includes the Fruholmen Formation, Tubåen Formation, Nordmela Formation and the Stø Formation which contains 85% of the Barents Sea hydrocarbon resources (Larsen et al.1993; Henriksen et al. 2011).

The major portion of the Stø Formation is medium to fine grained sandstone with good reservoir quality and better horizontal continuity. It has large-scale cross bedding. Trace fossils data show that these sediments were deposited along high energy shallow marine shoreline, tidal delta and shoreface environments (Seldal et al. 2005). In well 7120/1-2 the Stø Formation showed excellent reservoir quality (Stewart et al. 1995). Lower Cretaceous Marine sands, which were deposited along the flanks of the Loppa High due to erosion, holds good reservoir potential (Dore 1995). According to Seldal (2005) Lower Cretaceous turbidite sandstone, specifically the Knurr Formation, developed on the hanging wall towards the southern flank of the Loppa High contains good reservoir quality. Oil traces are present in this sandstone observed in the well 7120/1-2, whereas the Hauterivian age sandstone in the same well has some oil shows. Lower clastic wedge of the Knurr Formation is the only reservoir rock in the well 7120/1-2, in which oil is movable (NPD

2013). The well 7120/2-2 showed fair reservoir quality fan delta sands and favorable conditions for oil migration from source to trap. But the problem related to dry nature of this well is again may be the wrong timing of hydrocarbon generation (Knutsen et al. 2000).

**Reservoir rock correlation**

The main reservoir rocks in the study area as discussed above are the Stø and Knurr Formation which are present in the southern wells (7120/1-2 and 7120/2-2) of the area. Reservoir rocks of Jurassic and Cretaceous age are missing in the well 7120/2-1 due to erosion. Nordmela Formation and Tubåen Formation are only present in the well 7120/1-2. The Fruholmen Formation is present in the well 7120/1-1, 7120/1-2 and 7121/1-1.Triassic (Fruholmen Formation and Snadd Formation) strata are unconformably overlain by the Torsk Formation of Paleocene age. The dominating lithology of the Snadd Formation is shale, but there are also fine sand layers which can act as hydrocarbon reservoir. The correlation of the Snadd Formation from eastern well 7121/1-1 to the western wells 7120/2-1 and 7120/1-1 is shown in the Figure 2.10.

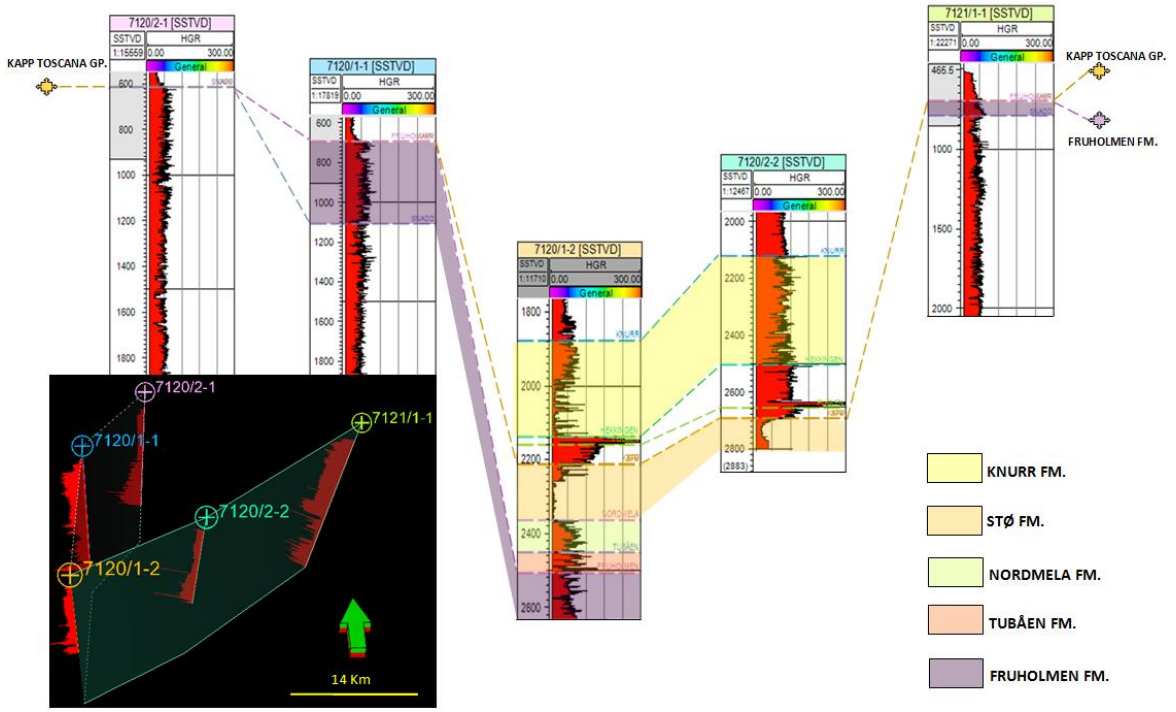


**Figure 2.11:** Correlation of clastic reservoir rocks of the five wells penetrated in the Loppa High area.

**Reservoir geometry**

The Kapp Toscana Group has variable thickness in the area. It has the major reservoir rocks with the porosity values ranging between 10 and 25%. The Stø Formation which is deposited in coastal marine environment during regression shows good reservoir quality. The net-to-gross for the Stø Formation is higher than 0.8. The porosity ranges from 16 to 18% whereas the permeability ranges from 200 to 800 mD (Selnes et al. 2004). The reservoir sands are deposited as clastic wedge during fault activity and the size of these wedges decreases upwards due to depreciation in fault activity. The 154 m thick bed of the Knur Formation

which is a wedge deposit. It has 17% average porosity with 0.80 net-to-gross (N/G) ratio in well 7120/1-2 (Fig.2.12) (Seldal et al. 2005).

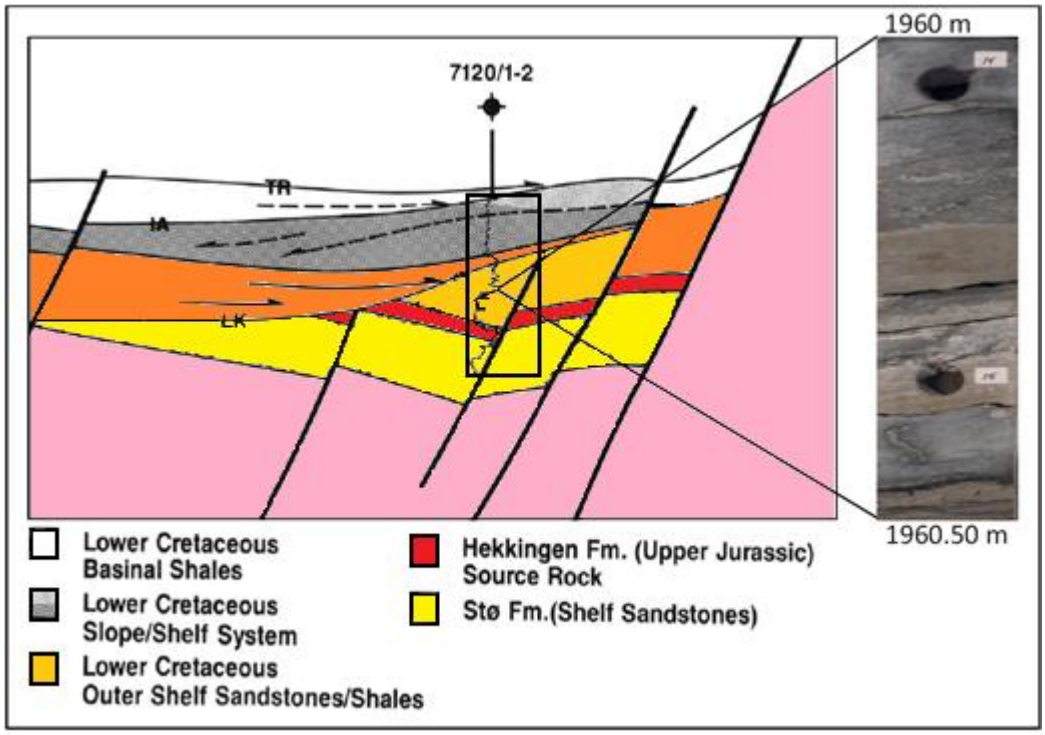


**Figure 2.12:** Geophysical log and core diagram of the well 7020/1-2 showing the Knurr Formation, with good reservoir sands between intervals 1958-2112m (Modified from NPD 2013; Stewart et al. 1995).

## 2.4.3 Traps and Seals

Stratigraphic and structural traps dominate in the Loppa High area (NPD 2013). The Late Paleozoic carbonates which are associated with the karstification of carbonate platform can act as stratigraphic seals (Henriksen et al. 2011). The Upper Jurassic shales of the Fuglen and the Hekkingen Formations are the main cap rocks for the Jurassic reservoirs. These formations in combination are extended over area of 100 m forming an effective seal (Stewart et al. 1995) The Cretaceous claystones and Lower Cretaceous claystones combines to form a good seal. The well 7120/2-1 shows that the play has good reservoir quality and also an active source rock but the traps breached to accumulate hydrocarbons (Seldal et al. 2005). The proven model from the well 7120/2-1 showed that traps failed at some stages to preserve hydrocarbon. The well 7120/2-2 studies showed that in the presence of good quality reservoir sandstone of the Lower Cretaceous and Oil prone source rock of Upper Jurassic once again trap failed to contain petroleum due to inadequate lateral, top or bottom seal (Knutsen et al. 2010).

## 2.4.4 The effects of uplift and erosion on petroleum system

For prospect evaluation it is important to consider the effects of uplift and erosion and the elements influenced by them, which are summarized in Figure 2.13 (Henriksen et al. 2011). The temperature decreased due to uplift and erosion, uplifted rocks which were supposed to generate oil have ceased oil generation because of decrease in temperature. This has affected

the charge to prospects, especially for the prospects which are depending on late migration due to late developments of the traps (Henriksen et al. 2011).

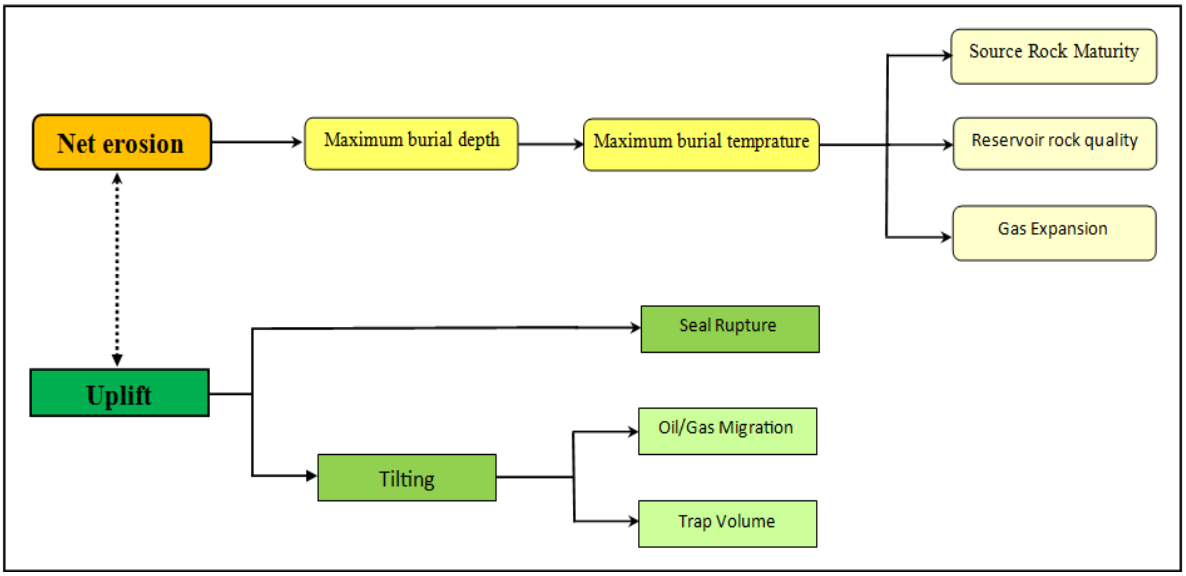


**Figure 2.13:** The effects of Uplift and Erosion on Petroleum system (modified from Henriksen et al. 2011).

The Loppa High is severely affected by Cenozoic uplift and erosion which is the biggest challenge for exploration in this area (Dore 1995). Figure 6 shows the estimated uplift in south-western part of the Loppa High area which is about 1400 m. The nature of uplift is orogenic-isostatic and the age of uplift is Palaeogene and Neogene (Henriksen et al. 2011). Dore´ and Jensen (1996) summarized the findings that reflect effects of uplift and erosion on petroleum systems

- Release in pressure and gas expansion which ultimately pushed oil below the spill point.
- Rupture of seal
- Deterioration of reservoir quality due to uplift.
- Fall in temperature of source rock resulting termination of hydrocarbon generation.
- Reorientation of traps causes spillage of petroleum.

# Chapter 3: Methodology and theoretical background

Detailed study of the geological background of the study area was the first most important task to start this work. After going through extensive literature review the given datasets (5 well log data) have been analyzed. After analyzing the data quality it has been found that there are many well log missing that could be valuable for this study. Using Interactive Petrophysics (IP) and the missing logs (temperature, water saturation, density porosity, clay volume etc.) were calculated using different empirical relationships. Excel spread sheets are generated from LAS format well data using IP software and used the extracted logs to calculate the most important but missing logs i.e. shear wave and average porosity. Elastic moduli (Young's modulus, shear modulus, bulk modulus, Lame's parameter and Poison's ratio) and seismic parameters (acoustic impedance, shear impedance and reflectivity) which are important for this study calculated using excel spread sheets. The AVO modeling is carried out using Hampson and Russel software.

Taking into account the original log data and calculated/estimated data the whole thesis workpakage is divided into three steps (Fig.3.1) given as;

- Petrophysical analysis of reservoir sandstones
- Rock physics diagnostic of reservoir sandstones
- AVO modeling of different reservoir horizons

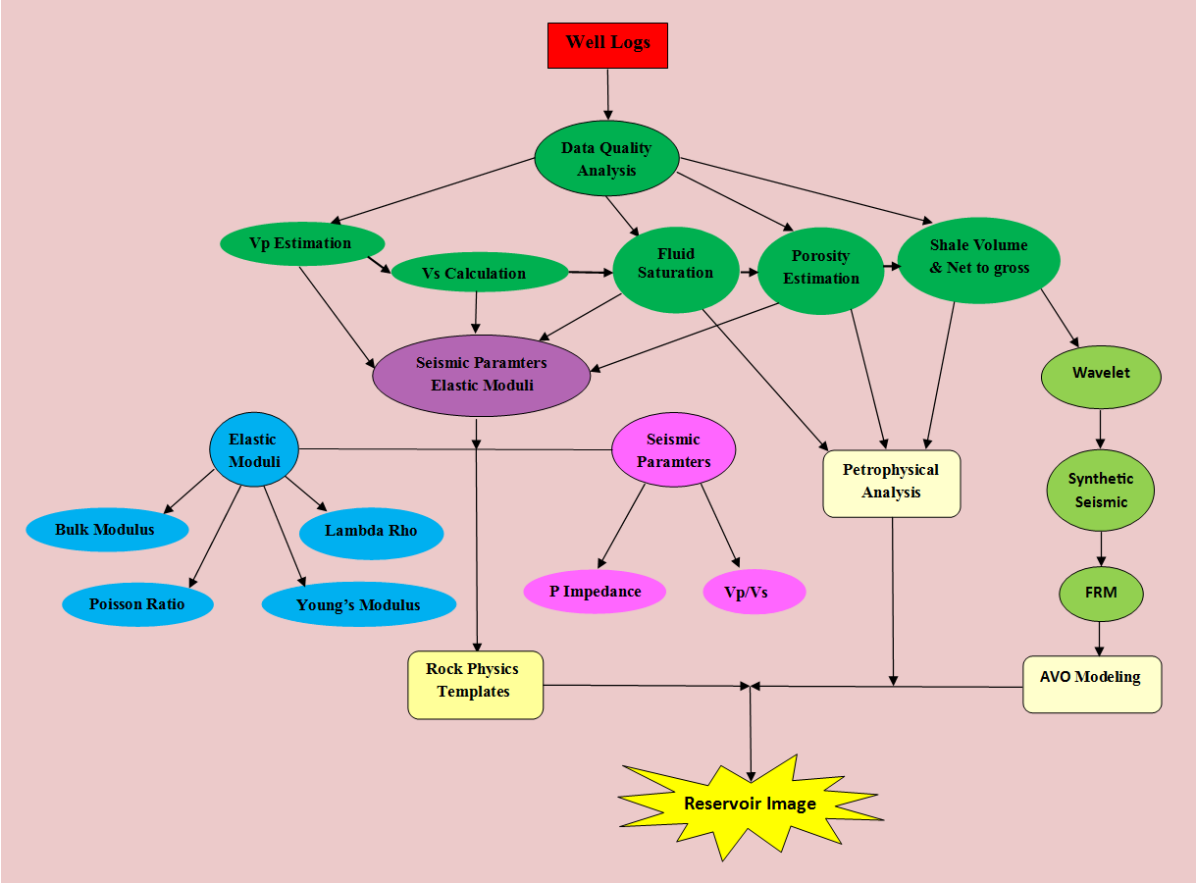


**Figure 3.1**: Flow diagram of the key steps of the thesis work.

The main thinking behind choosing these methods was to produce best results under limited data set and time. Only a single method is not always enough to predict the reservoir properties and could lead to ambiguity, which can be minimized by integrating different set of techniques and methods. At the later stages of this study all results have been compiled together and analyzed.

# 3.1 Petrophysical analyses of reservoir rocks

## 3.1.1 Net-to-gross (N/G) estimation

The net-to-gross (N/G) estimation for heterogeneous clastic reservoirs is commonly calculated by acoustic impedance inversion of 3D seismic data (Vernik et al. 2002). In nature we always not find clean sand reservoirs and we have many reservoirs with intercalating layers of shale and sand with quartz cement. It is very important to carefully observe the sandstone microstructure (quartz cement) and other heterogeneities (shale layers) in sandstone reservoirs. By definition N/G ratio is the proportion of permeable clean sand thickness to the thickness of whole reservoir (Avseth et al. 2009)

### 3.1.1.2 Volume of shale calculation

Calculation of shale volume is an important parameter for reservoir characterization. Asquith and Krygowski (2004), gave an imperial relation for the calculation of shale volume from any given gamma ray log. The equation is expressed as;

$$I_{GR} = \frac{GR_{log} - GR_{min}}{GR_{max} - GR_{min}} \quad \text{Eq.3.1}$$

Where, $I_{GR}$ is gamma ray index, $GR_{log}$ is the gamma ray reading in any target zone, $GR_{min}$ is the minimum value of gamma ray log and the $GR_{max}$ is the maximum value of gamma ray log.

Shale volume can be estimated with the help of a linear relation between $I_{GR}$ and $V_{shale.}$ Several authors suggested fine tuning of shale volume estimation and came up with their own imperial relations using $I_{GR}$. This study use the two following equations proposed by Larinov 1969.

Volume of shale for unconsolidated rocks is given by;

$$V_{sh} = 0.083(2^{2.7.I_{GR}} - 1) \quad \text{Eq.3.2}$$

Whereas, volume of shale for consolidated rocks is

$$V_{sh} = 0.33(2^{2.I_{GR}} - 1) \quad \text{Eq.3.3}$$

An example of shale volume calculation from gamma ray log is shown in Figure 3.2.

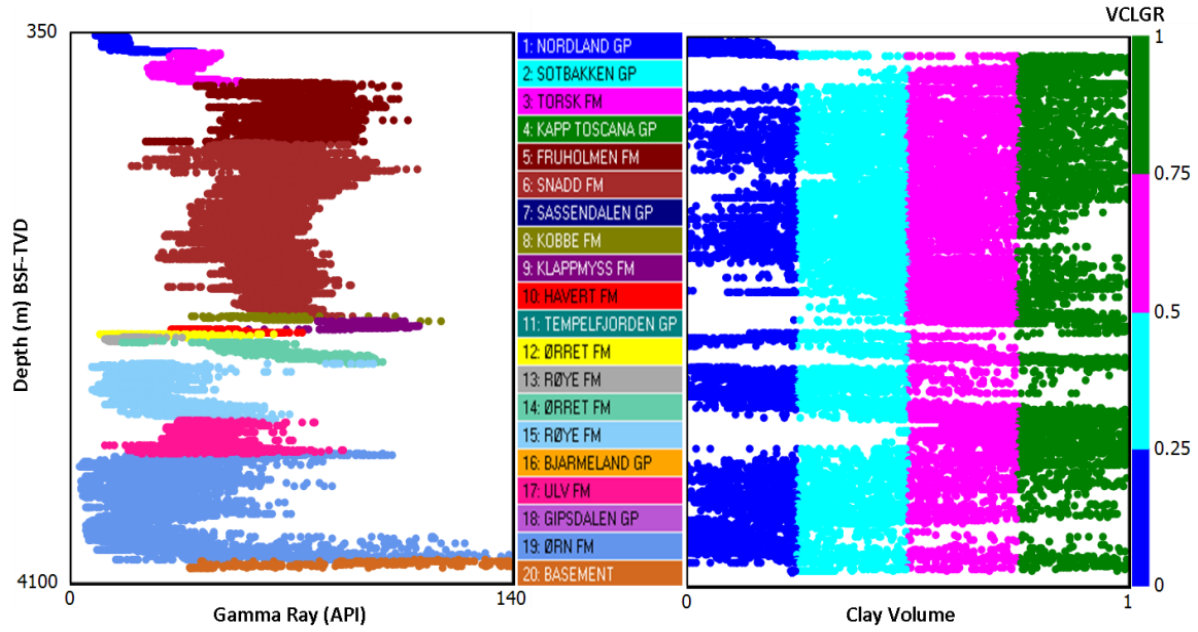


**Figure 3.2:** Volume of shale for the well 7120/1-1 is shown as a function of gamma ray depth trend.

### 3.1.2. Porosity estimation

Neutron porosity log is available in the given data but there are some uncertainties with the values of neutron porosity in gas saturated zone due to lower concentration of hydrogen. In gas zones the Neutron log shows low value of porosity. On the other hand, due to presence of water ion in shale the Neutron logs give higher value of porosity. Taking this factor into account porosity from density log is calculated by using the following formula;

$$Ø_{density} = \frac{(\rho_{matrix} - \rho_{bulk})}{(\rho_{matrix} - \rho_{fluid})} \qquad \text{Eq.3.4}$$

Where $Ø_{density}$ is the density log derived porosity, $\rho_{matrix}$ is the matrix density, $\rho_{bulk}$ is the density log reading at any area of interest and $\rho_{fluid}$ is the formation fluid density. For more precise calculation of porosity in shale and gas saturated zones the average porosity is calculated by computing density porosity and neutron porosity in the following equation;

$$Ø_{avg} = \sqrt{\frac{(Ø^2_{density} + Ø^2_{neutron})}{2}} \qquad \text{Eq.3.5}$$

### 3.1.3 Calculation of hydrocarbon saturation

Seismic properties of rocks (velocity, density and acoustic impedance) are drastically affected by pore fluids. During reservoir studies we usually come across three kinds of pore fluids which are brine, hydrocarbon gasses and hydrocarbon liquids. Due to inclusion of pore fluid the net bulk modulus and density increases compared to dry rock. Hydrocarbon gasses carry the largest pressure effect and the oils possess intermediate effect whereas brine has the smallest pressure effect (Batzle and Wang 1992).

The calculation of hydrocarbon saturation is an important factor for reservoir characterization. It is important to consider the geological factor as the pore fluid sensitivity can be affected by sandstone heterogeneity and microstructures (Avseth et al. 2009). The main principal for calculation of fluids saturation in the rock pores is Archie's equation. Quantitative use of resistivity log is the main tool to be used for measuring fluid saturation in rock pores (Donaldson and Siddiqui 1989). Archie's equation is given in following step;

$$R_o = F \times R_w \qquad \text{Eq.3.6}$$

Where $R_o$ is the resistivity of water filled formation and $R_w$ is the resistivity of water and F is the formation resistivity factor. The value of F can be calculated by knowing tortuosity (a) and cementation factor (m) by following equation;

$$F = \frac{a}{\emptyset^m} \qquad \text{Eq.3.7}$$

Water saturation ($S_w$) can be calculated by knowing the values of true formation resistivity ($R_t$) and water filled formation resistivity ($R_o$) by the equation given as;

$$S_w = \left(\frac{R_o}{R_t}\right)^{1/n} \qquad \text{Eq.3.8}$$

Computing values from equation 3.6 and 3.7 we can write equation 3.8 as;

$$S_w = \left(\frac{F \times R_w}{R_t}\right)^{1/n} \qquad \text{E.q.3.9}$$

$$S_w = \left(\frac{a \times R_w}{R_t \times \emptyset^m}\right)^{1/n} \qquad \text{Eq.3.10}$$

Where "a" is tortuosity factor and "n" is the cementation exponent and varies from 2.0 to 8 for strongly water wet, quartz sands to strongly oil wet rocks respectively. If the value of n is less than 8.0, minute errors of this parameter will results into a large error of estimation of water saturation. For example if value of n is taken 2 for water saturation calculation and the correct value is 3 it will give an error of 10% higher oil saturation. (Asquith and Krygowski 2004; Donaldson and Siddiqui 1989).

The available pore space is completely occupied by both hydrocarbon and water or only by water. So the total saturation of fluids in reservoir can be written as;

$$S_w + S_{hc} = 1 \qquad \text{Eq.3.11}$$

And the hydrocarbon saturation can be estimated as;

$$S_{hc} = S_w - 1 \qquad \text{Eq.3.12}$$

Where the saturation of water is $S_w$ and $S_{hc}$ is saturation of hydrocarbon.

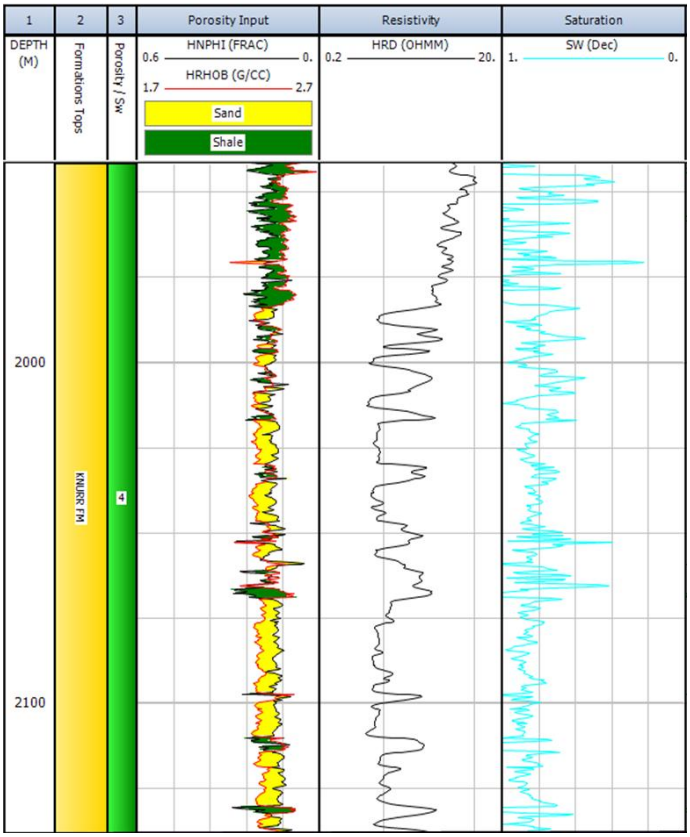


**Figure 3.3:** Water saturation of the Knurr Formation for well 7120/1-2.

**The Pickett Plot**

Using Archie's equation a plot of resistivity log and porosity log is made for the reservoir section which is called as the Pickett Plot. The value on X-axis is showing porosity form 0.01 to 1 and the Y-axis is showing value of deep resistivity log from 0.01 to 100 Ohm-m. A straight line is drawn from the Y-axis which gives the value of resistivity of water of the section measure. This line is called as water line (Glover 2005).

By combining the equation 3.6 and 3.7 we can write;

$$R_o = R_w \times \emptyset^{-m} \qquad \text{Eq.3.13}$$

This can be rearranged as;

$$\text{Log}\, R_o = \text{Log}\, R_w - m \times \text{Log}\, \emptyset \qquad \text{Eq.3.14}$$

For hydrocarbon bearing rock the above equations can be rewritten as;

$$R_t = I \times R_o = I \times R_w \emptyset^{-m} \qquad \text{Eq.3.15}$$

Where I represents resistivity index and m is the gradient of the line called cementation factor. The value of $R_w$ calculated from water line is used to calculate the saturation of water by computing the value in Archie's formula.

**Temperature gradient**

For fluid saturation calculation, temperature gradient is a necessary input. The temperature gradient for all wells in the data set is calculated by using following equation;

$$m = \frac{y-c}{x} \qquad \text{Eq.3.16}$$

Where m is geothermal gradient, y gives the bottom-hole temperature (BHT), c is surface temperature and x stands for the total depth of the bore hole. The geothermal gradients calculated by assuming surface temperature 4$^{o}$C. The water saturation has been calculated for the Knurr Formation (Fig. 3.3) and the Stø Formation which are the main sandstone reservoirs of the area penetrated by the wells 7120/1-2 and 7120/1-2.

# 3.2 Rock physics diagnostics

Rock physics is the integration of geophysical parameters (i.e. P-wave/S-wave velocity ratio $V_p/V_s$, elastic moduli, acoustic impedance and bulk density) and geologic reservoir constraints (porosity, saturation, clay content, sorting and cement). The basic purpose of rock physics diagnostics is to observe and interpret the seismic velocities in terms of reservoir constraints and extend it to the larger scale beyond the extent of available data to map the variation in lithology and pore fluid contents. Various depositional and compaction trends are altered to form new relations in cross-plots which give us better understanding of reservoir information that cannot easily gained by conventional methods. For the application of rock physics models it is necessary to have a better understanding of the geological parameters and the variation in rock properties in the area which leads to better extrapolation and minimum chances of uncertainties (Avseth et al. 2009; Avseth et al. 2010 ).

## 3.2.1 Porosity versus velocity relationships

Velocity-porosity relationship has a unique importance in rock physics diagnostics. The lithology and pore fluids can be analyzed with the help of this relationship. Gassman's (1951) equation describes the relationship between porosity, elastic properties of minerals and elastic properties of saturated rocks. The sensitivity of the rock modulus is directly proportional to the pore fluids and mineral constituents. Rocks that are soft show more seismic sensitivity to pore fluids whereas the rocks those are relatively stiff offer less sensitivity to pore fluids (Avseth et al. 2005). Here it is important to discuss the theory behind different background trends and models describing cementing and sorting trends, stiffness and softness of rocks.

The Willie time average equation is the best model to relate velocity to porosity. This equation is a heuristic model (Pseudo-theoretical), which fits very well for consolidated, clean water saturated rock units.

$$\frac{1}{Vp} = \frac{\emptyset}{V_{fluid}} + \frac{(1-\emptyset)}{V_{mineral}} \qquad \text{Eq.3.17}$$

### 3.2.1.1 Hashin-Shtrikman bound

Hashin-Shtrikman upper and lower bounds are useful heuristic models to describe cementing and sorting trends of rock units (Avseth et al. 2010). Hashin-Shtrikman (1963) derived the equation which describes the elastic moduli for two constituents without considering their geometry are given as;

$$K^{HS\pm} = K_1 + \frac{f_2}{(K_2 - K_1)^{-1} + f_1(K_1 + \frac{4}{3}\mu_1)^{-1}} \quad \text{Eq.3.18}$$

$$\mu^{HS\pm} = \mu_1 + \frac{f_2}{(\mu_2 - \mu_1)^{-1} + \frac{2f_1(K_1 + 2\mu_1)}{5\mu_1(K_1 + \frac{4}{3}\mu_1)}} \quad \text{Eq.3.19}$$

Where bulk moduli of the given constituents are shown by $K_1$ and $K_2$ and shear moduli of the constituents are shown by $\mu_1$ and $\mu_2$. For Hashin-Shtrikman upper bound stiffer material is taken as "1" and for lower bound "1" is taken for softer material.

### 3.2.1.2 Hashin-Shtrikman-Walpole bound

The best way to study the elastic properties of rocks is Hashin-Shtrikman bound (HS bound) which separates them into two end members, one with zero porosity shows the properties of mineral and the other at critical or highest porosity (40-45% for sands). These end two members are called upper HS bound representing stiffest material and the lower HS bound representing the softest material. The upper bound gives a good representation of cementation and the lower bound defines the effect of sorting (Avseth et al. 2010). Hashin-Shtrikman bound was modified later by Walpol (1966) which was then called Hashin-Shtrikman-Walpole bound given as;

$$K^{HS\pm} = K_1 + \frac{f_2}{(K_2 - K_1)^{-1} + f_1(K_1 + \frac{4}{3}\mu_m)^{-1}} \quad \text{Eq.3.20}$$

$$\mu^{HS\pm} = \mu_1 + \frac{f_2}{(\mu_2 - \mu_1)^{-1} + f_1[\mu_1 + \frac{\mu_m}{6}(\frac{9K_m + 8\mu_m}{K_m + 2\mu_m})]^{-1}} \quad \text{Eq.3.21}$$

All the variables are same as used by Hashin-Shtrikman despite of subscript "m" which is for maximum bulk ($K_m$) and maximum shear moduli ($\mu_m$).

### 3.2.1.3 Han's empirical relation between velocity and porosity

Han (1986) derived an empirical relationship between velocity and porosity which describes the increase or decrease in clay contents in sandstones. The equations for Vp and Vs assuming pressure 40 MPa are given as;

$$Vp = 5.59 - 6.93\emptyset - 2.13C \quad \text{Eq.3.22}$$

$$Vs = 3.52 - 4.91\emptyset - 1.89C \quad \text{Eq.3.23}$$

Where Vp and Vs are given in km/s, Ø is the porosity and C is the volume fraction of clay. Figure 3.4 shows the contours describing the change in clay contents with respect to changes

in velocity and porosity. Han's clay rich line describes the dirtier sands whereas the Han's clean contour shows clean sands.

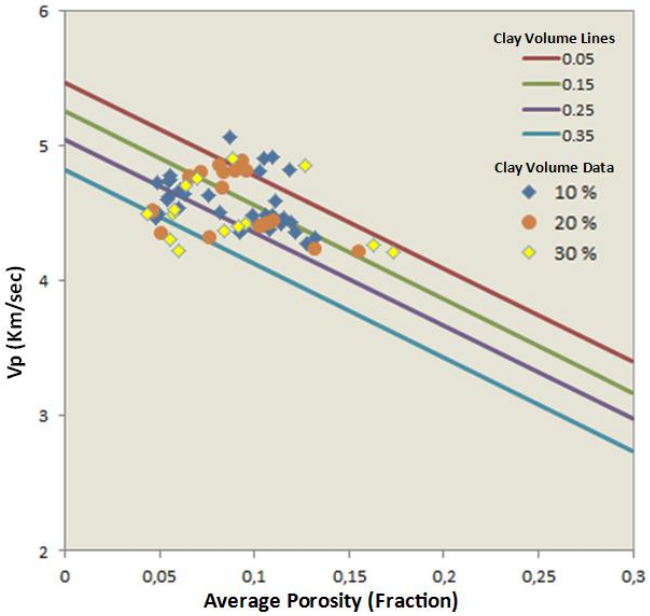


**Figure 3.4:** Digitized diagram of Han's clayey sand model, with clay data points (circles and diamonds) of the Tubåen Formation from the well 7120/1-2.

### 3.2.1.4 Rock Physics cement estimation

Reservoir heterogeneity and sandstone microstructures play a critical role in pore fluid sensitivity in sandstone reservoirs. When the rocks cross the temperature range of 60-80 $^{o}$C quartz precipitation starts over the grain surfaces. Thus the amount of cement in sandstone reservoirs severely changes the AVO signatures and also decreases the fluid sensitivity and pressure. The contact cementation theory thus explains the stiffness (Normal and shear) of a two grain combination with elastic cement at the contact. The shear and normal stiffness obtained from this theory can be utilized in different operative medium estimates. This model helps better to interpret the heterogeneous and cemented reservoirs. This model gives the better understanding of microstructures from velocity-porosity data and also helps to calculate the cement volume and degree of sorting (Dvorkin et al. 1996; Avseth et al. 2009). Cement models are further categories into three different heuristic hybrid models are explained in detail in the following section.

#### The friable sand model or unconsolidated sand line

This model for high porosity sands is first time introduced by Dvorkin and Nur (1996). It states the changes in velocity-porosity relation when grain sorting depreciates. The porosity of well sorted sand is around 40% (critical porosity). The friable sand model describes the deposition of fine grains in the well sorted friable sands and thus represents the two end members which are well sorted sands and poorly sorted sands. The poorly sorted sand possesses almost the same porosity but slightly higher shear modulus than the well sorted sand as shown in Figure.3.5 (Avseth et al. 2010).

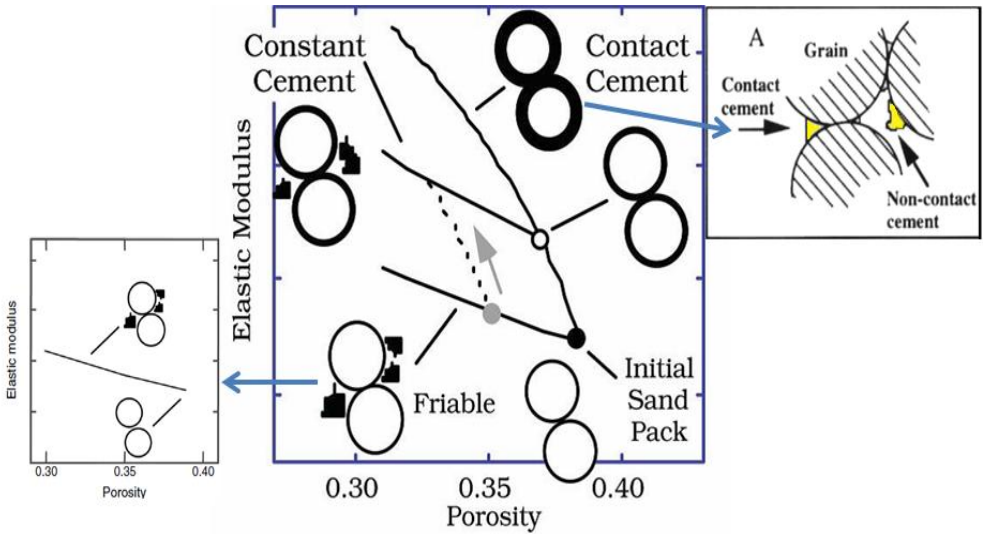


**Figure 3.5:** Different cement models and their relation to porosity and elastic moduli (Modified from Dvorkin and Nur 1995; Avseth et al. 2010).

**The contact-cement model**

During burial process sandstones undergo cementation process with different kinds of cements i.e. calcite, albite, diagenetic quartz and other mineral. This process makes sandstones stiffer as the grain surfaces are strongly bounded together with cement. Taking this process into account Dvorkin and Nur (1996) stated that initial porosity of sandstones decreases due the uniform deposition of sand layers around the grain surfaces and called it "the contact cement model". Figure 3.5 shows the uniform cementation around the sand grains has decreased the porosity and increased the elastic modulus (Avseth et al. 2000; Avseth et al. 2010).

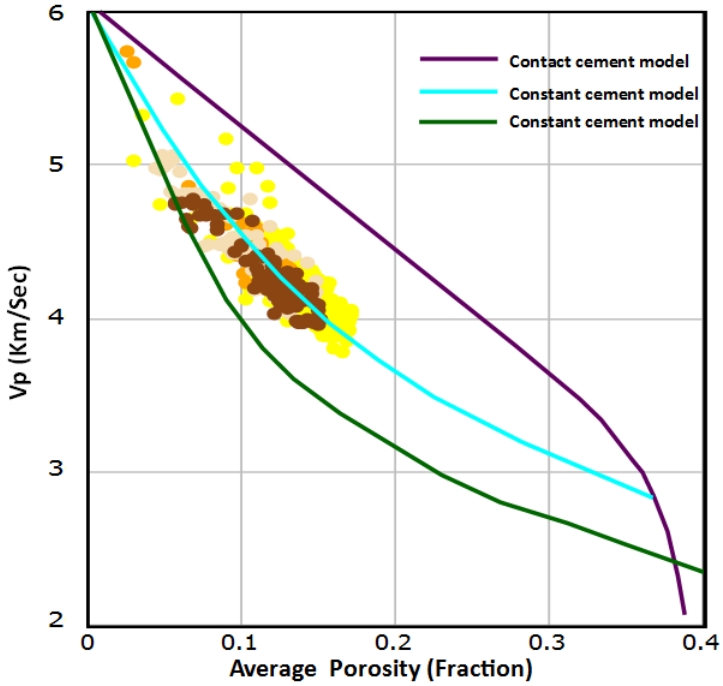


**Figure 3.6:** Background trend line of three cement models (digitized from Avseth et al. 2005) with data points of different reservoir rocks from Well 7120/1-2.

**The constant-cement model**

Avset et al. (2000) introduced another model which is the mathematical combination of first two cement models. It states that the sands of different porosity are carrying the same amount of contact-cement and the reduction in porosity is exclusively a function of non-contact pore-filling material. Standard background curves for all three cement models are shown in the Figure 3.6.

## 3.2.2 Vp versus Vs

Vp and Vs relationship is a good lithology indicator and also a direct indicator of pore fluids. The simplest and easiest way to describe this relationship is to; construct empirical relationship between Porosity, Vp and Vs for and individual pore fluid (mostly water) and then use the Gassman's (1951) relations to extrapolate this relationship for other fluids (Avseth et al. 2005).

Due to absence of Vs data different empirical relations is used to calculate Vs from Vp and then compared with the published relations suggested by Castagna et al. (1993) for different types of sandstones to choose the best fit equation. The famous Mudrock line was the first equation derived by Castagna et al. (1985) to calculate Vs form Vp is given below;

$$Vp = 1.16Vs + 1.36 \text{ (km/s)} \qquad \text{Eq. 3.24}$$

The very next year Hans (1986) came up with his equation to calculate Vs from Vp on the basis of a series of laboratory data;

$$Vs = 0.794Vp - 0.787 \qquad \text{Eq. 3.25}$$

Krief et al. (1990) derived another equation in which they used square of Vp and Vs and used some constant values for different types of sandstone and limestone (Table 3.1).

$$Vp = aVs^2 - b \qquad \text{Eq. 3.26}$$

**Table 3.1:** Constant values for different lithologies given by Krief et al. (1990).

| Lithology | a | b |
|---|---|---|
| Wet Sandstone | 2.213 | 3.857 |
| Sandstone with gas | 2.282 | 0.902 |
| Shaley Sandstone | 2.033 | 4.894 |
| Limestone | 2.872 | 2.755 |

Greenberg and Catagna (1992) derive the following equations for Vs calculation from Vp.

Vs for sandstone can be calculated by following equation;

$$Vs = 0.80416Vp - 0.85588 \quad \text{Eq. 3.27}$$

Vs for shales can be calculated by following equation;

$$Vs = 0.76969Vp - 0.86735 \quad \text{Eq. 3.28}$$

Castagna et al. (1993) revised their work and formulated another empirical relationship to suggest Vs prediction from Vp is given as;

$$Vs = 0.804Vp - 0.856 \quad \text{Eq. 3.29}$$

Most of the calculations for this study will be carried out with the equation given by Castagna et al. (1993) which gives relatively better results compared to the equations given by others.

### 3.2.3 Vp/Vs versus acoustic impedance (AI)

Two important parameters acoustic impedance (AI) and Vp/Vs are important outputs from geophysical data. When AI and Vp/Vs are used together in a rock physics template can infer lots of important information regarding fluid constituents, porosity trends for different lithologies and cementations trends. The cross-plot between AI and Vp/Vs (Fig.3.7) shows background brine sand trend line and curve for oil and gas saturated sands as a function of porosity. Nature does not always follow these trend lines so ambiguity of interpretation could be noticed i.e. increase in shale content can be misinterpreted with decrease in effective pressure.

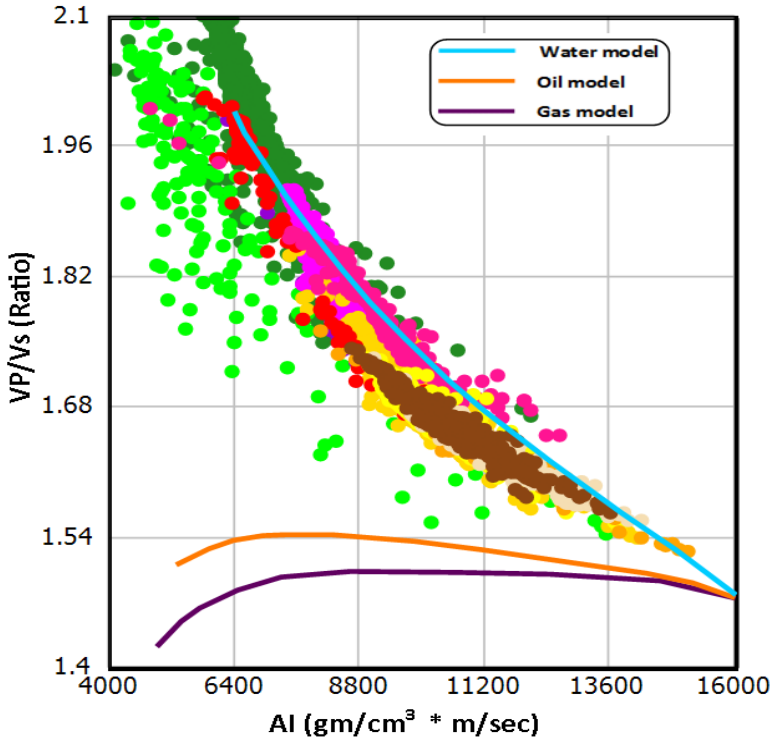


**Figure 3.7:** Background trend line of different fluid models with data points of different formations from the well 7120/1-2 in a cross-plot of AI versus Vp/Vs.

### 3.2.4 Lamda-Rho versus Mu-Rho

Compressibility and shear rigidity are fundamental rock properties and are easy to apprehend as compared to acoustic impedance and velocities. For examples understanding the higher compressibility of sponge as compared to brick is much easier than understanding their respective acoustic impedance (Gray et al. 1999). Lamda-Rho ($\lambda\rho$) versus Mu-Rho ($\mu\rho$) is an important RPT for lithology prediction and pore fluid discrimination. Lamda-Rho and Mu-Rho curves possess identical value ranges, they make a good crossover for gas zone where $\lambda\rho$ is less than $\mu\rho$. Whereas for thin and tight shale breaks $\lambda\rho$ is higher than $\mu\rho$ which shows different scenario from the gas zone (Fig.3.8) (Goodway et al. 2002).

Young's modulus ($\lambda$) is calculated by using equation;

$$\lambda = 2\mu(1+\gamma) \qquad \text{Eq.3.30}$$

Where $\lambda$ and $\mu$ are called Lame's parameters, $\mu$ is same as shear modulus and $\gamma$ is Poisson's ratio. The value for Poisson's is required for this calculation which can be estimated by the following equation;

$$\gamma = \frac{0.5(\frac{Vp}{Vs})^2 - 1}{(\frac{Vp}{Vs})^2 - 1} \qquad \text{Eq.3.31}$$

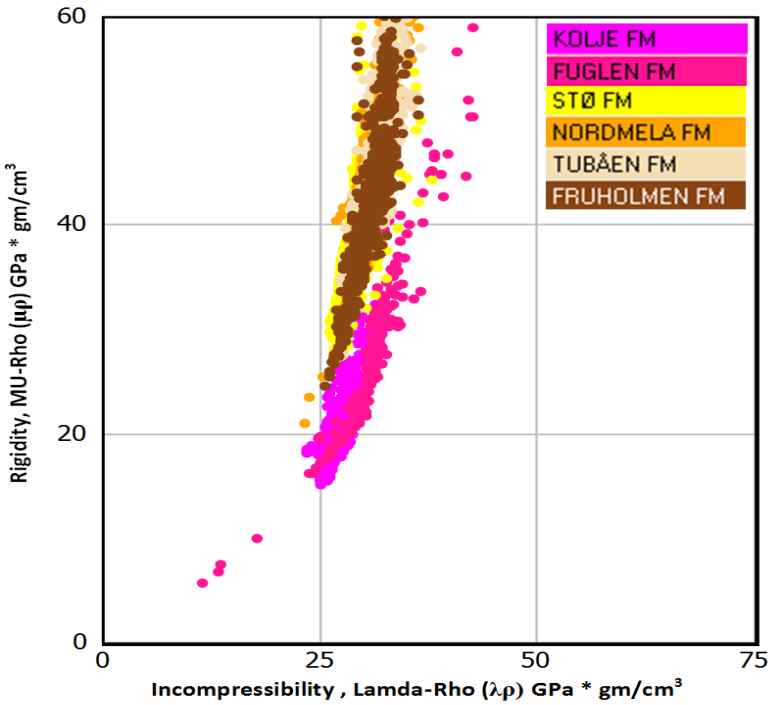


**Figure 3.8:** Lamda-Rho versus Mu-Rho cross-plot of reservoir sands and source rocks from the well 7120/1-2.

## 3.3 AVO modeling

Ostrander (1984) showed first time that the presence of gas sands under shale bed can cause a significant amplitude variation with offset using pre-stack seismic data. Since then, AVO

(amplitude variation with offset) modeling has evolved as integral tool for reservoir characterization. It has a significant role in seismic data acquisition design, processing and interpretation. The integration of AVO with other geophysical and geological data has become a common practice in hydrocarbon exploration which minimizes risks and uncertainties related to reservoir characterization (Li et al. 2007).

### 3.3.1 Gassman's Fluid substitution theory

The Gassman's (1951) equation describes the link between petrophysical properties (fluids, saturation of water and porosity) and seismic properties of rocks (bulk modulus and shear modulus), which is given as;

$$K_{sat} = K_{dry} + \frac{(1-\frac{K_{dry}}{K_o})^2}{\frac{\emptyset}{K_f}+\frac{1-\emptyset}{K_o}+\frac{K_{dry}}{{K_o}^2}} \quad \text{Eq.3.32}$$

$$\mu_{sat} = \mu_{dry} \quad \text{Eq.3.33}$$

This equation is later modified and called Gassman-Biot (1956) theory written as;

$$\frac{K_{sat}}{K_o - K_{sat}} = \frac{K_{dry}}{K_o - K_{dry}} + \frac{K_f}{\emptyset(K_o - K_f)} \quad \text{Eq.3.34}$$

Where $K_{sat}$ is the effective bulk modulus of saturated rock, $K_{dry}$ is the effective bulk modulus of dry rock, $K_f$ is the bulk modulus of fluid in the pore spaces, $K_o$ is the bulk modulus of mineral constituents of rock unit, $\mu_{sat}$ is the shear modulus of saturated rock, $\mu_{dry}$ is the shear modulus of dry rock and Ø is the porosity.

Gassman's equation is based on following assumption;

- All pores in the rock unit are connected (effective porosity)
- The fluid in pore spaces is homogenous and the pore volume is fully saturated with fluid
- The physical properties of all mineral constituents are same
- Applicable to low frequencies

The major drawback of this equation is that it does not predict the changes in bulk and shear moduli due to replacement of one fluid to the other fluid. The solution of this problem is very simple and can be done by using this equation in two steps, firstly from initial to dry state and then from dry to the newly substituted state. The equation is stated as;

$$\frac{K_{sat1}}{K_o - K_{sat1}} - \frac{K_{f1}}{\emptyset(K_o - K_{sat1})} = \frac{K_{sat2}}{K_o - K_{sat2}} \quad \text{Eq.3.35}$$

Where $K_{sat1}$ and $K_{sat2}$ are bulk modulus of rock saturation with respect to fluid 1 and fluid 2 respectively, and $K_{f1}$ and $K_{f2}$ are the bulk modulus of fluid 1 and fluid 2 respectively (Mavko et al. 2009).

### 3.3.2 Angle dependent reflection coefficient

Normal incident P-wave generates reflected and transmitted P-waves. When incidence angle θ is greater than zero then incident wave also generates reflected and transmitted S-wave. The incident wave conversion into four type of wave is called "mode conversion" (Fig.3.9). Both reflected and refracted wave follow the Snell's law given as;

$$\frac{\mathrm{Sin}\theta_1}{\mathrm{Sin}\theta_2} = \frac{V_1}{V_2} \qquad \text{Eq.3.36}$$

Where $V_1$ is the velocity in medium 1 and $V_2$ is the velocity in medium 2.

Angle of reflection and reflection coefficient ($R_o$) are the key parameters for AVO analysis.

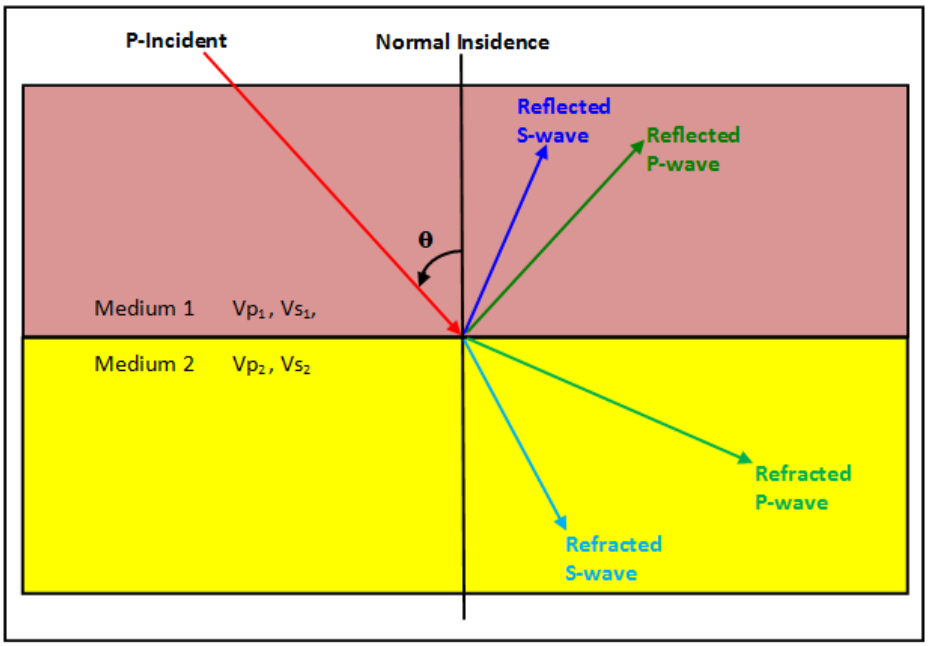


**Figure 3.9:** Mode conversion of seismic waves showing the rock properties in different medium determine the energy distribution (Modified from Mondol, 2010).

- **Knot_Zoeppritz equations**

The equation explains that the reflection coefficient which varies with the variation in angle of incidence for a single interface. Zoeppritz equations do not deliver a simple physical meaning to apply practically. This equation is then modified by several approximations. Aki and Richards (1980), came up with their well know approximation for P-wave reflection. Zoeppritz approximation is best fit to small angles ($35^o$). Wiggens or Gelfand's approximation is the most simplified form of all approximation, assuming Vp/Vs and small angles ($\tan\theta \approx \mathrm{Sin}\theta$) given as;

$$\mathrm{Rpp}\,(\theta) \approx \mathrm{Rp} + B\mathrm{Sin}^2\,\theta \qquad \text{Eq.3.37}$$

Where;

$$\mathrm{Rp} = \frac{1}{2}\left(\frac{\Delta Vp}{Vp} + \frac{\Delta\rho}{\rho}\right) \qquad \text{Eq.3.38}$$

$$Rs = \frac{1}{2}\left(\frac{\Delta Vs}{Vs} + \frac{\Delta \rho}{\rho}\right) \quad \text{Eq.3.39}$$

$$B = Rp - 2Rs. \quad \text{Eq.3.40}$$

Where Rpp (θ) is the reflection coefficient of P-reflected at an angle of incident (θ). Rp is the AVO intercept and B is the AVO gradient. Zero offset reflection coefficients for Vp and Vs are represented by Rp and Rs. ΔVp and ΔVs are difference in P-wave and S-wave velocities across the interface respectively. Similarly Δρ is the difference in density of the two layers and ρ is the average density of two layers.

**Aki-Richards approximation**

Aki-Richards approximation is much simpler and easily applicable in AVO analysis. Intercept stack and gradient stack the AVO quantities which can be plotted separately as well as combined section can be drawn. Combined section is good for bright spot detection and also used for the shear wave enhancement (Gelius and Johansen 2010). Some important AVO equations are shown in Table 3.2

**Table 3.2:** Shows the simplified AVO equations, assumptions and their limitations (Li et al. 2007).

| | | |
|---|---|---|
| Shuey (1985) | $R(\theta) = R_p + G\sin^2\theta + C(\tan^2\theta - \sin^2\theta)$ | |
| | Solves for: | Assumptions and limitations: |
| | $R_p$, $G$ | 3rd term is truncated and for angles ≤ 25°. Change in gradient could indicate change in fluid content, but could also be caused by a change in lithology. |
| Hilterman and Verm (1995) | $R(\theta) = R_p\cos^2\theta + \frac{\Delta\sigma}{(1-\sigma)^2}\sin^2\theta$ | |
| | Solves for: | Assumptions and limitations: |
| | $R_p$, $\frac{\Delta\sigma}{(1-\sigma)^2}$, or $R_\sigma$ | Based on Shuey's equation. Ignores angles > 30°. Assumes $V_P/V_S = 2$, and makes no density assumptions. Change in Poisson 'reflectivity' could indicate change in fluid content, but could also be caused by a change in lithology. |
| Smith and Gidlow (1987) | $R(\theta) = \left\{\frac{\Delta V_P}{V_P}\right\}\left\{\frac{1}{2}(1+\tan^2\theta) + g\left(1-2(V_S/V_P)^2\sin^2\theta\right)\right\} \times \left\{\frac{\Delta V_S}{V_S}\right\}\left\{4\left(\frac{V_S}{V_P}\right)^2\sin^2\theta\right\}$ $g$ is from Gardner's equation $\rho = aV_P^{\,g}$. | |
| | Solves for: | Assumptions and limitations: |
| | $\Delta V_P/V_P$, $\Delta V_S/V_S$ | Assumes density follows Gardner's equation. Fluid factor $\Delta F$ based on velocity. Less than critical angle. Makes no assumption about $V_P/V_S$. |
| Fatti et al. (1994) | $R(\theta) = \frac{1}{2}\left(\frac{\Delta I_P}{I_P}\right)(1+\tan^2\theta) - 4\left(\frac{V_S}{V_P}\right)^2\left(\frac{\Delta I_S}{I_S}\right)\sin^2\theta$, 3rd term truncated | |
| | Solves for: | Assumptions and limitations: |
| | $R_P$, $R_S$ | For angles < 50°. Requires no assumptions about $V_P/V_S$ and density. Fluid factor $\Delta F$ based on impedance. |
| Gray et al. (1999) | $R(\theta) = \frac{1}{2}\left(\frac{\Delta\lambda}{\lambda}\right)\left(1-\left(\frac{V_S}{V_P}\right)^2\right)\sec^2\theta - \left(\frac{\Delta\mu}{\mu}\right)\left(\frac{V_S}{V_P}\right)^2\left(\frac{1}{2}\sec^2\theta - 2\sin^2\theta\right) + \frac{1}{2}\left(\frac{\Delta\rho}{\rho}\right)\left(1-\frac{1}{2}\sec^2\theta\right)$ | |
| | Solves for: | Assumptions and limitations: |
| | $\Delta\lambda/\lambda$, $\Delta\mu/\mu$ | Makes no assumptions about $V_P/V_S$ and density. For angles < 60°. |

### 3.3.3 AVO classification of reservoir sands

Rutherford and William (1989) classify reservoir gas sands on the basis of AVO characteristics and impedance contrast. This classification was based on the magnitude and sign of the reflection coefficient ($R_o$) of the sand top. It was observed that cape rock (shale) has the high Poisson's ratio value as compared to gas sands, with the increase in offset the negative reflection coefficient increased. They classify gas sands into three AVO classes.

Castagna and Swan (1997) proposed graphical representation of AVO classes by plotting normal incident reflectivity against a measure of the offset dependent reflectivity. They called this representation as AVO intercept and AVO gradient (Fig.3.10). AVO class 4 was also introduced which was a part of Rutherford and William's AVO class 3 (Young and LoPiccolo 2003)

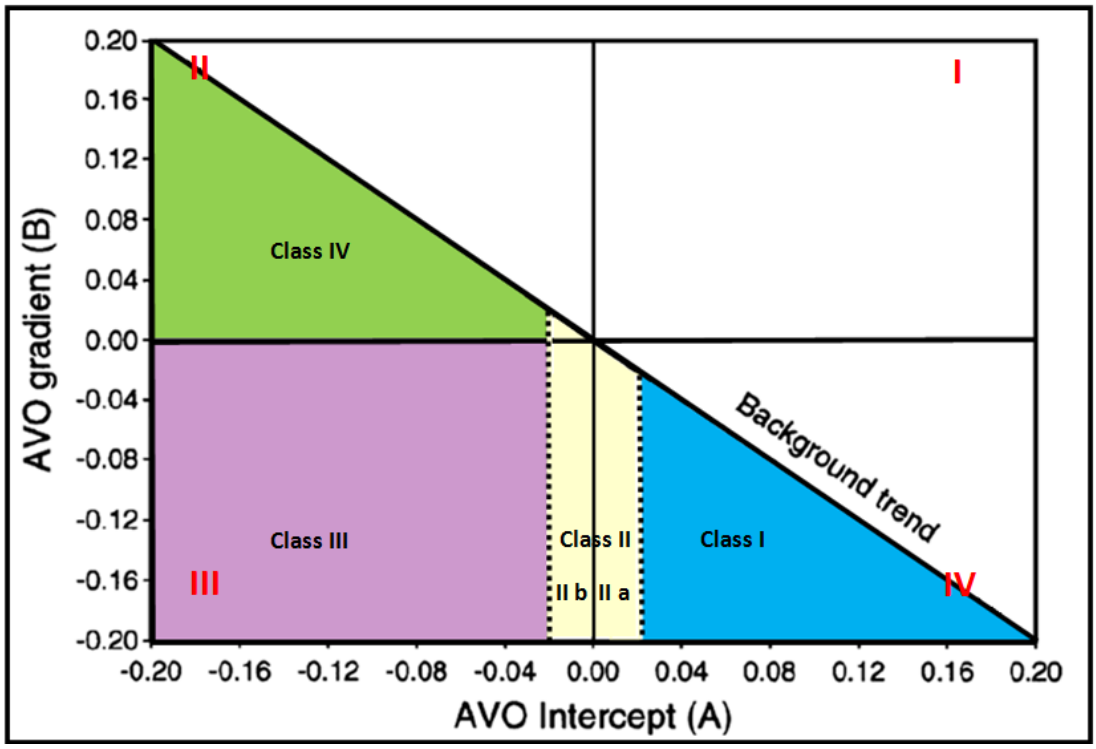


**Figure 3.10**: Four classes of gas sands shown in AVO intercept versus AVO gradient cross-plot (Modified from Castagna et al.1997).

**Class I: high impedance sand**

High impedance sand has a positive reflection coefficient at zero offset and the magnitude decreases initially with offset. The class I sand shows higher magnitude as compared to the class II and class III (Rutherford and William 1989). At the availability of suitable angle/offset polarity also changes.

**Class II: near-zero impedance contrast sands**

The class II sand compared to overlying shale bed holds low impedance contrast. It shows small offset/angle reflectivity which is close to zero and presence of noise makes it undetectable at times. A polarity change occurs when the reflectivity is positive but it is hard

to detect because the noise level is higher than the signal (Rutherford and William 1989). Class II sands are found in both offshore and onshore environments.

**Class III and Class IV: low impedance sand**

Like the class II sands, class III and class IV also have low impedance contract as compared to overlying shale units. These are usually unconsolidated sands and have negative zero-offset/angle reflectivity. Both class III and Class IV sands are found in marine environment. Class III shows increasing reflectivity with offset whereas class IV shows decreasing reflectivity with offset (Fig.3.11) (Castagna et al. 1997).

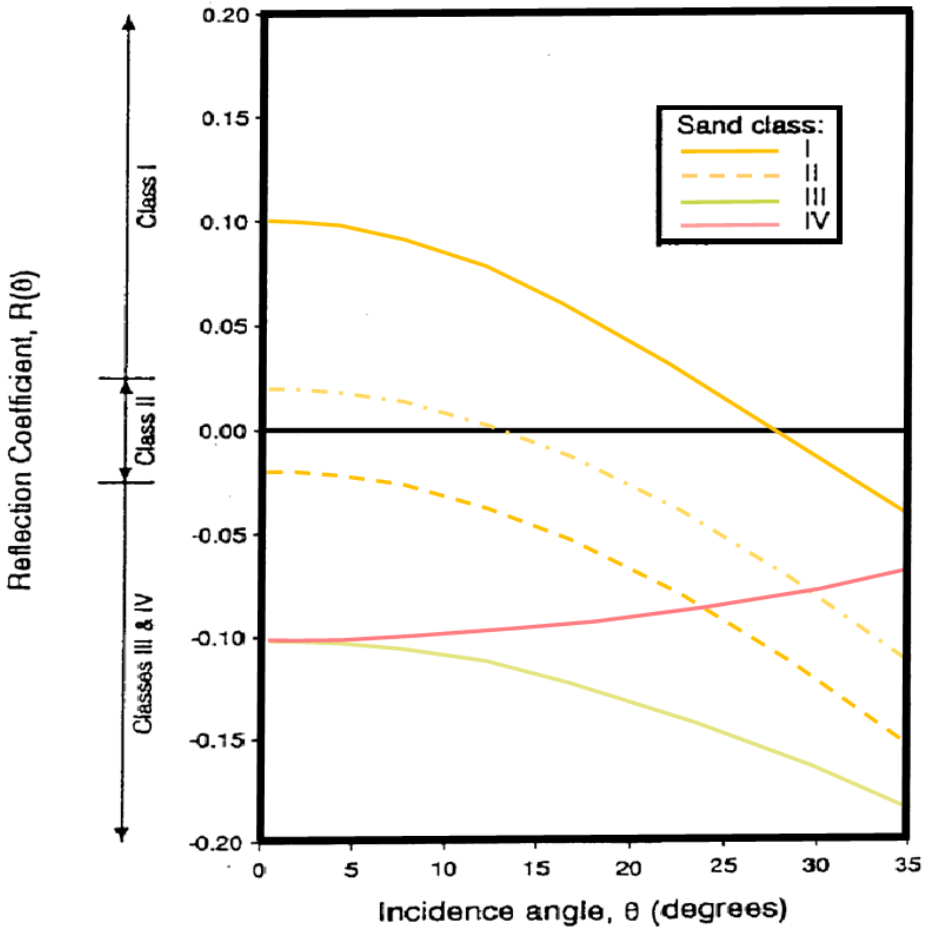


**Figure 3.11** Intercept gradient cross-plot of different AVO sand classes (Castagna et al. 1997).

# Chapter 4: Petrophysical analyses of reservoir rocks

## 4.1 Petrophysical analyses

One of the main steps in the evaluation of subsurface formations is the petrophysical analysis. In this analysis, useful information (as obtained from wireline logs, core data and mud logging data) are used to analyze the chemical and physical properties of the formation, penetrated by the wells. This investigation is mainly focused on (1) the mineral composition of the formations, (2) pore spaces and (3) the fluids (gas, oil and water) entrapped between the pores. In the second phase, the formation containing hydrocarbon is differentiated. Ultimately, all these data are combined to estimate the presence of hydrocarbons in the area, which then used to formulate reservoir management policies (Glover, 2005). In this chapter, the results of the petrophysical analysis will be discussed based on the interpretations of the geophysical well logs.

### 4.1.1 Net-to-Gross ratio

The main silisiclastic reservoir rocks in the Loppa High area are present in the Knurr Formation and Stø Formation (see section 2.3.5 and 2.36 for their lithology and depositional environment). Also, the Snadd Formation is regarded as a reservoir potential and thus includes in the analysis of reservoir properties. All three formations are classified as heterogeneous sandstones with fair amounts of clay contents. Therefore, the volume of shale and/or clay will be the basic parameters used to characterize shaly sandstones. Since shale is usually more radioactive than sandstones and carbonates, the gamma ray log is used to calculate the volume of clay using Equations 3.1-3.3.

The estimated net-to-gross (N/G) ratios for the different formations are summarized in the Table 4.1. The clay volume was assumed to be greater than 0.25 and the cutoff was applied in the Net/Gross estimation. The ‘Net’ represents the clean reservoir sand and the ‘Gross’ stands for the total thickness of the reservoir. Since the upper part of the Knurr Formation (well 7120/1-2) is of claystone, the N/G ratio was only estimated for the lower part (1982-2135m TVD_KB).

**Knurr Formation**

The N/G of the Knurr Formation varies significantly from the wells 7120/1-2 to 7120/2-2. In the well 7120/1-2 the N/G is high (0.78) but in the well 7120/2-2 (dominated by claystone) the N/G value is very low (0.31). The maximum data points in the well 7120/1-2 are located below the sand line suggesting that the lower part of the Knurr Formation is comprised of sandstone (Fig.4.1a). In the well 7120/2-2, the maximum data points are above the sand line but the shaly part confirms the shaly/clayey nature of this location in the Knurr Formation.

**Stø Formation**

In contrast to the Knurr Formation, the N/G from the two wells (7120/1-2 & 7120/2-2) in the Stø Formation are almost identical. The maximum data points are located below the sand line. The upper part of Stø Formation is shaly sandstone, the amount of shaly sandstone decreases from the western well 7120/1-2 to the eastern well 7120/2-2. Figures 4.1 (C) and

(D) show the comparison of these two wells. There are almost negligible data points found above the sand line in the well 7120/2-2.

**Table 4.1:** Net-to-gross calculated of five studied wells for possible reservoir sands.

| Formations | Wells | Gross | Net | Net/Gross |
|---|---|---|---|---|
| **Knurr Fm.** | 7120/1-2 | 157.90 | 123 | 0.783 |
| | 7120/2-2 | 382.20 | 117.04 | 0.306 |
| **Stø Fm.** | 7120/1-2 | 153.30 | 135.73 | 0.885 |
| | 7120/2-2 | 100.30 | 86.43 | 0.862 |
| **Nordmela Fm.** | 7120/1-2 | 87.20 | 21.55 | 0.247 |
| **Tubåen Fm.** | 7120/1-2 | 54.00 | 6.45 | 0.117 |
| **Fruholmen Fm.** | 7120/1-1 | 413.00 | 196.66 | 0.322 |
| | 7120/1-2 | 124.00 | 53.00 | 0.428 |
| **Snadd Fm.** | 7121/1-1 | 1412.00 | 454.50 | 0.322 |
| | 7120/2-1 | 1321.00 | 26656 | 0.202 |
| | 7120/1-1 | 1179.00 | 546.14 | 0.463 |

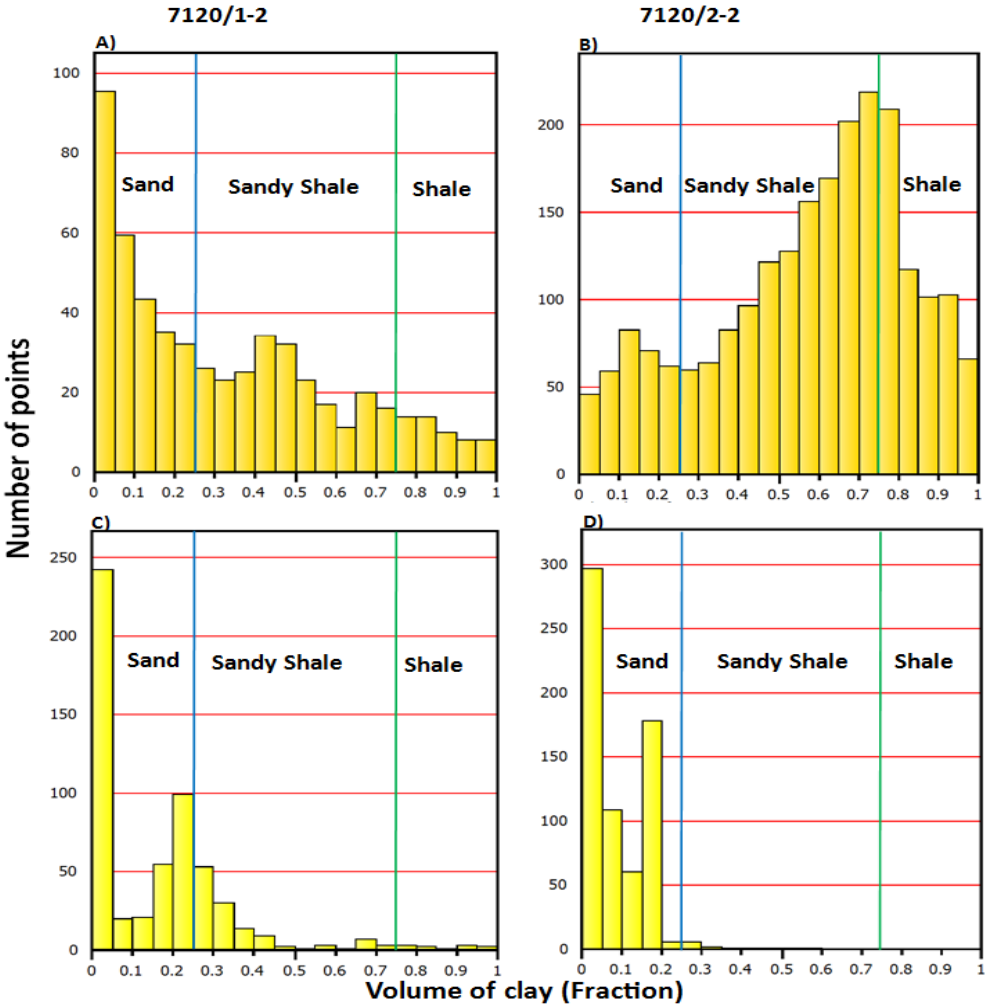


**Figure 4.1:** Histogram of clay volume for Knurr Formation in (A) and (B) and Stø Formation in (C) and (D), sand line (BLUE) discriminating reservoir sand from shale.

**Snadd Formation**

The net-to-gross for the Snadd Formation is calculated for the wells 7120/2-1, 7120/1-1 and 7121/1-1. Majority of dataset is falling in sandy shale and shale zone as shown in Figure 4.2 (B). Table 4.1 shows the net-to-gross values calculated for these wells, the highest values among these three wells is 0.46 for the well 7121/1-1. The highest points are falling in shale zone in the wells 7120/2-1 and 7121/1-1 whereas the highest number of points is falling in sandy shale zone.

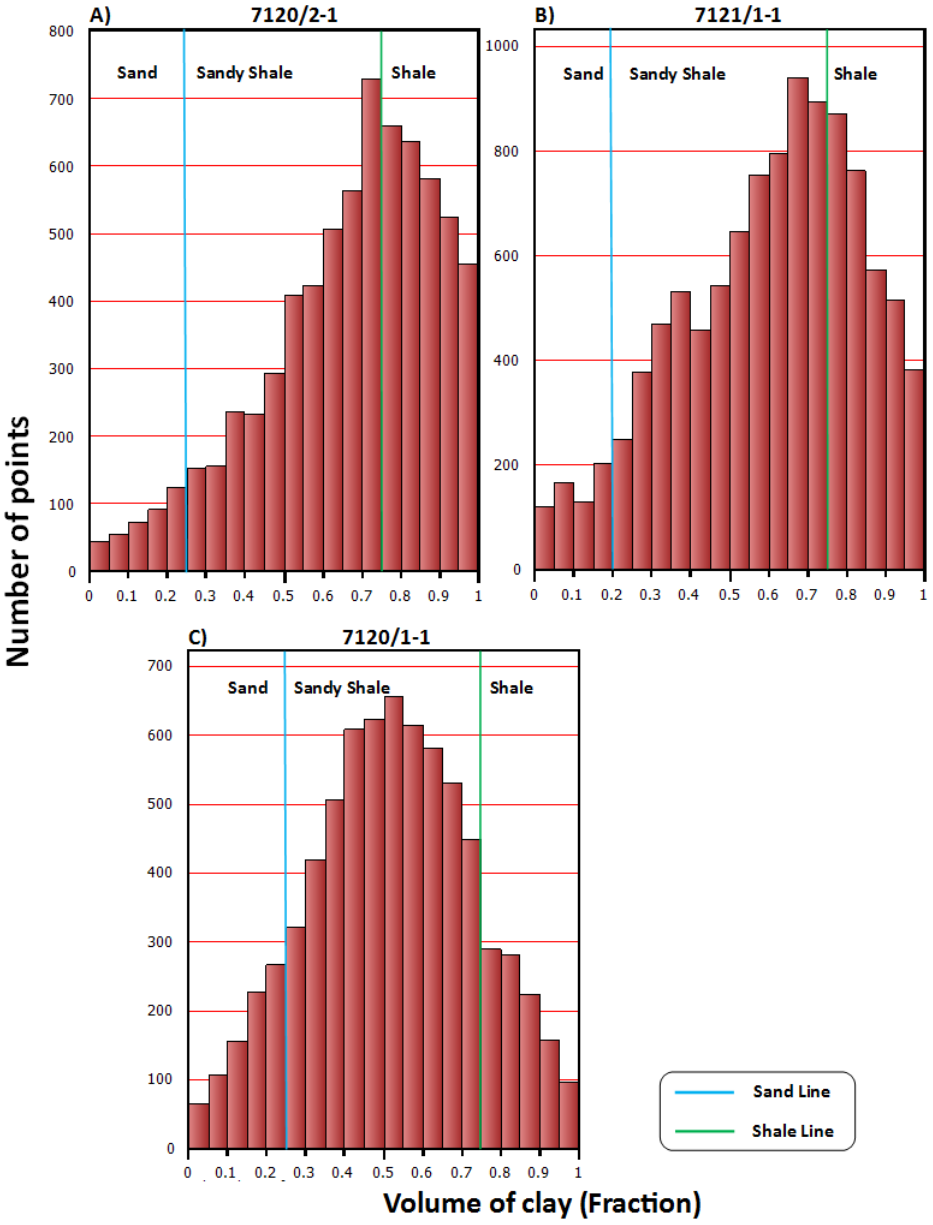


**Figure 4.2:** The histogram representation of clay volume of the Snadd Formation.

## 4.1.2 Porosity estimation

Porosity is defined as the ratio of the volume of the empty space available between the solid grains of the rock to the total volume of the rock. The space covers all the pores, fractures, inter and intra-granular spaces and vugs. Porosity is represented by the symbol Ø and it is

expressed by either percentage (0 to 100%) or by fraction (0 to 1). The fractional form is always used for calculations. The value of porosity for reservoir rocks varies from 0 to 40%. When the value of porosity increases from 40% the grain-to-grain contact diminishes and this value thus called as critical porosity. Grain shape, grain size and grain orientation are the initial microstructural parameters affects the porosity whereas cementation is the secondary factor which reduces the porosity (Glover 2005).

For higher accuracy in porosity estimation core data is required. Since no core data is available an approach to determine the porosity for the reservoir section is calculated by well log data explained in detail in section 3.1.2. The three main logs for porosity estimation are neutron, density and sonic. Neutron logs measures the concentration of hydrogen in a formation, in water filled shale free formation it gives the porosity of formation occupied by water. Neutron log underestimates the value of porosity in gas filled reservoir as gas contains lower concentration of hydrogen ions than oil and water. Density log is the electron density of a rock unit. This density is related to the bulk density of the formation given in $g/cm^3$. The sonic log is the interval transit time of P-waves through a rock unit. This measurement is in µs/m or µs/ft and related to the porosity of the formation (Asquith and Krygowski 2004).

Due to the limitation of well logs, which does not fit well to all situations in the bore hole, there is a common industrial practice to make crossover between neutron and density logs. This gives reliable values of porosity and is also good for detecting gas zones and discriminating lithology. The average porosity was calculated by equation 3.5. Neutron-density combination is drawn for the reservoir section in the wells 7120/1-2 and 7120/2-2 (Fig. 4.3). The porosity curves of neutron, density and average porosity depicts good resemblance in the sandy portion but not for the shaly part where the peaks are not identical. The matrix density for porosity calculation is 2.65 $g/cm^3$ which show strong correlation with the sandy part but lower correlation with the shaly section. The average porosity calculated from neutron and density logs is given in table 4.2.

**Table 4.2:** The average porosity calculated for reservoir sections.

| Formation | Well name | Neutron-Density (Avg.) |
|---|---|---|
| **Knurr Fm.** | 7120/1-2 | 17% |
| | 7120/2-2 | 13% |
| **Stø Fm.** | 7120/1-2 | 16% |
| | 7120/2-2 | 10% |
| **Nordmela Fm.** | 7120/1-2 | 12% |
| **Tubåen Fm.** | 7120/1-2 | 11% |
| **Fruholmen Fm.** | 7120/1-2 | 12% |
| **Snadd Fm.** | 7120/1-1 | 11% |
| | 7120/2-1 | 12% |
| | 7121/1-1 | 14% |

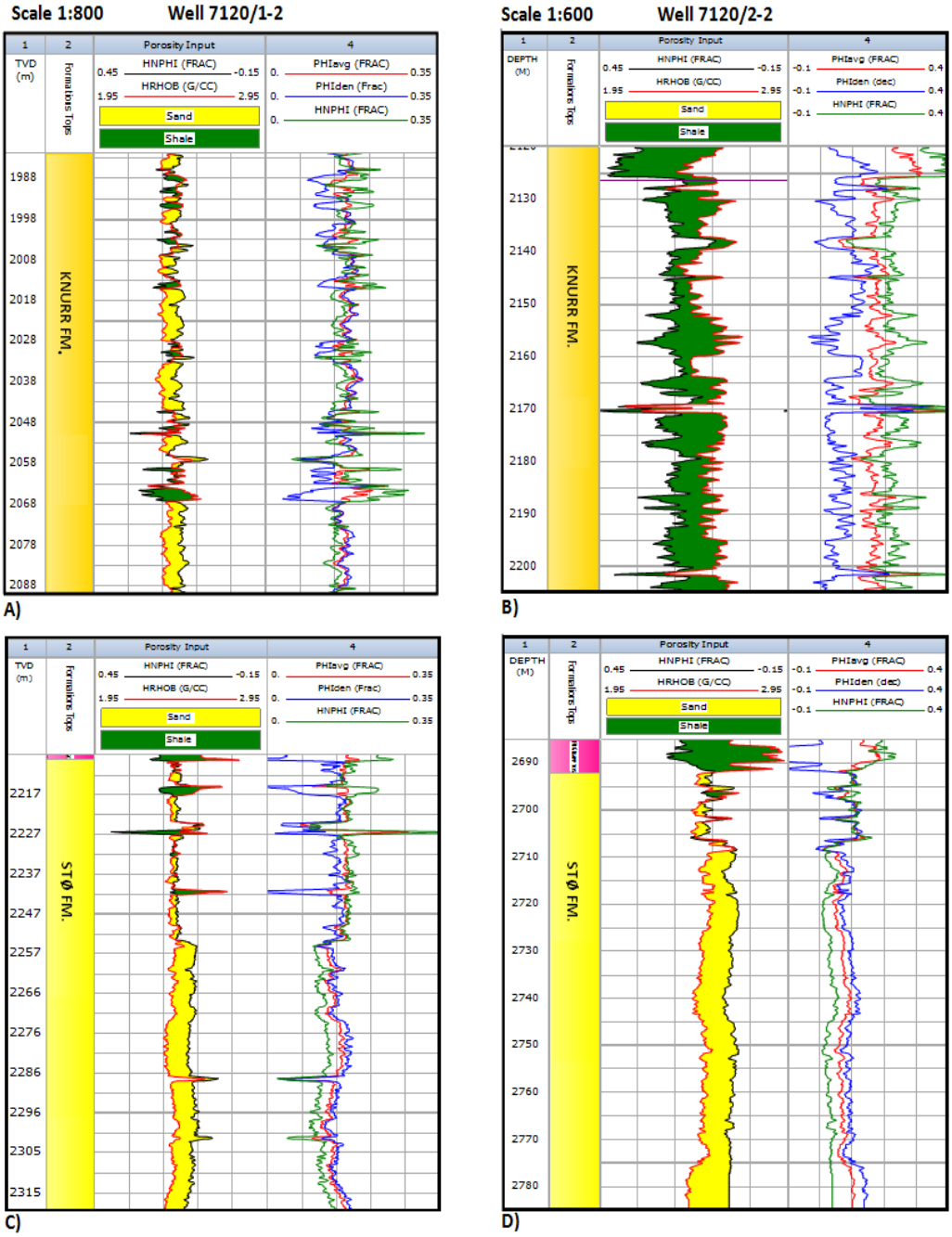


**Figure 4.3:** Neutron porosity, density porosity and average porosity curves are shown with neutron density crossover for the Knurr Formation in (A) and (B) and the Stø Formation in C and D for the wells 7120/1-2 and 7120/2-2 respectively.

The density and neutron porosities are then used to make cross-plot for the discrimination of sandy and shaly parts in a reservoir. The cross-plot between neutron porosity and density porosity is drawn for reservoir and source rocks of the well 7120/1-2. Figure 4.4 shows clear lithology discrimination between clean sand, sandy shale and shale. The upper part of Knurr Formation is claystone which is shown by data points towards the shale line and the clean sandy reservoir part is shown by data points by the clean sand line (Fig. 4.4). The Fuglen Formation and the Hekkingen Formation are shales with most of the data points located around the shale line.

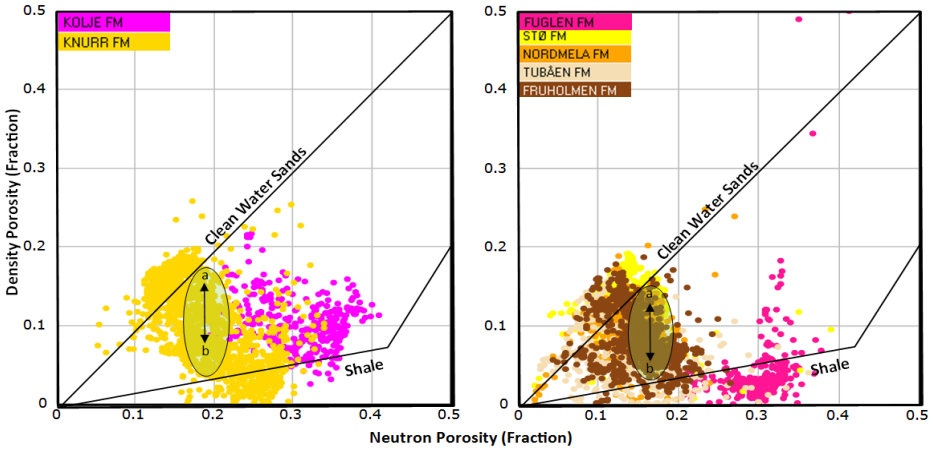


**Figure 4.4:** Cross-plot of density-porosity and neutron-porosity for the well 7120/1-2 is a good lithology discriminator, point 'a' shows clean sands and point 'b' for shales, between these two points is the area for shaly sand and sandy shale.

### Knurr Formation

The relationship between neutron-porosity and density-porosity for the Knurr Formation in the well 7120/1-2 shows higher concentration of dataset around clean water sand line (Fig. 4.5 A). The same cross-plot for the Knurr Formation in the well 7120/2-2 shows high concentration of data points in between water sand and shale line (Fig. 4.5 B). There are very few data points above clean water sand line represents higher shale contents in this well.

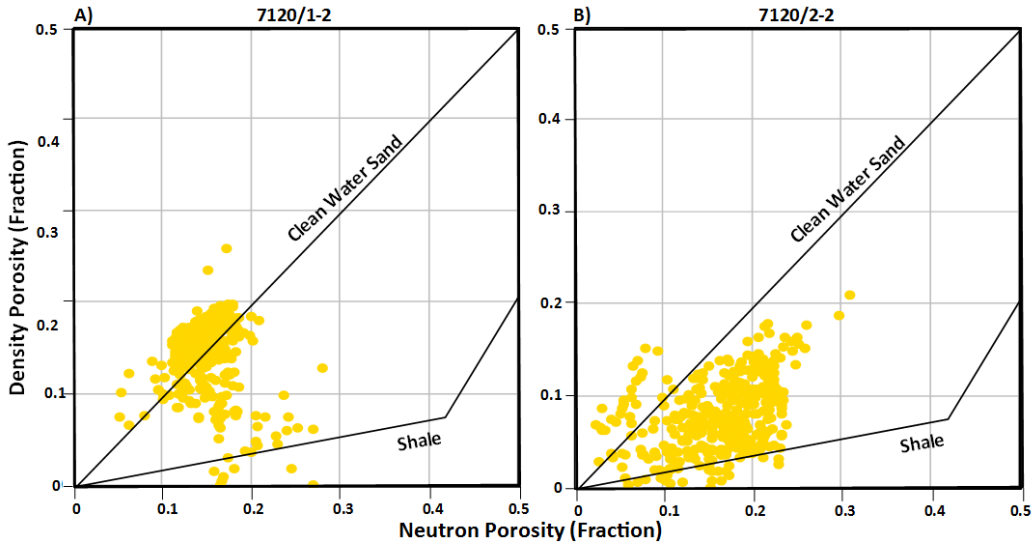


**Figure 4.5:** Neutron-porosity and density-porosity cross-plots of the Knurr Formation in the two wells.

### Stø Formation

The neutron density cross-plot for the wells 7120/1-2 and 7120/2-2 confirms that the Stø Formation is clean sandstone (Fig. 4.6). The average porosity value for the Stø Formation in well 7120/1-2 is around 16-18%. The porosity value for the Stø Formation in the well 7120/2-2 is quite low (8-12%) as compared to the well 7120/2-1.

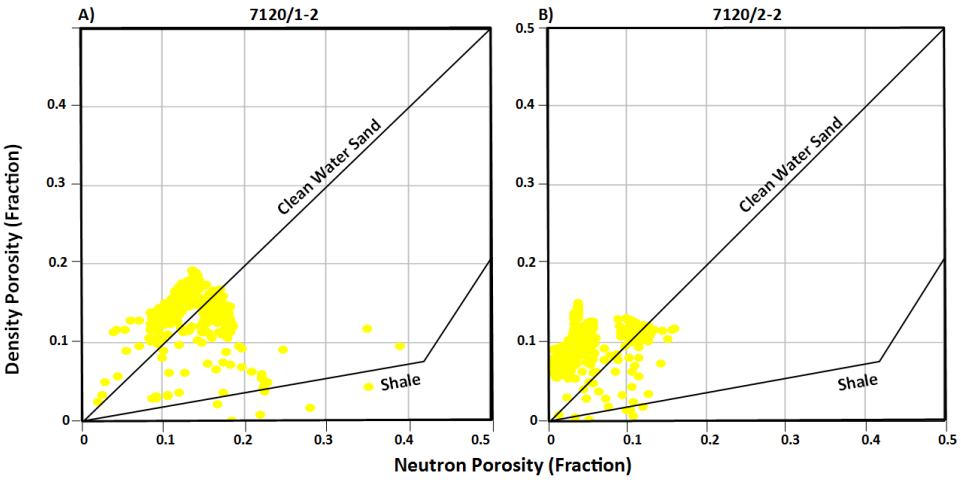


**Figure 4.6:** Neutron-porosity and density-porosity cross-plots of the Stø Formation.

### Snadd Formation

The neutron porosity and density porosity cross-plot showed quite different results from the Knurr and Stø Formation. The majority of data points (as expected from net-to-gross calculation) are falling in sandy-shale and shaly-sand domain (Fig. 4.7). Few data points from the well 7121/1 and 7120/2-1 are situating closer to the clean water sand line whereas the well 7120/1-1 which is located at the most south-western vicinity of the Loppa High probably has no clean water sand within this formation (Fig. 4.7 C).

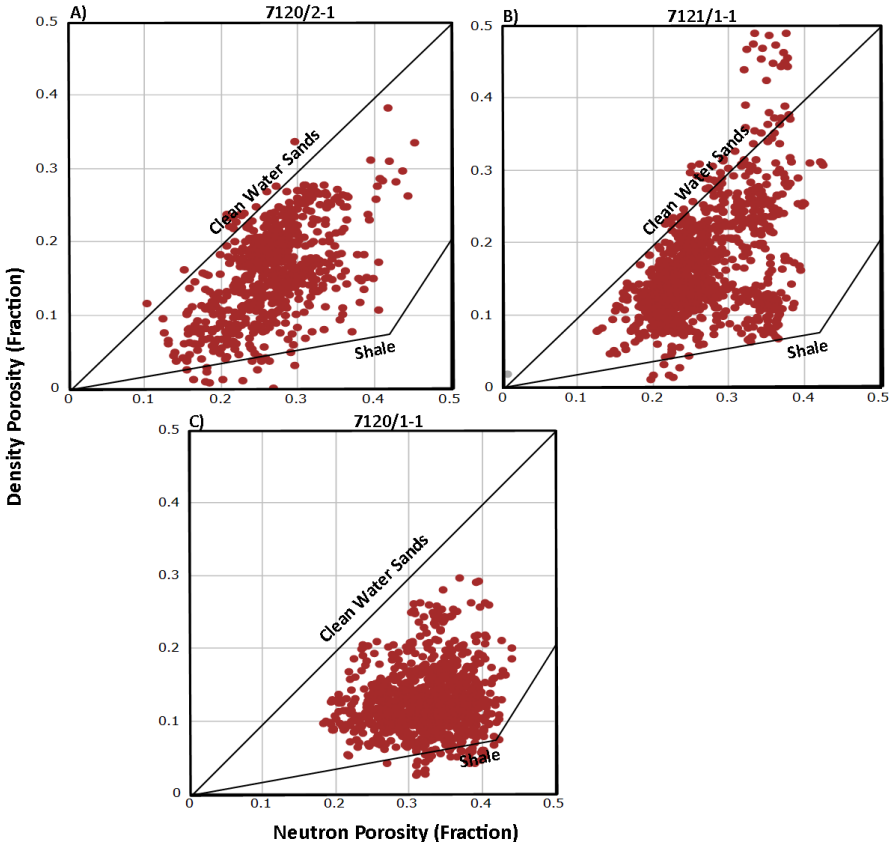


**Figure 4.7:** Neutron-porosity versus density-porosity cross-plot of the Snadd Formation for the well 7120/2-1, 7121/1-1 and 7120/1-1.

### 4.1.3 Calculation of hydrocarbon saturation

Fluids saturation in rocks can be measures by knowing their electrical resistivity, which is the resistance to flow of electrical charge through saturated rocks. It can be measured from resistivity logs and its unit is ohm-m. In sedimentary rocks, the value of resistivity varies from 0.2 to 2000 ohm-m. The value of resistivity depends on the effective porosity, salinity of formation water, the hydrocarbon contents in the pore space and temperature of the formation. With the increase in temperature and hydrocarbon contents resistivity increases whereas the increase in porosity shows an inverse relation to the resistivity (Djebbar & Donaldson 2004). For saturation calculation deep resistivity log ($R_t$) has been used as it gives the true resistivity value of the fluids in the un-invaded zone.

**The Pickett Plot**

Saturation of water for the reservoir sections (Knurr and Stø Formations) has been calculated for the wells 7120/1-2 and 7120/2-2 using Archie's equation. Before applying Archie's equation geothermal gradient for the well is required and is calculated by Equation 3.13. The geothermal gradient for five wells is calculated and given in the Table 4.3.

**Table 4.3** The geothermal gradient of all 5 wells in the study area.

| Well Name | Total Depth | Oldest Unit Penetrated | Bottom Hole Temperature ($^oC$) | Geothermal Gradient ($^oC$/Km) |
|---|---|---|---|---|
| **7120/2-1** | 3484 (TVD) | Basement | 97 | 26.7 |
| **7121/1-1R** | 5000 (MD) | Ørn Fm | 146 | 28.4 |
| **7120/1-1R2** | 3978 (TVD) | Basement | 125 | 30.41 |
| **7120/1-2** | 2613 (TVD) | Fruholmen Fm. | 77 | 27.93 |
| **7120/2-2** | 2794 (MD) | Stø Fm. | 87 | 29.70 |

The Picket plot is generated for water saturated portion (2325-2350m) of well 7120/1-2 (Fig. 4.8) assuming value of "a" equal to 0.81, n and m equal to 2 which are the values for consolidated sandstone. The value of $R_w$ from the water line is 0.0288 ohm-m.

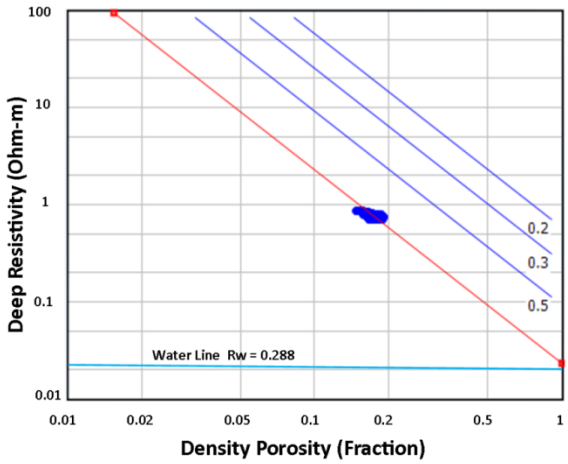


**Figure 4.8:** Pickett plot between porosity and resistivity of the Stø Formation water saturated part (well 7120/1-2) showing the value of Rw from water line.

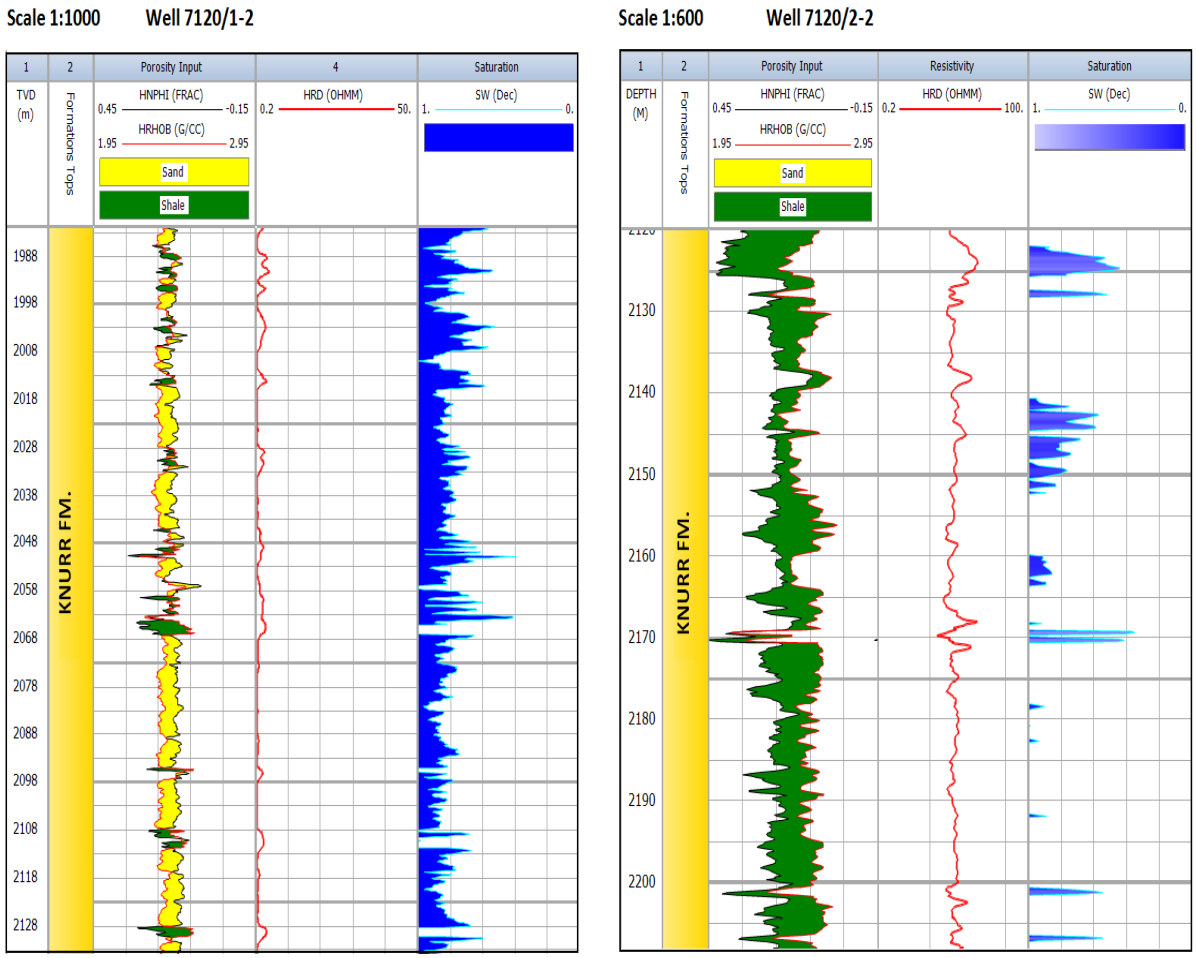


**Figure 4.9:** Hydrocarbon saturation of the Knurr Formation in wells 7120/1-2 and 7120/2-2.

### Knurr Formation

The water saturation of the Knurr Formation for wells 7120/1-2 and 7120/2-2 is calculated using Archie equation show in Figure 4.9 with their respective deep resistivity curve. Well 7120/1-2 holds about 70-75% water saturation and 25-30% hydrocarbon saturation in the lower clastic part of the Knurr Formation (1982m to 2135m TVD-KB). The Knurr Formation in well 7120/2-2 is about 100% water saturated with minor oil shows represented by sharp resistivity peaks.

### Stø Formation

The water saturation in the well 7120/1-2 is about 65-70% and the oil saturation is shown in track 5 of the Figure 4.10. The Stø Formation in the well 7120/2-2 is fully water saturated with minor shows of hydrocarbons. Figure 4.10 represents the water saturation calculated for the wells 7120/1-2 and 7120/2-2.

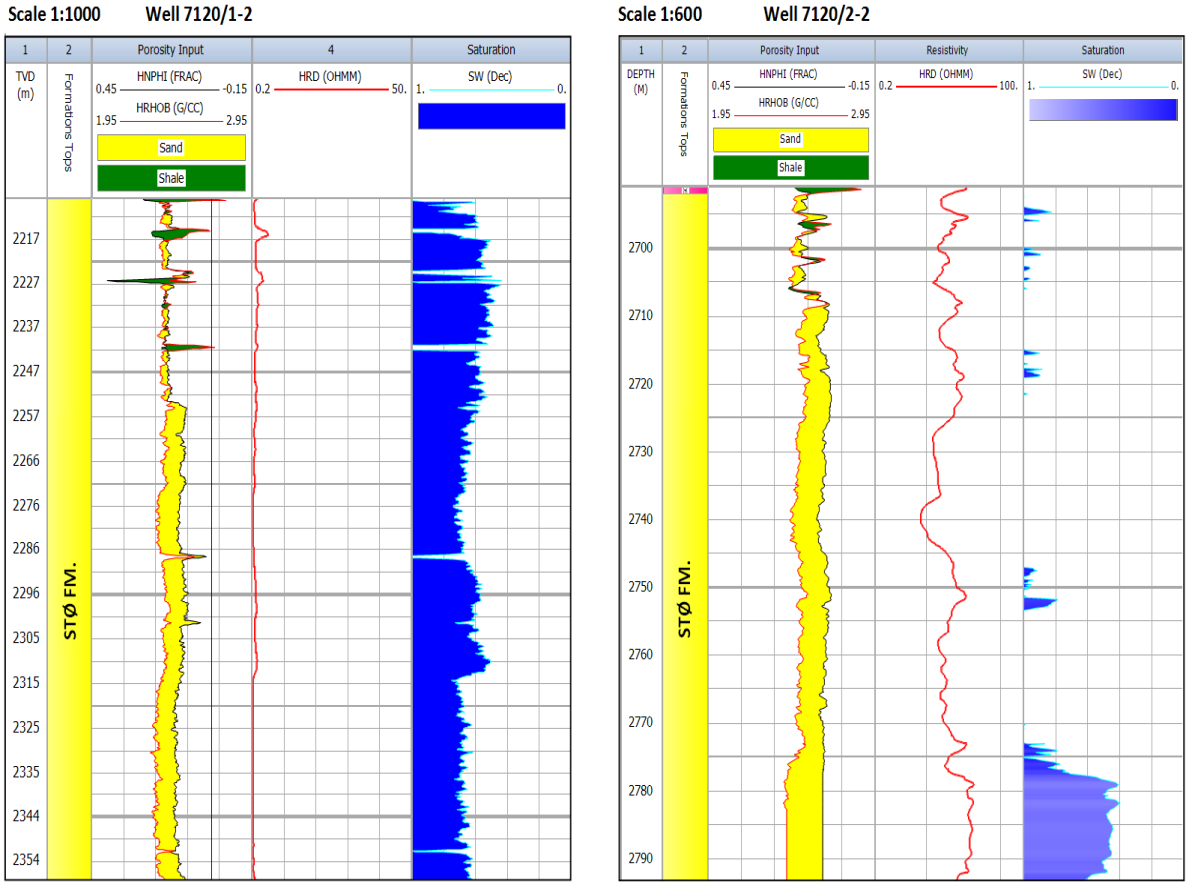


**Figure 4.10:** Hydrocarbon saturation of the Stø Formation for the wells 7120/1-2 and 7120/2-2.

### Snadd Formation

The hydrocarbon saturation has been calculated for all three wells penetrating the Snadd Formation. The well 7120/1-1 is basically water saturated with 10 to 15% patchy saturation of hydrocarbons. There are thin patches shows about 40% hydrocarbon saturation. Hydrocarbon saturation found throughout the Snadd Formation in the well 7120/2-2 from 612 to 1933 m TVD_KB. Similarly well 7121/1-1 also shows good saturation of hydrocarbons at different intervals.

## 4.2 Discussion

In this chapter, a detailed petrophysical analysis is presented for the Knurr and Stø Formations penetrated by the wells 7120/1-2 and 7120/2-2 and the Snadd Formation penetrated by well 7120/1-1, 7120/2-1 and 7121/1-1. There are significant differences between the reservoir properties of the Knurr and the Stø Formations and also even within the formation from one well to the other. The reservoir properties of the Snadd Formation varies from the eastern well 7121/1-1 to the western well 7120/1-1.

### Knurr Formation

The lower part of the Knurr Formation in the well 7120/1-2 possesses high N/G (0.78). The 154 m thick bed of the Knurr Formation belonging to the clastic wedge, possesses low shale

contents in the well 7120/1-2. The well 7120/2-2 which is on the eastern side to the well 7120 /1-2 possesses very low (0.36) N/G. The burial depth of the Knurr Formation in the eastern well is high and is located relatively far from the fault block. So the wedge deposited in the eastern side carried a relatively low amount of sands. Similarly the porosity in lower part of the Knurr Formation in the well 7120/1-2 is 17% but the porosity in the well 7120/2-2 is about 13%. The porosities in both wells are fair to good for hydrocarbon production. The main effect which deteriorates the reservoir quality is the shale contents or low N/G. Despite of the fact that there is a fair porosity value in the well 7120/2-2 the connectivity of pores is very low due to high clay content in the pores which reduces the permeability. But in the well 7120/1-2, the porosity is higher than the well 7120/2-2 with low shale contents proves the good reservoir quality in the well 7120/1-2. This finding proves the existing literature; according to Knutsen et al. (2010) the L. Cretaceous wedge play (lower part of the Knurr Fm.) holds very good reservoir quality in the well 7120/1-2 but the same play holds very poor reservoir quality in the well 7120/2-2.

**Stø Formation**

The Stø Formation in both wells has high N/G (avg. 0.88). The good porosity values (16-18%) and hydrocarbon saturation confirms the good reservoir quality of the Stø Formation in the well 7120/1-2. The porosity of the Stø Formation in well 7120/2-2 is 10%. Prior to uplift the present day depth and temperature of the Stø Formation in the well 7120/2-2 is much higher than the well 7120/1-2 which validates the presence of high quartz cementation in the well 7120/2-2. Selnes et al. (2004) stated that the N/G for the Stø Formation is over 0.8 and the porosity ranges from 18 to 20%. There is a good match between the calculated reservoir properties in this study and the published data for the well 7120/1-2. But at the same time the porosity value for the well 7120-2-2 is quite far from published results. Selnes et al. (2004) also stated that the presence of stylolitation and the effect of quartz cementation in Stø Formation, which can reduce porosity. Although no core data studied for the Stø Formation but the huge variation in porosity from one well to the other depicts the presence of stylolitation/cementation. The present day burial temperature of the Stø Formation in the well 7120/2-2 is also above 80$^{o}$C which shows the Stø Formation is in chemical compaction domain. The detail effect of the quartz cementation can be seen in section 5.1.1.2.

**Snadd Formation**

As discussed by different authors that the dominant lithology of the Snadd Formation is shale and sandy shale with interlayers of siltstone and sandstones. The N/G calculation and neutron-density porosity cross-plot confirmed that major part of the Snadd Formation is shale. The well 7121/1-1 which is the north-eastern well in the study area holds relatively more sandy content than the western and south-western wells. Henriksen et al. (2011) stated that the reservoir section of the Snadd Formation was deposited during transgression. The well 7120/1-1 is located on the hanging wall which can be the reason behind its more shaly nature. Because during sea level changes the hanging wall remained relatively deeper than the foot wall (Fig. 4.11). The storm derived silt and sand deposits (Dalland et al. 1988) seem to be not that effective in this part as compared to the footwall blocks.

The average porosity calculated for the Snadd Formation in the area is 12-14% with the highest value of porosity found in the well 7121/1-1. The values of porosity seem to be fair but the high shale contents (low N/G) put a question mark on the connectivity of pores which reduces the effective porosity. According to Henriksen et al. (20011) the Snadd

Formation possesses fine to medium sand and silt deposited which are gone through high temperature and diagenesis. This also depicts the digenetic effect increases from east to west due to greater burial depth and higher temperature. The diagenesis also reduces the porosity and in the same pattern affects the reservoir quality.

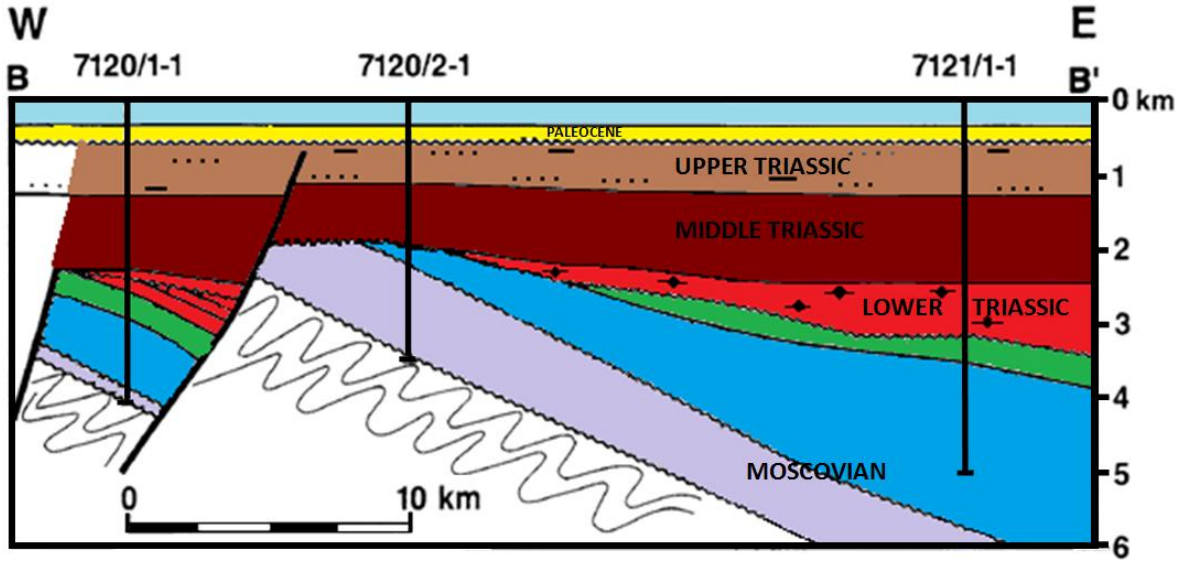


**Figure 4.11:** The E-W cross-section of the Loppa High, shows the variation in the thickness of source and reservoir rocks (modified from Stewart et al. 1995).

Figure 4.11 shows the thickness of the L. Triassic source rock which reduces from east to west. The supply of hydrocarbon is directly depended on the presence, maturity and thickness of the source rock. Since the thickness of the source rock in the eastern well 7121/1-1 is high, probably it has higher supply from the source and ultimately has the higher saturation of hydrocarbons than the western wells.

# Chapter 5: Rock physics diagnostics

Rock physics emerged as a key tool for reservoir geophysics and plays an important role in quantitative seismic interpretation. It bridges the seismic properties (i.e. bulk density, P-wave/S-wave velocity ratio "Vp/Vs", acoustic impedance and elastic moduli) with reservoir geology constraints (i.e. porosity, lithology, sorting, saturation, clay contents). By knowing porosity and elastic wave velocity we can diagnose rock texture of sandstones and shales. The velocity-porosity data used and plotted on theoretical cemented rock trends, which tells us whether the rock is cemented or not. Hence, the rock physics analysis reduces the risk in lithology prediction and helps to predict the microstructures in heterogeneous reservoirs (Avseth et al. 2010; Polyaeva et al. 2011).

## 5.1 Rock Physics Templates

The upper and lower boundaries of any rock formation can be best inferred with the help of seismic velocities by knowing the mineralogical composition, porosity and elastic moduli of the mineral components. For detail seismic interpretation geometrical arrangement of the mineral components in the rock is required. Dvorkin and Nur (1996) used rock physics diagnostics to interpret the microstructures in rocks for the first time by using velocity and porosity relationship. The rock physics templates are the best combinations of petrophysical and geophysical information with which geological information can be extracted from seismic and well log data (Avseth et al, 2005). Different cross-plots are generated to construct the rock physics templates (RPTs) i.e. velocity verses porosity, AI verses Vp/Vs, AI verses EI and $\lambda\rho$ versus $\mu\rho$. With the help of these cross-plots valuable information can be extracted that helps to predict lithology and pore fluid type and their saturation (Avseth et al, 2005). The study area is carrying heterogeneous reservoirs of L. Cretaceous (Knurr Fm), M. Jurassic (Kapp Toscana Gp) and M. Triassic (Snadd Fm) age. In the following section, the detailed analysis of these reservoir rocks will be carried out using different rock physics templates (RPT's) to investiagte the lithology and fluid contents. As mentioned earlier, the shear wave (Vs) data is not available in any well so the Vs using here is calculated by Castagna et al. 1993.

### 5.1.1 Porosity versus velocity relationships

The most important rock physics models are drawn by predicting the relationship between velocity and porosity. Using velocity-porosity relationship, the lithology of different rocks and microstructures can be interpreted. Same approach is applied here for the studied wells to predict the lithology and microstructures of reservoir rocks.

#### 5.1.1.1 Han's model

Section 3.2.1.3 briefly describes the Han's (1986) model predicting the effect of clay content on Vp-porosity relationship. Han's model is applied to heterogeneous sandstones of the Knurr and Stø Formations for both wells 7120/1-2 and 7120/2-2 and their results are compared. Data points of 0-0.1, .10-0.2 and 0.2-0.3 clay bearing sandstones are plotted over Han's clay contours of 0.05, 0.15, 0.25 and 0.35 clay volumes fraction.

### Knurr Formation

Figure 5.1 shows the data points of the Knurr Formation from the wells 7120/1-2 and 7120/2-2. There is no significant difference among the data points of two wells. The data points of different values are scattered around the contours from clean sand line to dirty sand line (shaly sand). 0 to 10% clayey sand data points are found from cleanest to dirtiest sand line and same is the case for data points 10-20 and 20-30% clayey sandstones. The well 7120/2-2 has more shaly content than the well 7120/1-2, shown by higher density of data points below dirty sand line in the well 7120/2-2 (Fig. 5.1).

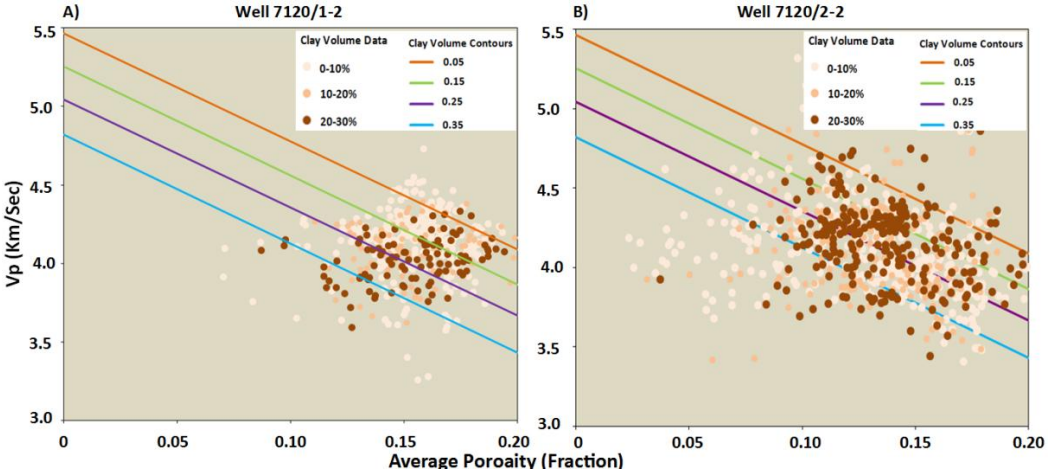


**Figure 5.1:** Han's model superimposed by data of the Knurr Formation from the wells 7120/1-2 and 7120/2-2.

### Stø Formation

The Stø Formation data points are plotted over Han's contours. In the well 7120/1-2 (Fig. 5.2 A) majority of data points of 0-10%, 10-20% and 20-30% clay volume are scattered between 0.05 to 0.25 (fraction) clay lines. The data points from the well 7120/2-2 (Fig. 5.2 B) are scattered between 0.05 to 0.35 (fraction) clay lines. Some of the data points are also observed below the dirty sand line.

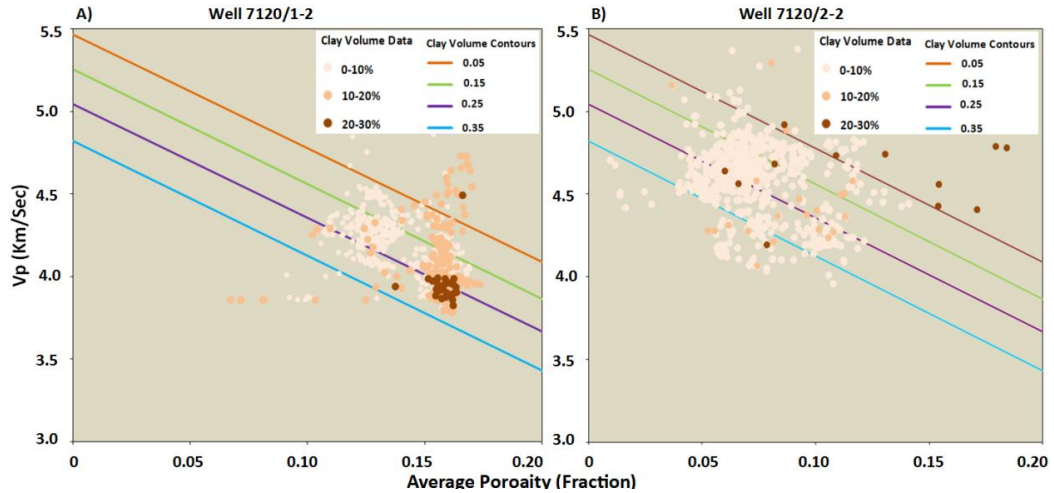


**Figure 5.2:** Han's model superimposed by data of the Stø Formation from the wells 7120/1-2 and 7120/2-2.

**Snadd Formation**

The thick deposit of the Snadd Formation is penetrated by wells 7120/1-1, 7120/1-2 and 7121/1-1, which basically consists of shale and siltstone with sandstone. The data points of variable clay contents are superimposed over Han's model (Fig. 5.3). There is a great spread of data in all wells and no synchronization among the data points and the Han's clay contours.

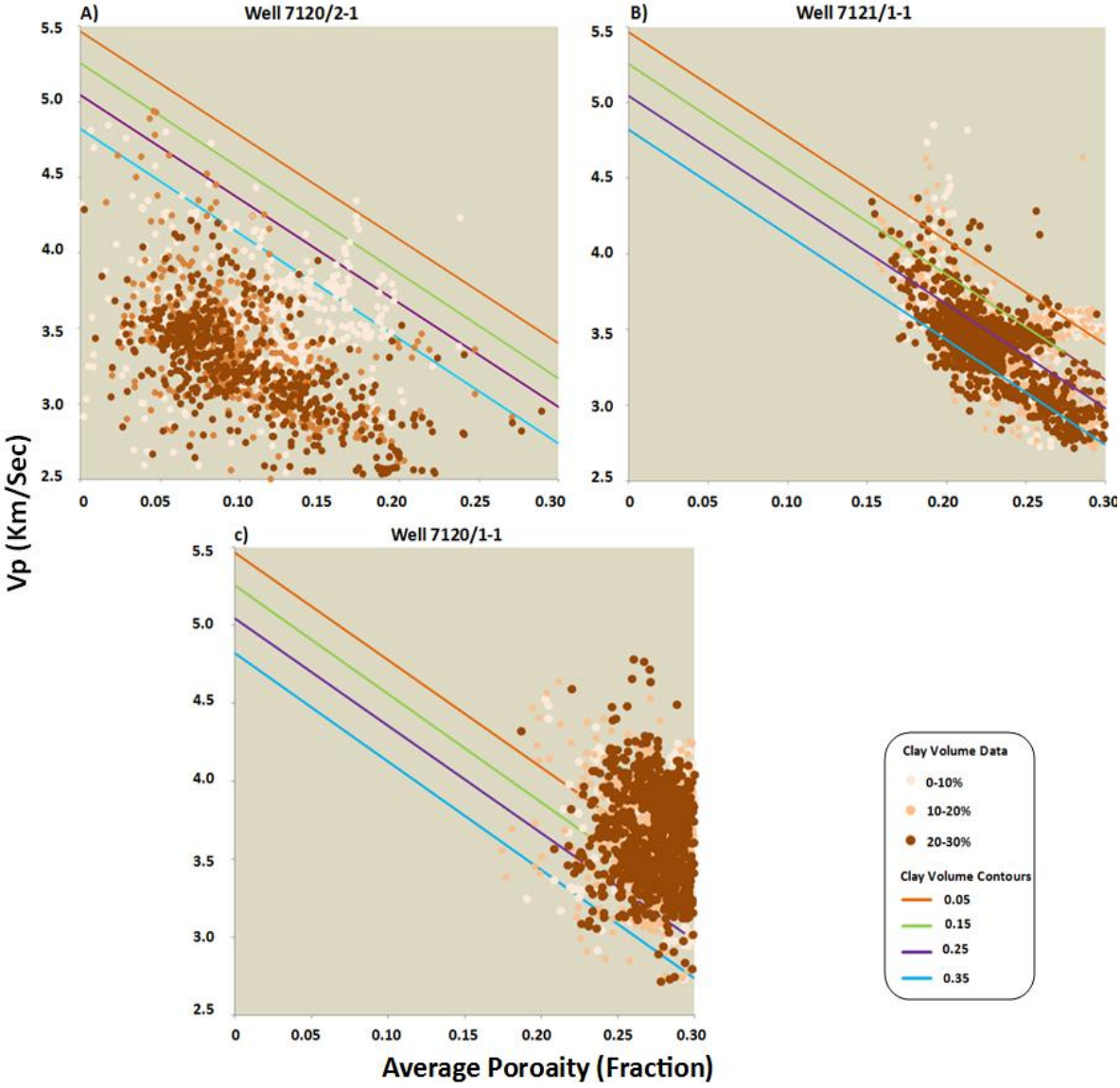


**Figure 5.3:** Han's model superimposed by data of the Snadd Formation from the wells 7120/1-1, 7120/2-1 and 7121/1-1.

### 5.1.1.2 Rock physics cement models

The relationship between seismic velocity and porosity can be used to predict the rock diagenesis, sorting and cementation. This can be done by assuming two end members; the first one is at zero porosity where the rocks must show the properties of its mineral constituents. The second end member is the critical porosity limit where the rocks loose

states of minimum grain-to-grain contact. Using these two end members, Hashin-Shtrikman (H-S) upper and lower bounds are constructed. Rock physics cement models are made on the basis of H-S upper and lower bounds. Three rock physics cement models are explained in detail in section 3.2.1.4. Cement models for Cretaceous Knurr Formation and Kapp Toscana group are calculated using well log data of the SW Loppa High area (Fig. 5.4). Cement models are digitized from Avseth et al. (2005) and cement volume for constant-cement model is taken as 2%.

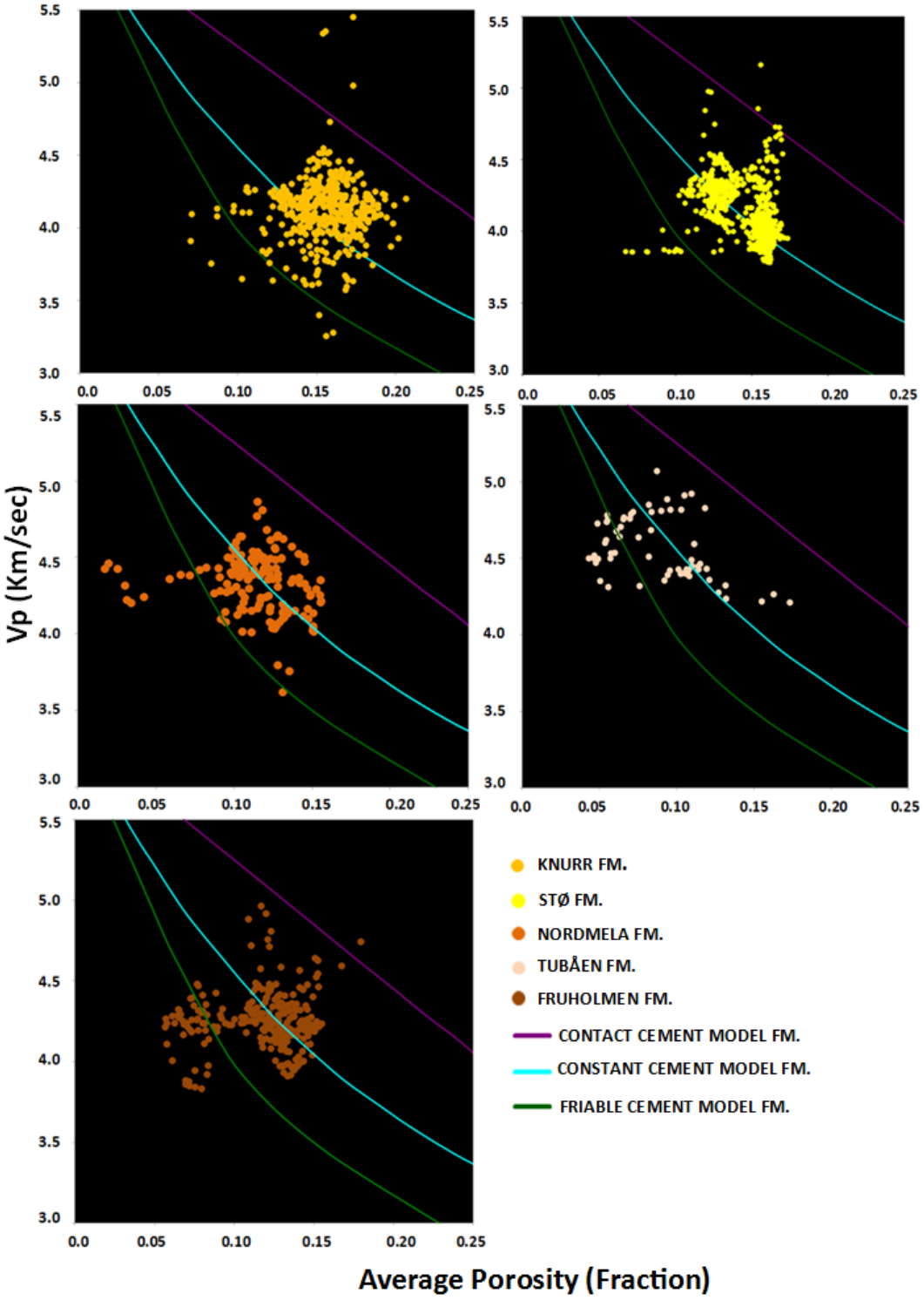


**Figure 5.4:** Reservoir rocks from the well 7120/1-2 plotted on rock physics cement models.

**Knurr Formation**

The data points from the Knurr Formation from the wells 7120/1-2 and 7120/2-2 are plotted over standard cement models shown in the Figure 5.5. The velocity ranges from 3.5 km/s to 4.5 km/s whereas the average porosity is 16%. The data points fall along constant-cement line show a nice sorting and cementing trend. Neglecting the uplift in the area, cementation in well 7120/2-1 is not justifiable with the present day temperature.

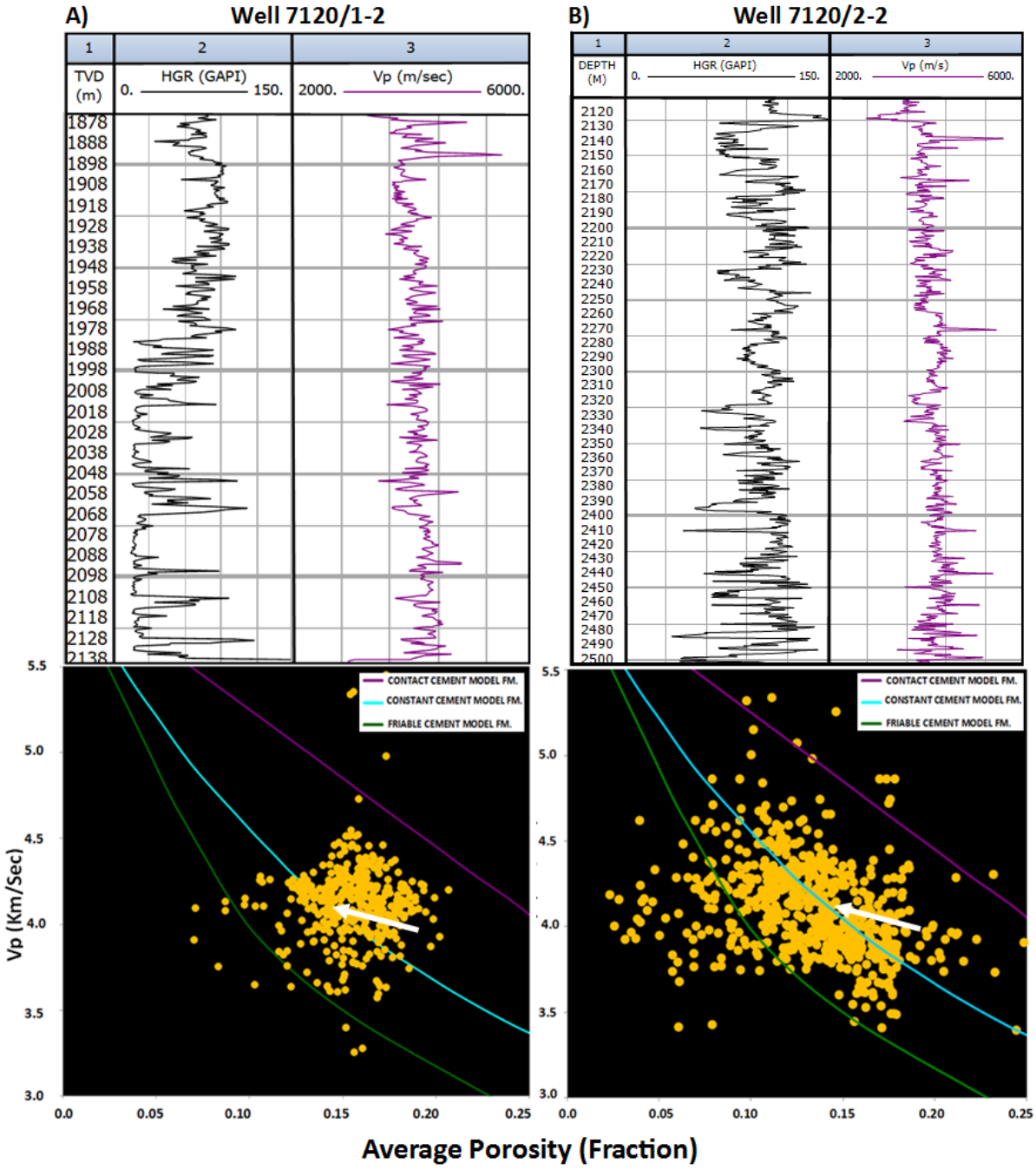


**Figure 5.5:** The Knurr Formation from the wells 7120/1-2 and 7120/2-2 superimposed on rock physics cement models, Vp and gamma logs of respective wells are also shown, white arrows are showing sorting trend.

Well 7120/2-2 has thick unit of about 380m claystones with very thin units of fine sandstones and siltstones shown by sharp peaks of low gamma ray values. The data points are scattered in a wide range of porosity from 0.07% to 20% and velocity ranging from 3.5 km/s to 4.5 km/s. In this well, the Knurr Formation is following both the friable and constant-cement models. The present day burial temperature of the formation is varying from 60-65$^{o}$C.

**Stø Formation**

The Stø Formation data from the wells 7120/1-2 and 7120/2-2 is superimposed on the rock physics cement model. Two distinct trends of the Stø Formation in both wells are observed can be seen in the Figure 5.6 shaded in blue and green colors.

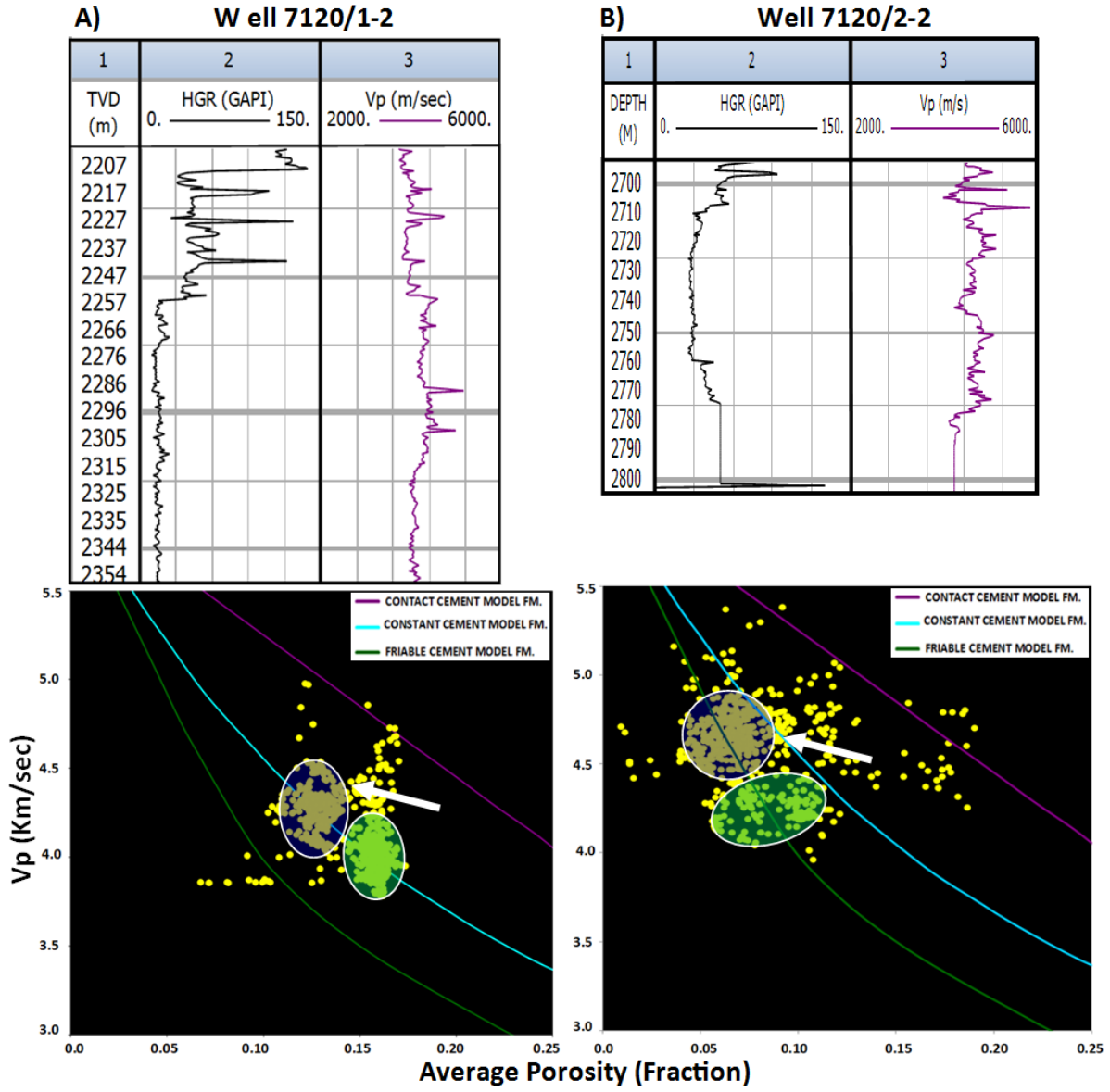


**Figure 5.6:** The Stø Formation from wells 7120/1-2 and 7120/2-2 plotted on cement models, Vp and gamma ray logs of respective wells are also shown, white arrows are showing the sorting trend.

The data points of the Stø Formation in the well 7120/1-2 are falling along the contact-cement line. The data can be separated into low porosity-high velocity and high porosity-low velocity members. The green shaded area in the Figure 5.6A shows porosity averaging 17% and velocity ranging from 3.7 to 4.2 km/s. This is the area belonging to high gamma ray values. These data points are from relatively shallower part as compared to the data points shaded in blue. The blue shaded data points in the same figure show average porosity of 13% and velocity ranging from 4.1 to 4.5 km/s. These data points belong to deeply buried part of the Stø Formation can be seen with the low gamma ray values. The total thickness of the Stø Formation in this well is 152 m. So, there is no significant variation in temperature in both parts and it ranges from 58 to 62$^{o}$C.

A total 102 m thick sequence of the Stø Formation in well 7120/2-2 is plotted over the cement models (Fig. 5.6 B). The results show that the majority of the data points along the friable-sand model but there are also a significant amount of data situated between friable and constant-cement models, some of the data points are situated between constant and contact-cement models. There are two sets of data points, the first one shaded in green color depicts relatively high porosity (above 10%) and velocity ranging from 4 to 4.4 km/s whereas the data points shaded in blue show very low porosity 5 to 10% and high velocity ranging from 4.5 to 5.1 km/s shown in track 3 in Figure 5.6 B. The present day burial depth is around 2700 m and the temperature value of the Stø Formation in this well is between 80 to 85$^{o}$C.

**Snadd Formation**

Sandy portion of the Snadd Formation from the wells 7120/1-1, 7120/2-1 and 7120/2-2 is superimposed on rock physics cement models (Fig.5.7). Since, the Snadd Formation in all wells possesses thick deposit of over 1100 m depth, so the data points are color coded with depth to show the variation of data with depth. Figure 5.7(A) is showing the P-wave velocity versus average porosity cross-plot of the well 7120/1-1. This well is located in the SW part of the Loppa High shows thickest deposits of the Snadd Formation (1418 m.) as compared to the other wells in the area. Majority of data points for this well fall along the constant-cement line and between constant and contact-cement line. Some of the shallow data points from depth 600 to 1000 m are following friable-cement line. The P-wave velocity is increasing with increase in depth.

The well 7121/1-1 is the eastern most well in the area, data points from the Snadd Formation are plotted over the rock physics cement models are shown in Figure 5.7 (B). The data followed the friable and constant cement models. There is an ambiguity observed that the data points from 1100 to 1300 m depth show very low to very high velocity. Similarly data points over 2100 m depth showing a large variation in porosity with no change in velocity.

The data points of the Snadd Formation from well 7120/1-1 superimposed on cement models are shown in Figure 5.7 (C). The results are quite different from the other wells. Data points followed the contact-cement line, with a massive crowd of data between contact-cement and constant-cement lines. The variations in velocity and porosity are not that significant as observed in the wells 7120/2-1 and 7121/1-1. Here again in the well 7121/1-1 shallow data points (1100-1300 m) shaded with blue show very high velocity as compared to deeply buried part.

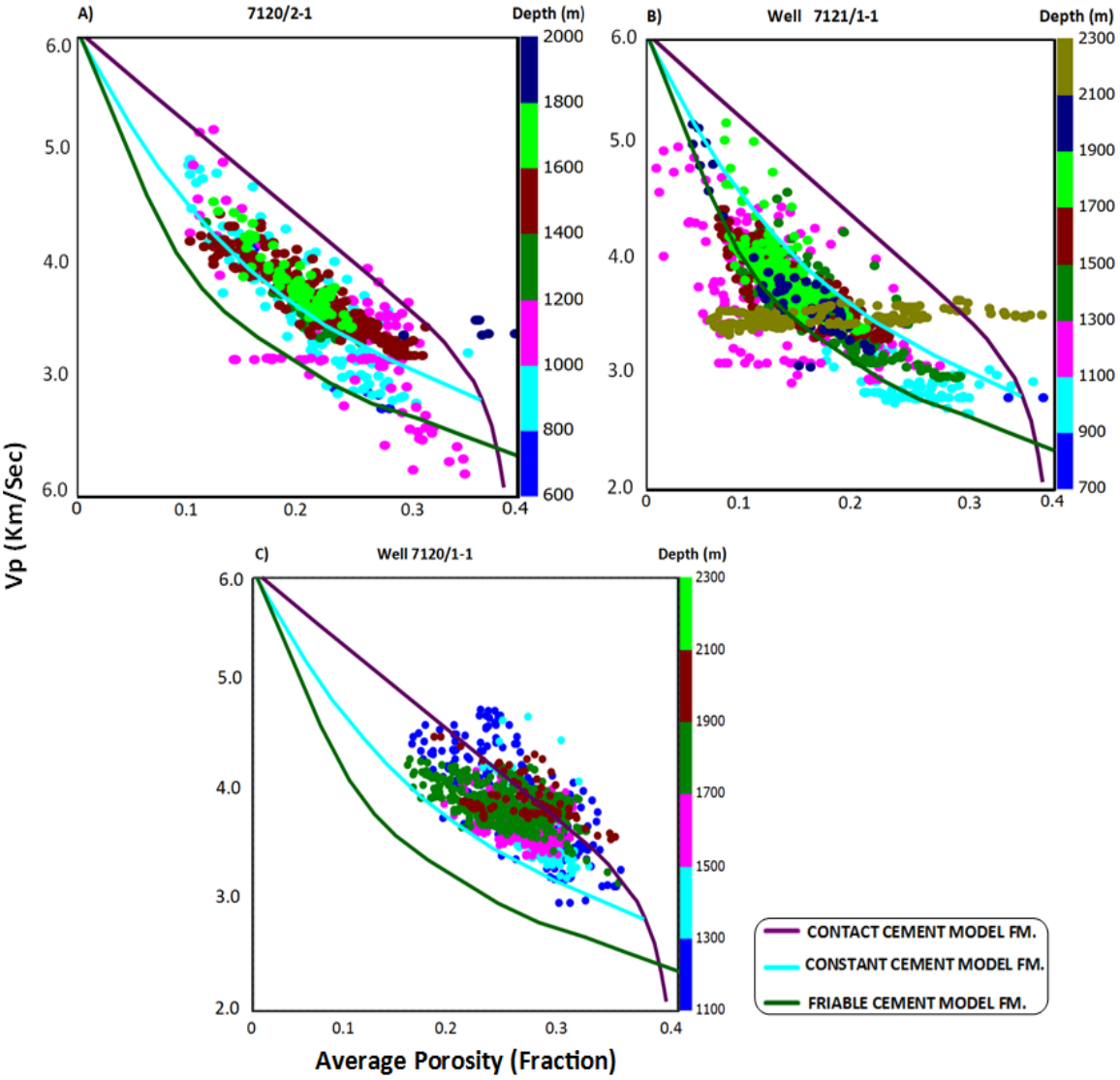


**Figure 5.7:** The Snadd Formation from three wells, color coded with depth superimposed on rock physics cement models.

## 5.1.2 Vp versus Vs

Vp versus Vs cross-plot is generated for different lithologies belonging to the well 7121/1-1. This cross-plot is considered to differentiate different lithologies. Since original Vs data is not available for any well so Vs is calculated by different empirical equations and used in this cross-plot, shown with different colors in the Figure 5.8. Different equations showed almost similar results and the resultant lines overlapped each other except Greenberg-Castagna 1992 shale line. To show different lines in the diagram, different depths are taken for these equations. There is no lithological variation observed among these lines and all equations resulted into straight lines showing increase in Vp and Vs with the increase in depth.

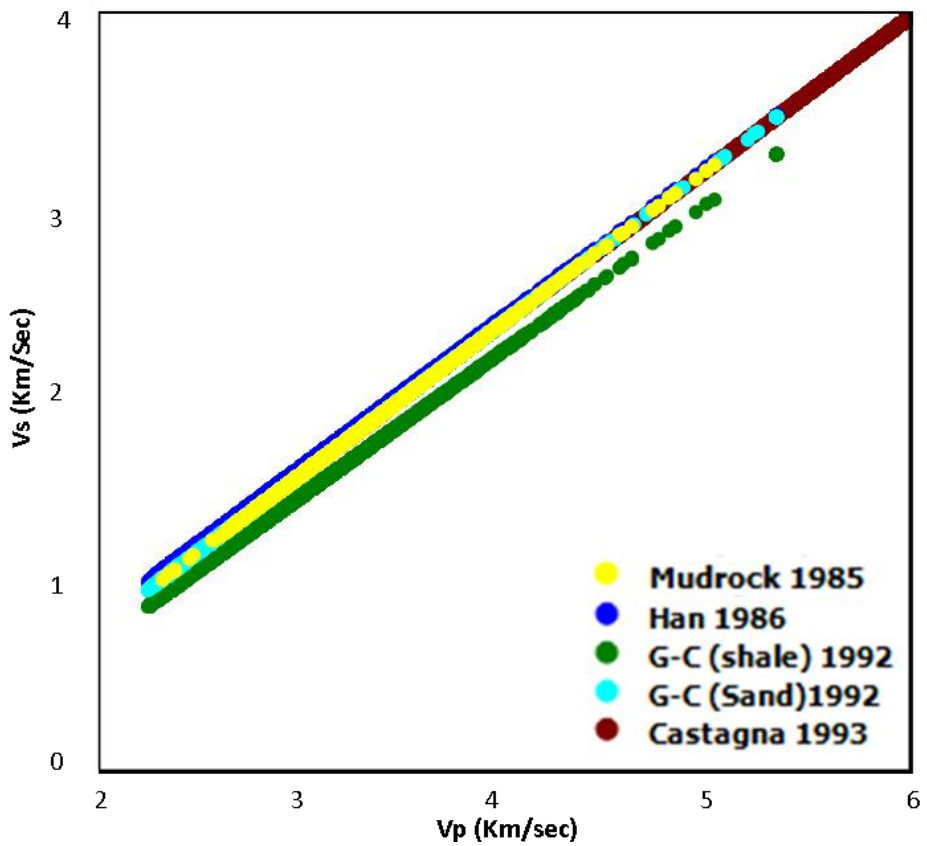


**Figure 5.8:** Cross-plot of Vp versus Vs showing trend lines of Vs derived for the well 7121/1-1, from different empirical equations.

### 5.1.3 Vp/Vs versus acoustic impedance (AI)

The ultimate focus of petroleum geosciences is to explore and discriminate the hydrocarbon bearing rock bodies. Qualitative interpretation of lithology and fluids can be done by seismic amplitude maps generated from 3D seismic data. Rock physics fluid models are good to distinguish the fluid and lithology effects quantitatively from the well log data (Avseth, 2005). In the following section, the rock physics fluid models are discussed for different reservoir sections in the study area. These results are compared to the results generated from petrophysical analysis of reservoir rocks (Chapter 4).

Vp/Vs versus AI cross-plot is a good RPT for fluid discrimination under certain geological conditions. Reservoir sections of the given area are superimposed on fluid models and results are observed. Figure 5.9 shows the Vp/Vs versus AI cross-plot of Jurassic and Cretaceous reservoir rocks in the well 7120/1-2. All the reservoir units are following the water line, showing the rocks are water saturated. The points of high Vp/Vs ratio are belonging to relatively shallow depth than the points of low Vp/Vs ratio which represents the deeply buried rock section. There are fair resemblances from the results of petrophysical studies which showed these rock are water saturated but there are some deviations from the previously observed results in this model which are debatable.

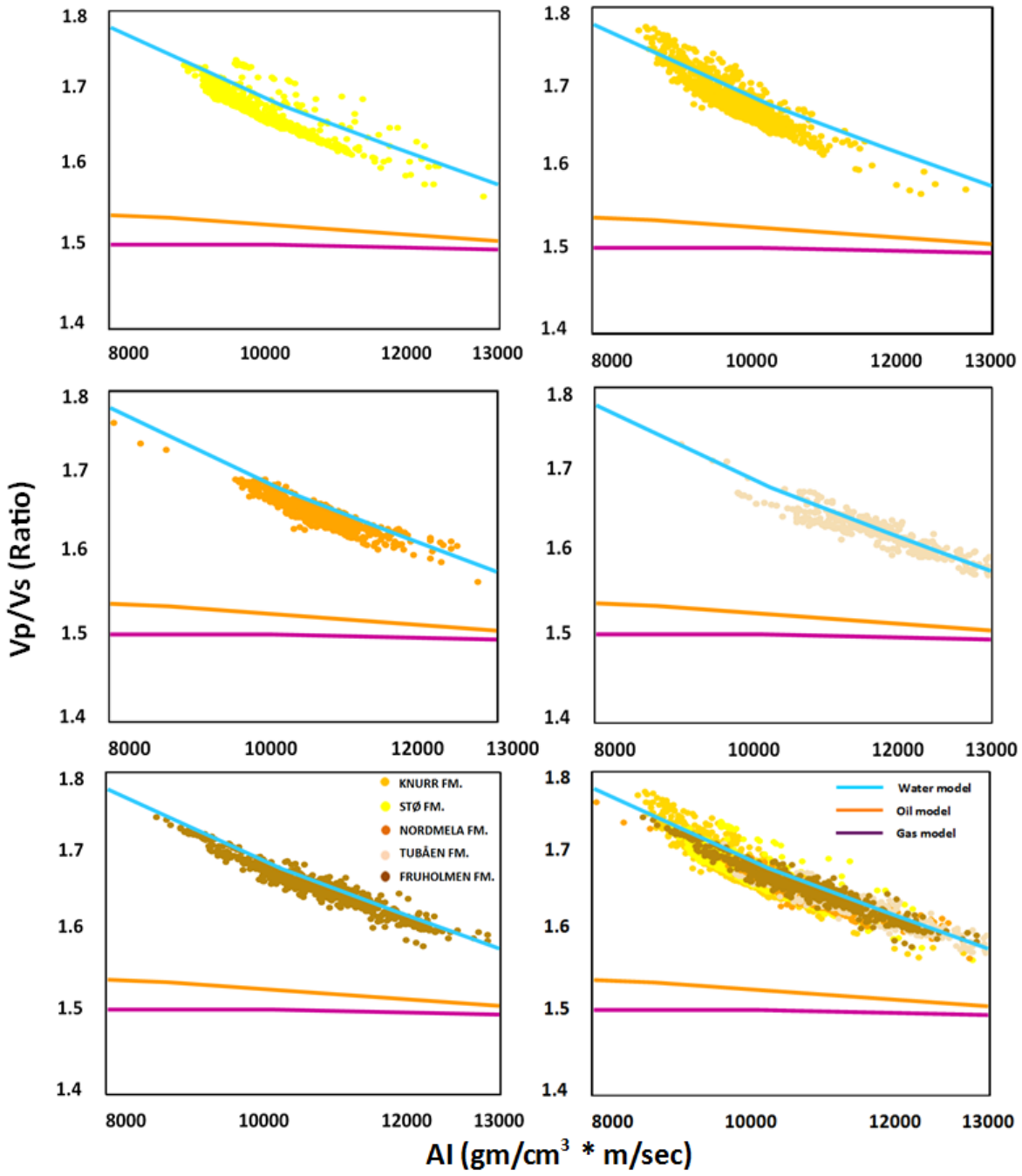


**Figure 5.9:** The Rock physics fluid models superimposed by reservoir rocks from the well 7120/1-2.

### Knurr Formation

The Knurr Formation data points from the well 7120/1-2 and 7120/2-2 are plotted on Vp/Vs versus AI cross-plot (Fig. 5.10). Data points from both wells are following the water model trend line. Data points from the well 7120/2-2 show relatively high Vp/Vs ratio and AI values. The data points from the well 7120/1-2 show little deviation toward the oil trend line showing low Vp/Vs and AI value.

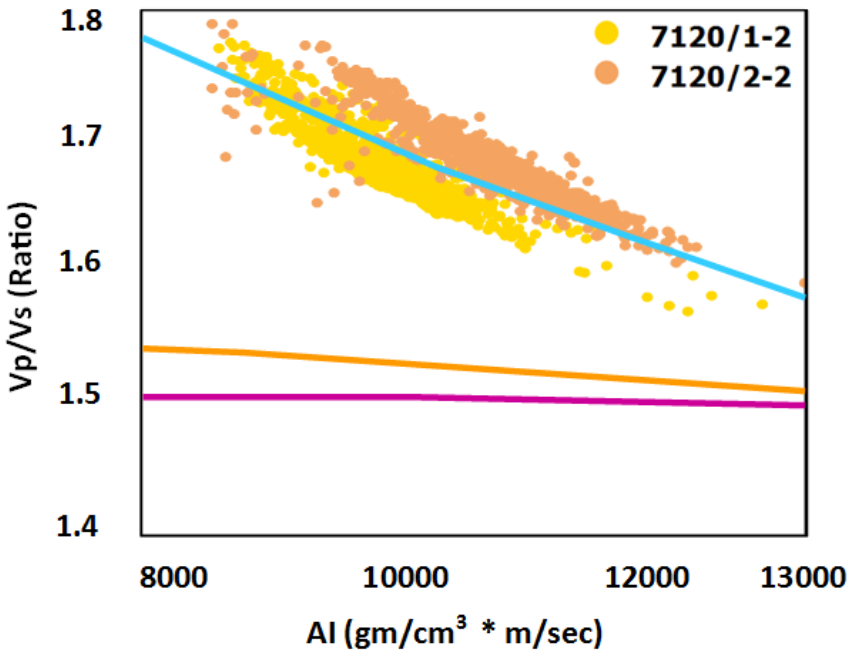


**Figure 5.10:** Vp/Vs versus AI cross-plot superimposed by the Knurr Formation from the wells 7120/1-2 and 7120/2-2.

**Stø Formation**

The data points of the Stø Formation from the wells 7120/1-2 and 7120-2-2 are plotted over fluid models. The data points are following the same trend and no distinction between two wells is observed as data is overlapping (Fig 5.11). Some data points from the well 7120/1-2 show high Vp/Vs ratio whereas the data points from the well 7120/2-2 show high AI.

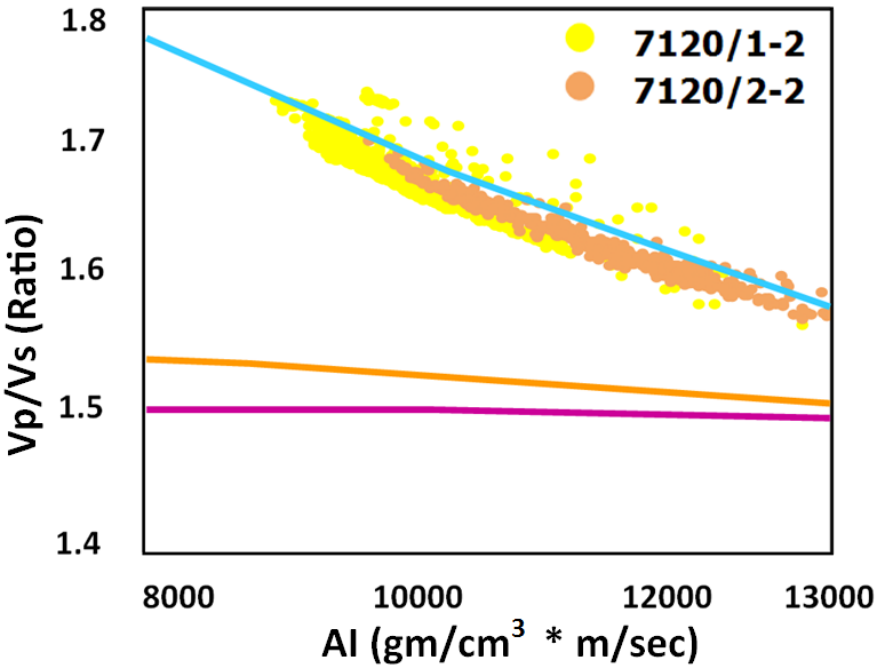


**Figure 5.11:** Vp/Vs versus AI cross-plot superimposed by the Stø Formation from the wells 7120/1-2 and 7120/2-2.

**Snadd Formation**

The data points from thick units of the Snadd Formation from the wells 7120/1-1, 7120/2-1 and 7121/1-1 are superimposed on the fluid models. Figure 5.12 (A) and (B) are showing the Snadd Formation data points from 7120/2-1 and 7121/1-1 respectively. Majority of data in both wells is following water model. The data points from shallow depth holds AI value below 8000 g/cm$^3$*m/sec are falling above water model. In the well 7121/1-1 the data points shown with olive green color in the Figure 5.12 (B) fall below the water line.

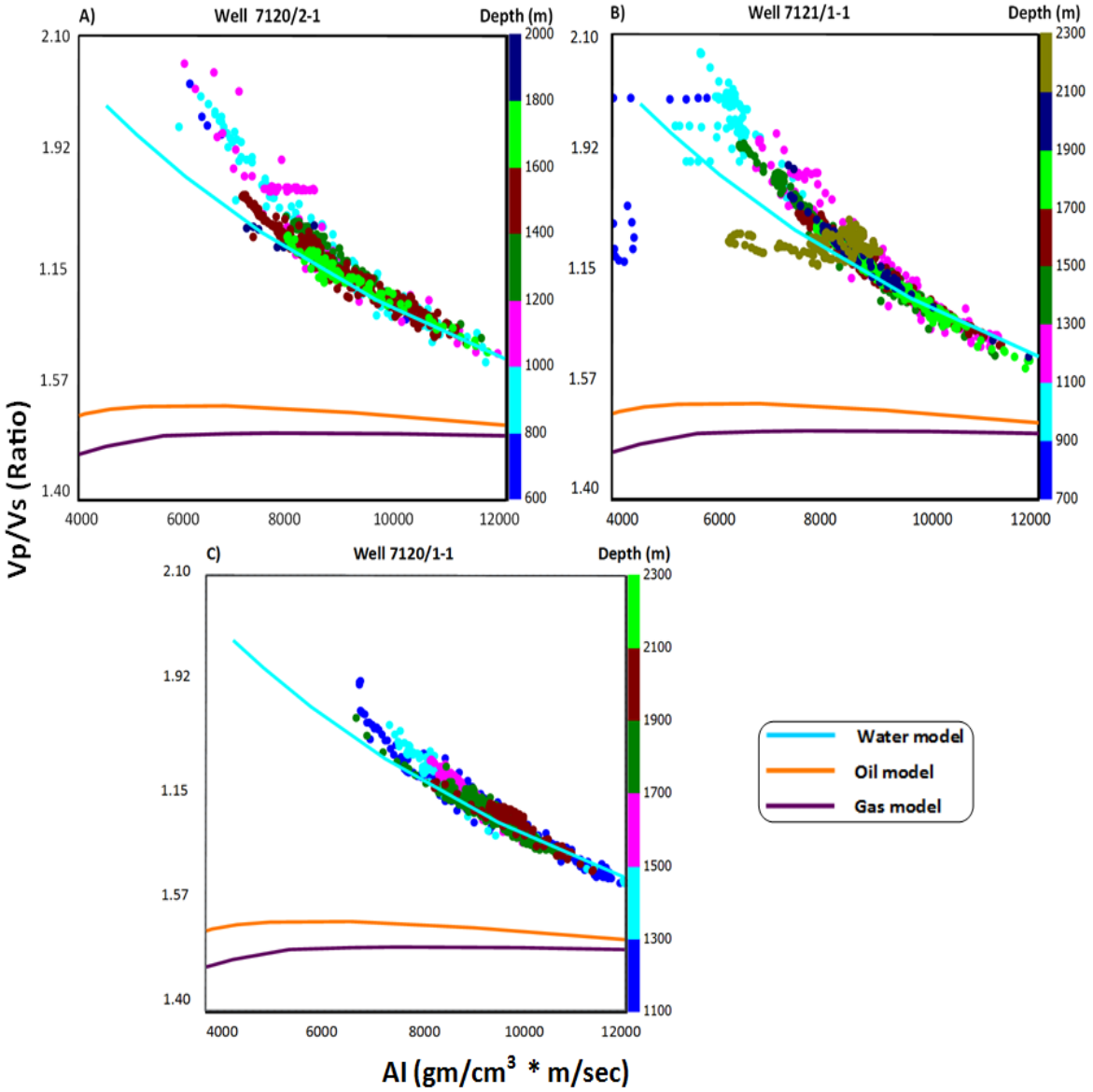


**Figure 5.12** The Snadd Formation from the wells 7120/1-1, 7120/2-1 and 7121/1-1 superimposed on rock physics fluid models.

The Snadd Formation in the well 7120/1-1 is shown in the Figure 5.12 (C) where all the data points are following water model. The data points from shallow depth are showing abnormally very high AI values. The same behavior of high AI values at very shallow depth is observed in the well 7120/2-1.

## 5.1.4 Lamda-Rho versus Mu-Rho

Lamda-mu-rho (LMR) technique is widely applied in petroleum industry for lithology and fluid discrimination. One of the basic reasons behind the success of this technique is that all the parameters (λ,μ,ρ) can directly be derived from seismics as well as well log data (Ujuanbi et al. 2008). The Lamda-rho stands for incompressibility whereas the Mu-rho stands for rigidity. However, rocks and fluids do not compress easily but gas quite significantly. This technique is applied to the given data set to prove its validity and check the presence of hydrocarbon contents in the reservoir rocks in the study area.

### Knurr Formation

Majority of the data points of the Knurr Formation from the well 7120/1-2 is situated in the sand zone where some of the data points are also spread in shale zone and tight sand/carbonate zones. The well 7120/2-2 replicates the scenario for the Knurr Formation in LMR cross-plot. But there is wide spread of data points falling in the shale and cemented sand zones (Fig. 5.13A).

### Stø Formation

The LMR cross-plot for the Stø Formation showed the majority of data points from the well 7120/1-2 are located in the sand zone where some of the data points are also located in the cemented sand zone (Fig. 5.13B). The Stø Formation in the well 7120/2-2 shows almost equal spread of data points in sand cemented sand zone. There is no clear separation of data points observed toward gas saturated zone for both the Knurr and the Stø Formations.

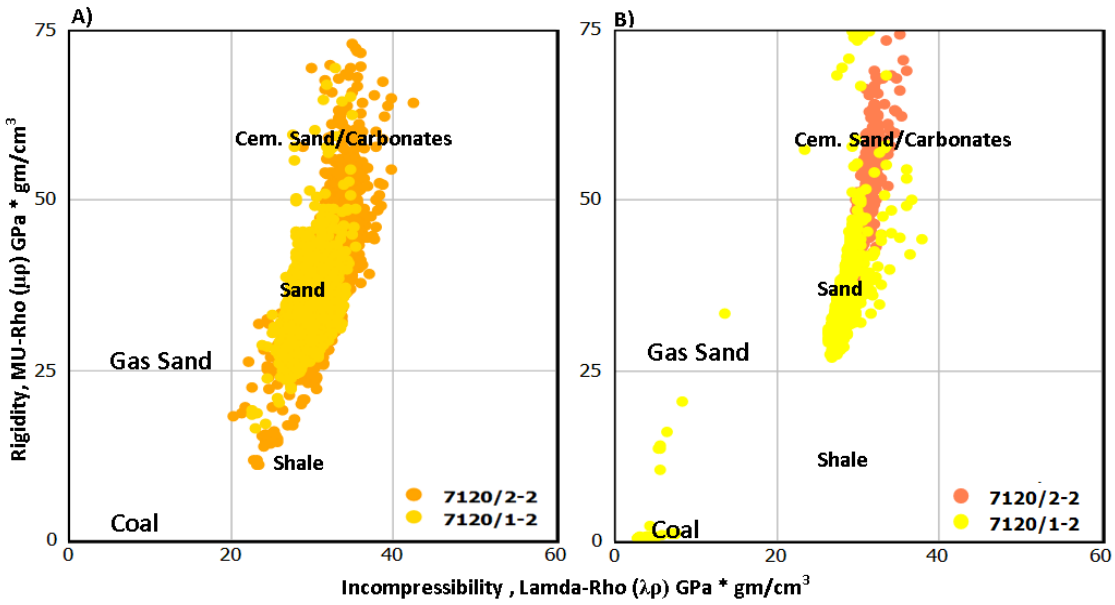


**Figure 5.13:** Lamda-Rho and Mu-Rho cross-plot for the Knurr (A) and Stø (B)and Knur Formations from the wells 7120/1-2 and 7120/2-2.

### Snadd Formation

LMR cross-plot for the Snadd Formation showed quite variable results from the three wells 7120/2-1, 7121/1-1 and 7120/1-1. The data points of Snadd Formation from well 7120/2-1

show a nice spread from shale to cemented sand/carbonate zone in LMR cross-plot (Fig. 5.14 A). There is a little change in incompressibility whereas a wide range of rigidity values. Majority of the data points are located in sand and cemented sand zones whereas some of the data points are situated in the shale zone.

The well 7121/1-1 shows similar trend of data spread in sand and cemented sand zone but there is a fair shift of data points toward gas sand zone and coal zone (Fig. 5.14B). These points are quite similar to the zone (shaded area in Fig. 5.15) observed in fluid models. The Snadd Formation from the well 7120/1-1 showed a quite different results in LMR cross-plot as almost no data points are located in shale zone whereas almost equal proportion of data points are found in sand and cemented sand zone (Fig. 5.14 C).

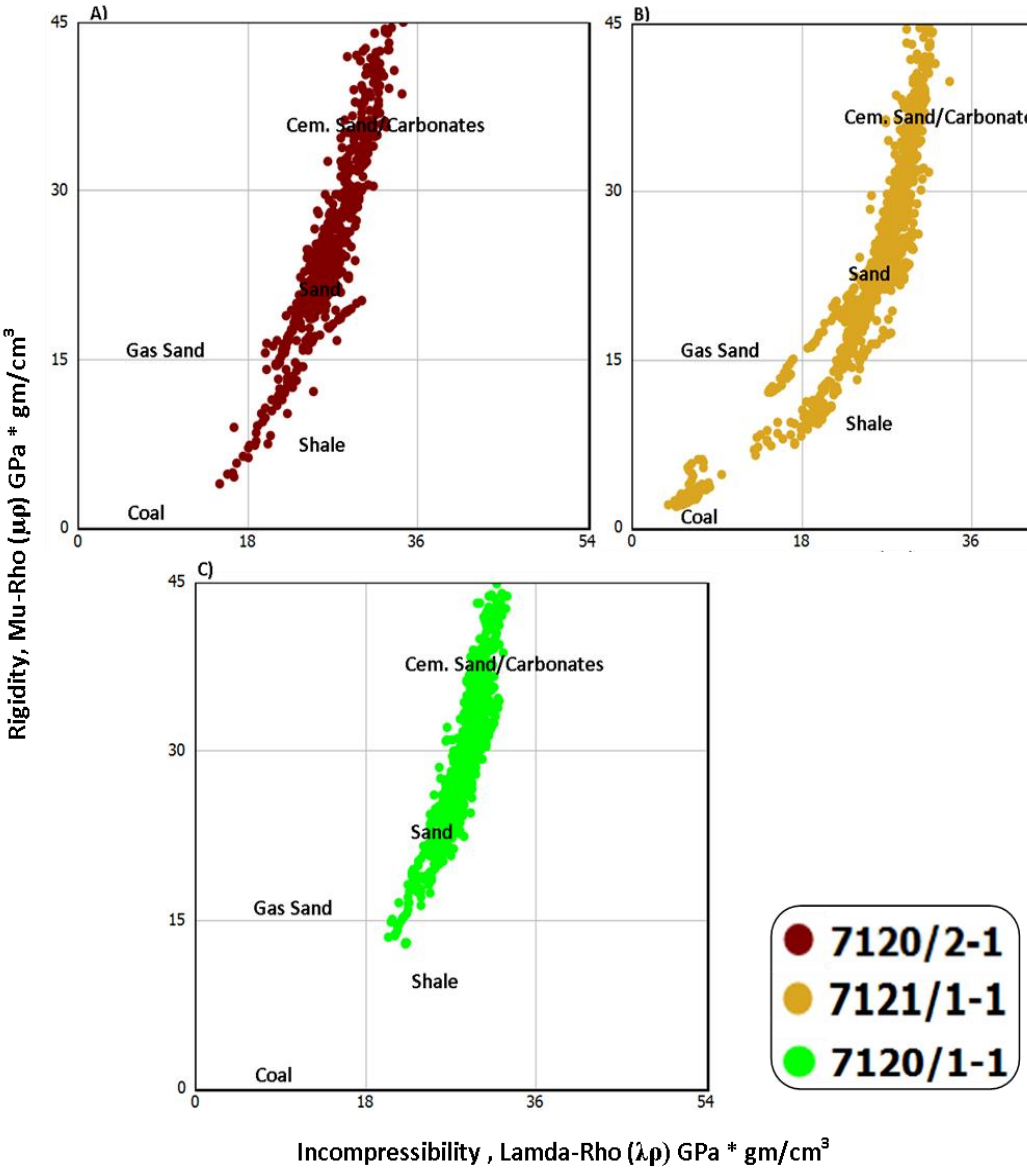


**Figure 5.14:** LMR cross-plot of the Snadd Formation from the wells 7120/1-1, 7120/2-1 and 7121/1-1.

# 5.2 Discussion

## 5.2.1 Porosity versus velocity relationships

### 5.2.1.1 Han's model

The most important factor which should be assumed during interpretation of Han's model is the behavior of Vp versus porosity of clayey sandstones. Avseth et al. (2005) stated that if the porosity remained constant with the inclusion of clay contents in sandstone body, then the velocity decreases, in case of laminated clay or clay coating around sand grains. Contrary if the porosity decreases as the clay contents increase in sandstone, then the velocity might increase as the pore spaces are occupied by clay particles. This can be the one possible reason behind the deviation of data points from the Han's contours. Secondly, the log derived average porosity and log derived clay volume can easily lead us to uncertainty if we compare it to lab derived methods and models. Seldal et al. (2005) stated the gamma ray peaks in the well 7122/2-1 in the L. Cretaceous sand body are proved to be conglomerates. This suggests that high gamma ray peaks in this area could also mislead to estimate clay volume because usually these peaks stand for claystones.

The comparison between the Stø Formation and Snadd Formation from different wells depicts that there will be more misleading results if data points are taken from very thick units (over 1100 m thick units). For better estimation of the porosity and clay volume core data is the most reliable source. Since Han assumed 40 MPa effective pressure for his experiment so exact measurement of effective pressure is also required. The Loppa High is an uplifted area which shows the stiffness of rocks higher than the present day burial depth. The original burial depth for the rock units is also required to predict the effective pressure.

### 5.2.1.2 Rock physics cement model

The well 7120/1-2 is located at the margin of the Loppa high and the clastic wedge is deposited due to the erosion of uplifted foot wall. The Knurr Formation from the well 7120/1-2 is plotted over cement model trend lines it follows the 2% constant cement line, also shows cementing and sorting trend. Contrary the Knurr Formation from the well 7120/2-2 is claystone with sandstone stringers shown by low gamma ray values. This data plotted over cement models. The data points are scattered from friable to contact-cement model. The higher density of data points from constant-cement line to the friable-cement line and below depicts the increase of clay contents and decrease of cement fraction (Fig. 5.5 B). There is significant variation in porosity and velocity due to the variation in clay contents.

The Stø Formation in contrast to the Knurr Formation is sandstone in both wells 7120/1-2 and 7120/2-2. It follows the constant-cement model and shows two trends of relatively high and low porosity which belongs to relatively shallow and deep burial depths respectively. The data points of the Stø Formation in the well 7120/2-2 are situated in between friable and constant-cement model. The porosity values as already discussed in the section 4.2 are very low. The burial depth of the Stø Formation in the well 7120/2-2 is about 400 m deeper than the well 7120/2-1 which is one of the reasons for high Vp values in the well 7120/2-2.

The lithology of the Snadd Formation varies from claystones, siltstones to tight cemented sandstones with intercalation of limestone and dolomite. The cement models from three

wells (7120/1-1, 7120/2-1 and 7121/1-1) showed variable rock properties. High P-wave velocity is observed in all wells for shallow data points which do not follow the principles of rock physics if we only assume claystone or unconsolidated sandstone. That high value of Vp shows presence of carbonates or pyrite in sandstones. When published well reports are studied, limestone band is observed at the same depth which is giving high velocity values in well 7120/1-1. Similarly dolomite stringer around 1390 m depth is found in the well 7121/1-1 justifying the higher velocity at that depth. The data points below 2100 in the well 7121/1-1 (olive green in the Fig. 5.7B) are showing a huge variation in porosity but the velocity is very low, which is due to decrease in density. Comparing the results from published well reports revealed that the data points are from organic-rich siltstones. This zone is investigated in detail in section 5.2.3 and 5.24 to verify whether there are any hydrocarbons or not.

### 5.2.2 Vp versus Vs

Vp versus Vs cross-plot does not give much information about the lithological variation in this study. The main reason behind this anomaly is the use of linear equation for Vs calculations. This cross-plot is also good for fluid discrimination but there is no such kind of information observed in our cross-plot negating the saturation calculation made during petrophysical analysis. But, final conclusion about the rock properties cannot be made on the basis of only one RPT observation. For digging deep into the reservoir properties it is better to sketch different RPT's which can help to make a clear image of reservoir quality and properties. The Vs is derived from Castagna et al. (1993) is directly dependent on the Vp value. As it is a linear equation so Vp versus Vs cross-plot fails to give any information about lithology when derived Vs is used for rock physics analysis.

### 5.2.3 Vp/Vs versus AI

Figure 5.10 plotted from the data of the Knurr Formation of well 7120/1-2 shows little deviation towards the oil line whereas the data points from the well 7120/2-2 are showing high Vp/Vs ratio confirming the high shaly/clayey contents in this well. The Stø Formation data points are follows the same trend in both wells (Fig.5.12). High AI values in the well 7120/2-2 show the high cementation effect than the well 7120/1-2. Very few data points from well 7120/1-2 are above water line confirms the results of high N/G and low shale contents.

Vp/Vs versus acoustic impedance (AI) cross-plot of the wells 7120/2-1 and 7120/1-1 (Fig.5.12 A & C) shows some of the data points from shallow depth found with high AI values. This anomaly can be a carbonate band or due to the presence of heavy minerals i.e. pyrite in the sandstone. When the concerning depth is investigated from well completion reports, a dolomite band found at shallow depth in well 7120/1-1. Moreover the shallow buried sandstone in the same well is very tight holds pyrite and calcite cement. Similarly the Snadd Formation in well 7120/2-1 is carrying heavy minerals i.e. olivine and also gone through cementation which caused the high AI at shallow depth.

Figure 5.12 depicts that the Snadd Formation in all wells is saturated with water. This observation is contradicting the results of calculated hydrocarbon saturation presented in the chapter 4. The well 7121/1-1 shows some deviation towards hydrocarbon line. The Snadd Formation from this well is plotted over fluid models with color codes of resistivity and

saturation of water (Sw) in Figures 5.15 (A) and (B) respectively. The shaded zone in the Figure 5.15 (A) shows relatively high resistivity value. There is a huge range of data following that resistivity range which is hard to predict whether it is hydrocarbon bearing or not? The solution for this question is solved by plotting the same data with color coded with saturation of water (Sw). The zone (shaded area in the Fig. 5.15.B) under investigation showed saturation of hydrocarbon higher than 50%. The hydrocarbon saturated area shows tilt toward the hydrocarbon line but still far away from the model line. There are several reasons behind that deviation; here linear equation is applied for shear wave calculation which can give us only a general trend but still have some ambiguities. Secondly, the present day depth of this zone is 2130-2150m TVD which depicts the presence of cementation. Since, seismic velocities are not much sensitive to fluids in cemented zone so this can be a reason behind presence of hydrocarbon saturated data closer to water line.

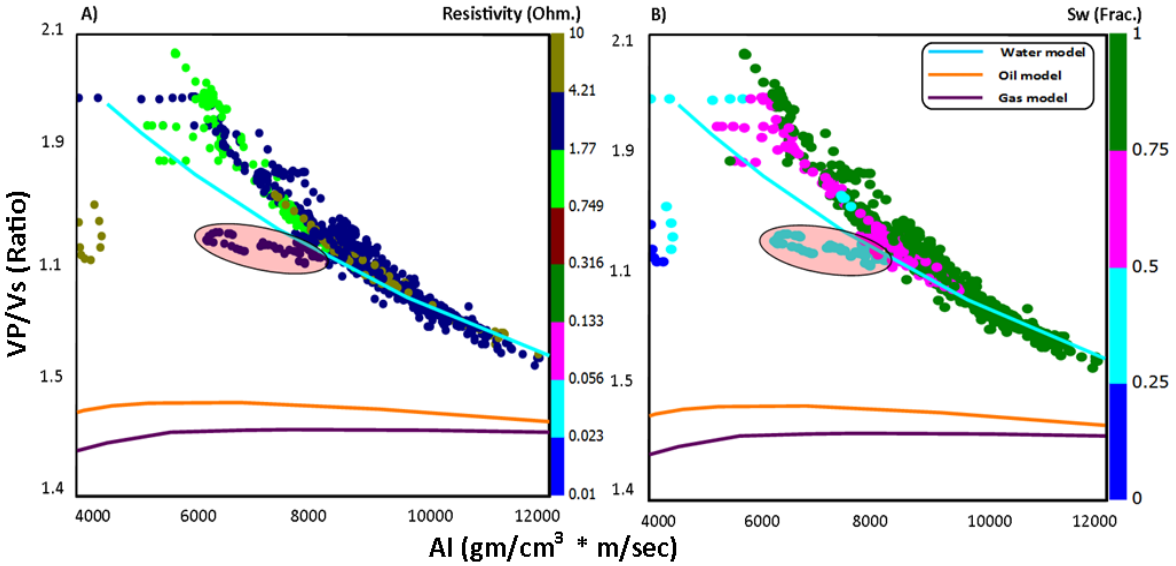


**Figure 5.15:** Vp/Vs versus AI cross-plot of the Snadd Formation from the well 7121/1-1.

## 5.2.4 Lamda-Rho versus Mu-Rho

The LMR cross-plot for the Knurr Formation showed clear discrimination among sandy and shaly sections of the wells 7120/1-2 and 7120/2-2 (Fig.5.13A). In the well 7120/1-2, the reservoir part is much cleaner than the well 7120/2-2. Only few data points from the well 7120/1-2 are falling in shaly part where some data points falling in cemented zone showing less evidences of cementation, whereas in the well 7120/2-2 the Knurr Formation is more shaly and cemented than the well 7120/1-2. There is a nice correlation among the findings from cement models and fluid model for the Knurr Formation in the wells 7120/1-2 and 7120/2-2. The higher proportion of cement in the well 7120/2-2 is due to relatively deep burial and temperature from the well 7120/1-2. The LMR cross-plot for the Knurr Formation from well 7120/1-2, color coeded with Sw and resistivity (Figs. 5.16 A & B ) shows that the data points with relatively high resistivity and low Sw are more compressible.

The Stø Formation data from the wells 7120/1-2 and 7120/2-2 is superimposed over LMR cross-plot. It shows both wells have no shaly portion (Fig. 5.13B). Majority of the data points from the well 71250/1-2 are falling in sandy zone showing relatively low proportion of cement. Data points from well 7120/2-2 are falling in sand as well as a high proportion of

data points falling in cemented sand zone showing relatively higher cementation in the well 7120/2-2 than the well 7120/1-2. The LMR cross-plot for the Knurr Formation from well 7120/1-2, color coded with Sw and resistivity (Figs. 5.16 C & D) shows that the data points with relatively high resistivity and low Sw are more compressible.

No major deviation of data points towards gas saturated zone is found for any formation in both wells. The reason is the low saturation of hydrocarbon and cementation effect in both wells. LMR cross-plot is good to discriminate gas sands and less sensitive for oil saturation. This depicts that there is no economic hydrocarbon saturation in these two wells. These results are also validating the presence of only oil/gas shows of these wells reported by Stewart et al.(1995), Seldal et al. (2005) and NPD (2013) in well completion reports.

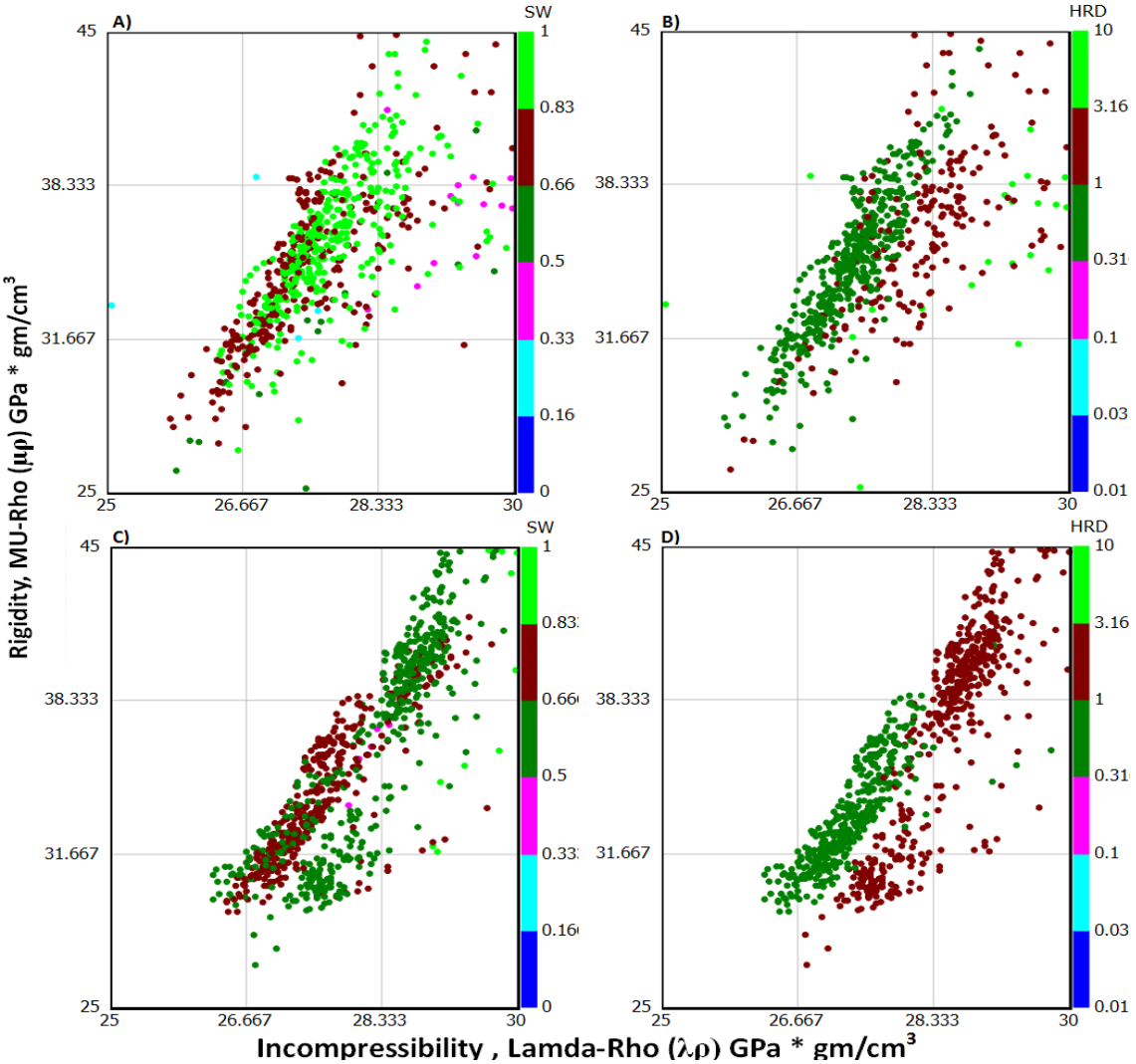


**Figure 5.16:** LMR cross-plot of the Knurr Formation (A and B) and Stø Formation (C and D) from the well 7120/1-2, color coded by Sw and deep resistivity.

Vp/Vs versus AI and LMR cross-plots of the Snadd Formation also show interesting results. The data points from the well 7120/1-1 are falling in sand and cemented sand zone (Fig. 5.14 C). There is a little increase in incompressibility for the cemented sand zone. There are also some carbonate bands proven, studied in section 5.2.3 for shallow depth are also falling in the zone of high rigidity and high incompressibility. There is no evidence of gas saturation or

presence of coal found as no incompressible data is encountered in LMR cross-plot. These results have clear synchronization with the cement model as well as fluid model discussed in the sections 5.21 and 5.2.3 respectively. There are very weak hydrocarbon shows reported by the NPD well completion reports, which are not possible to discriminate in this cemented zone.

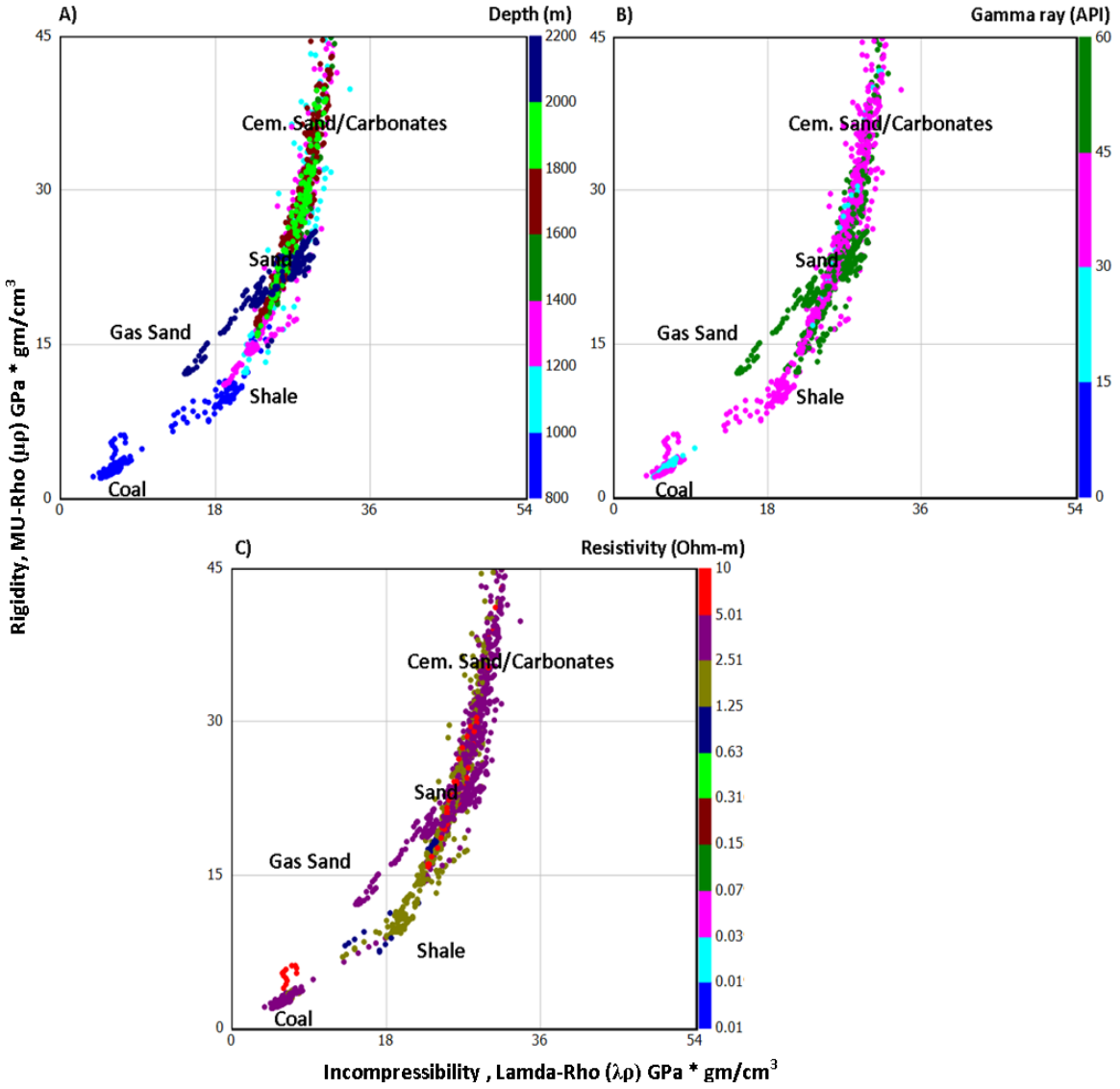


**Figure 5.17:** LMR cross-plot of the Snadd Formation color coded with depth, gamma ray and resistivity from the well 7121/1-1.

LMR cross-plot for the well 7120/2-1 showed some data points in coal and shale zones. Well completion reports also confirmed the thin beds of coal within the Sandd Formation in this well. Majority of the data points are falling in sand and cemented sand/carbonate zones (Fig. 5.14C). There are thin dolomite and limestone bands in the Snadd Formation already been discussed in section the 5.2.3 which is showing high rigidity and incompressibility.

Vp/Vs versus AI cross-plot for the well 7121/1-1 also shows clues of hydrocarbon presence. Considering the previous results this well is superimposed on LMR cross-plot with color codes of depth, gamma ray and resistivity (Fig. 5.17).When the data points are color coded

with depth they showed an anomalous behavior of deeply buried section with very low incompressibility values falling in gas saturated area (dark blue data points in Fig. 5.16 A). This proves that the data points are same, which are shaded with red color in the Figure 5.15. These points show relatively high gamma ray values between 45 and 60 API (Fig. 5.17B). The high resistivity values of these data points proved that there is fair saturation of hydrocarbons in this section (Fig. 5.17C). The data points falling in coal section are have highest resistivity values and belonging to very shallow depth. Both presence of coal and hydrocarbon saturation in this well proved by published well completion report and the previous discussion resulted from petrophysical and RPT's analyses.

# Chapter 6: AVO Modeling

## 6.1 Introduction

AVO modeling is carried out for 'in-situ' and 'what-if' scenarios. The Knurr and Stø Formations penetrated in the well 7120/1-2 are selected for AVO modeling. The Knurr Formation is relatively unconsolidated and less cemented than the deep buried Stø Formation. As previously discussed the lower part of the Knurr Formation in the well 7120/1-2 is clastic wedge which holds good reservoir properties and the upper part is claystone which can act as cap rock. So the claystone in the Knurr Formation is chosen as cap rock and the sandy part is chosen as reservoir rock for AVO modeling. The Fuglen Formation is cap rock for the Stø reservoir in this well. The total thickness and present day depth of the Knurr and Stø reservoir are given in the Table 6.1. The main input logs, required for AVO modeling, are P-wave, S-wave and density logs. As mentioned earlier the Shear wave data are not available in the log suites in five studied wells and so it is calculated by empirical relation of Castagna et al. (1993). A suit of given and generated logs for the reservoir and cap rock sections are given in the Figure 6.1.

**Table 6.1:** The thickness and present day depth of reservoir section of the well 7120/1-2.

| Formation | Thickness (m) | Depth TVD-KB (m) |
|---|---|---|
| Knurr Formation | 258 | 1876 |
| Knurr Reservoir | 70 | 2067 |
| Stø Formation | 154 | 2208 |

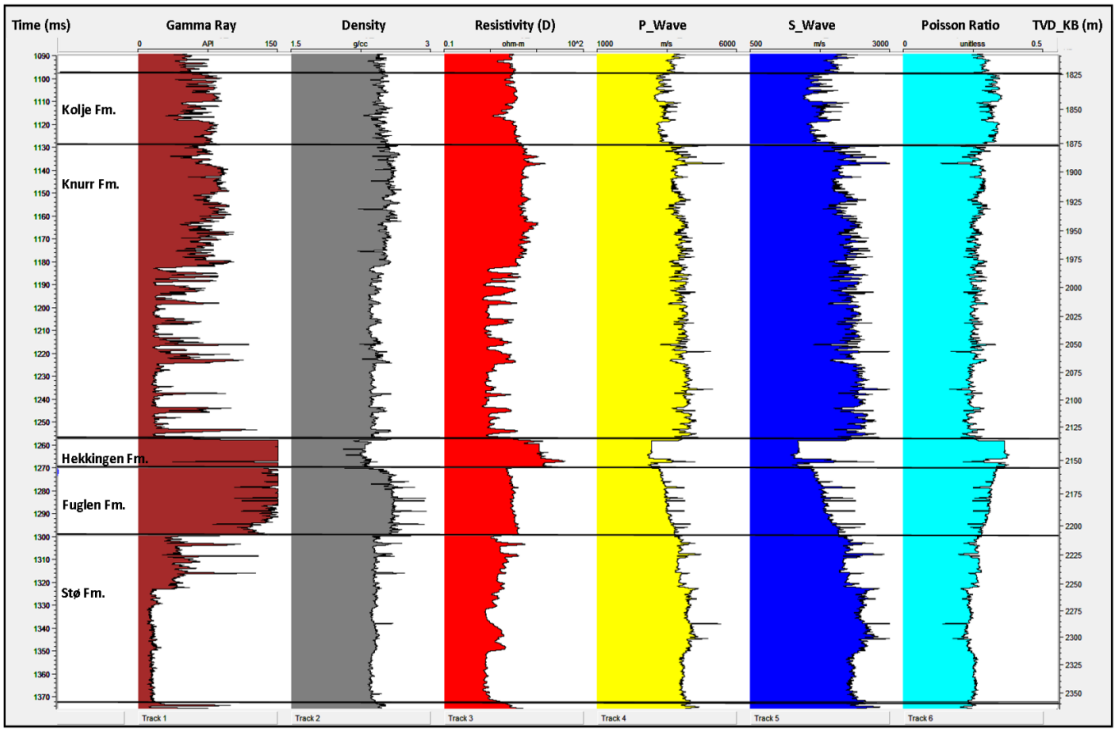


**Figure 6.1:** The original and calculated logs of reservoir and cap rocks of the well 7120/1-2.

The second step for AVO modeling requires generating a synthetic seismogram. A default Ricker wavelet is used as seismic wavelet to generate synthetic seismogram. The increase in the peak sharpness represents increment in acoustic impedance. Figure 6.2 shows the Ricker linear wavelet have 45 Hz frequency. The wavelength of this wavelet is 200 ms and sample rate is 2ms. This wavelet has average zero phase with no side lobes which make finest signal-to-noise ratio. The vertical resolution of synthetic seismic is higher than the original seismic exploration survey.

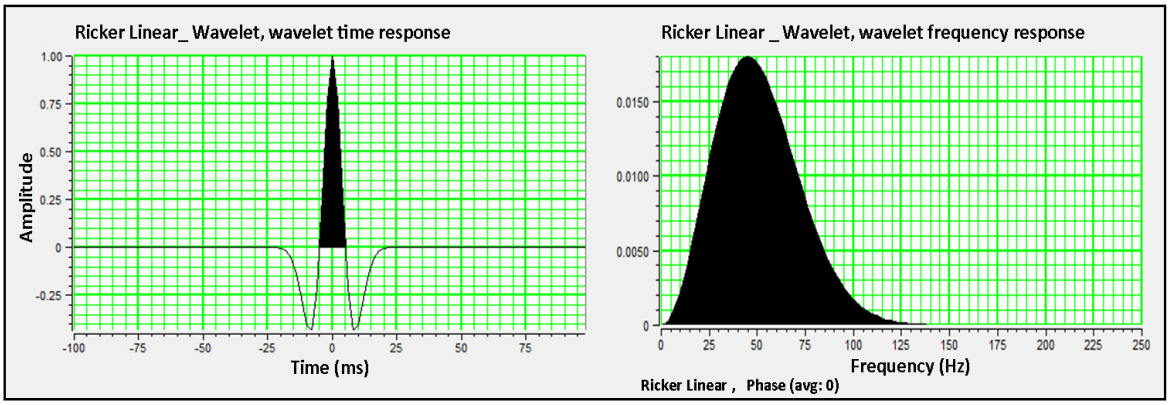


**Figure 6.2:** The Ricker Linear wavelet in time and frequency domain, used for AVO modeling.

## 6.2 Fluid replacement modeling (FRM)

Biot-Gasmann method is applied for fluid replacement to analyze the 'what if' scenario for different amount of fluid saturation. The matrix and fluid properties are assumed to be constant as given in the Table 6.2. Pressure assumed to be 20 MPa for FRM. The porosity value for FRM is set same as input porosity for different values of fluid substitution.

**Table 6.2:** Matrix and fluid properties assumed for FRM.

| Matrix/Fluid Type | Density (g/cc) | Bulk Modulus (GPa) | Shear Modulus (GPa) |
|---|---|---|---|
| Sandstone | 2.65 | 37 | 44 |
| Clay | 2.58 | 20.90 | 6.9 |
| Brine | 1.04 | 2.38 | ----- |
| Gas | 0.13 | 0.04 | ----- |

### 6.2.1 Effect of FRM on rock properties

As discussed earlier in the chapter 5, rock properties are affected by the change of fluid saturation. Cemented rocks are less sensitive to the changes in fluid saturation whereas unconsolidated rocks are more sensitive to these changes. The FRM is applied to the two reservoir sections in the well 7120/1-2 to observe the changes in rock properties in shallow, relatively low cemented (Knurr reservoir) and relatively high cemented (Stø reservoir) rocks. Four cases of fluid saturation (In-situ water, 10% gas, 50% gas and 100% gas saturation) are considered for FRM.

**Knurr Formation reservoir section**

The top of Knurr reservoir is taken as 2067 m TVD_KB and thin claystone bed is chosen as cap rock. Assuming the reservoir section is 100% brine saturated. Introduction of 10% gas in the rock unit caused the slight decrease of both Vp and density whereas increase of Vs is also observed. When gas saturation increased from 10% to 50%, density decreased significantly whereas a minor decrease in Vp is observed. There is slight increase in Vs is observed. Finally, 100% gas substitution to the system decreases the density sharply while slight increase in Vp and Vs is observed. The average values of seismic waves and density calculated from the reservoir section after different values of gas saturation are given in the Table 6.3.

**Table 6.3:** Values of seismic waves and density after changes in gas saturation in the Knurr reservoir.

| Fluid Substitution (%) | Density (g/cc) | P-wave (m/sec) | S-wave (m/sec) |
|---|---|---|---|
| In_Stiu Water | 2.43 | 3939 | 2223 |
| 10 % Gas | 2.42 | 3675 | 2228 |
| 50% Gas | 2.38 | 3667 | 2249 |
| 100 % Gas | 2.32 | 3705 | 2276 |

**Stø Formation**

The Stø Formation is relatively deeply buried and has upper shaly part from 2208 to 2251m TVD-KB whereas the lower part is clean sandstone till its bottom. When 10% gas is introduced to the system, slight decrease in density and sharp depreciation in Vp is observed. There is very minute increment in Vs also observed (2249 to 2257 m/s). On 50% gas substitution, the density sharply decreased whereas Vp and Vs are slightly increased (Table 6.4). On 100% gas saturation, density significantly decreased whereas a slight increase in Vp and Vs is observed.

**Table 6.4:** Values of seismic waves and density after changes in gas saturation in the Stø reservoir.

| Fluid Substitution (%) | Density (g/cc) | P-wave (m/sec) | S-wave (m/sec) |
|---|---|---|---|
| **In_Stiu Water** | 2.35 | 3970 | 2249 |
| **10% Gas** | 2.34 | 3784 | 2257 |
| **50% Gas** | 2.32 | 3806 | 2287 |
| **100% Gas** | 2.24 | 3869 | 2327 |

## 6.2.2 AVO classification of reservoir sands

Three layers model is used for AVO classification of reservoir sands considering two interfaces, the top and bottom of the reservoir. In-situ water model is used and then replaced by different amount of gas saturation.

**Knurr Formation reservoir section**

AVO classes are observed for in-situ water, 10% and 50% gas saturation for the top and bottom of the reservoir section of the Knurr Formation shown in the Table 6.5. The top of the reservoir section remain consistent after FRM. It gave AVO "class II a" for all cases with relatively high positive reflectivity of in-situ water case than the 10% and 50% gas saturated sand. The bottom of the reservoir showed different results. For in-situ water saturated case the bottom of reservoir represents class IV sand with high negative reflection coefficient.

**Table 6.5:** AVO classes for top and bottom of reservoir sands with respect to in-situ water, 10% and 50% gas.

| Fluid Saturation (%) | AVO Class | |
|---|---|---|
| | Reservoir Top | Reservoir Bottom |
| In-situ water | II a | IV |
| 10% Gas | II a | III |
| 50% Gas | II a | III |

The intercept-gradient analysis is also carried out for these reservoir sections (Fig.6.3). The intercept (A) for all cases remain positive for reservoir tops whereas for the bottom of reservoir it remained negative. The gradient (B) remained negative for reservoir top but it shows variation for the reservoir bottom, where for in-situ water saturated sand it gives positive values and for 10% and 50% gas saturation it remains negative (Table 6.6). The top of reservoir sand in all substitution cases is situated in fourth quadrant of A-B cross-plot. The reservoir bottom for in-situ water case is situated in second quadrant and for 10% and 50% gas substitution case the reservoir bottom is located in third quadrant of A-B cross-plot.

**Table 6.6:** The intercept (A) and gradient (B) values for the Knurr reservoir top and bottom for in-situ water, 10% and 50% gas saturation.

| Fluid Saturation (%) | Quadrant | | Intercept (A) | | Gradient (B) | |
|---|---|---|---|---|---|---|
| | Res. Top | Res. Bottom | Res. Top | Res. Bottom | Res. Top | Res. Bottom |
| In-situ water | 4 | 2 | + | - | - | + |
| 10% Gas | 4 | 3 | + | - | - | - |
| 50% Gas | 4 | 3 | + | - | - | - |

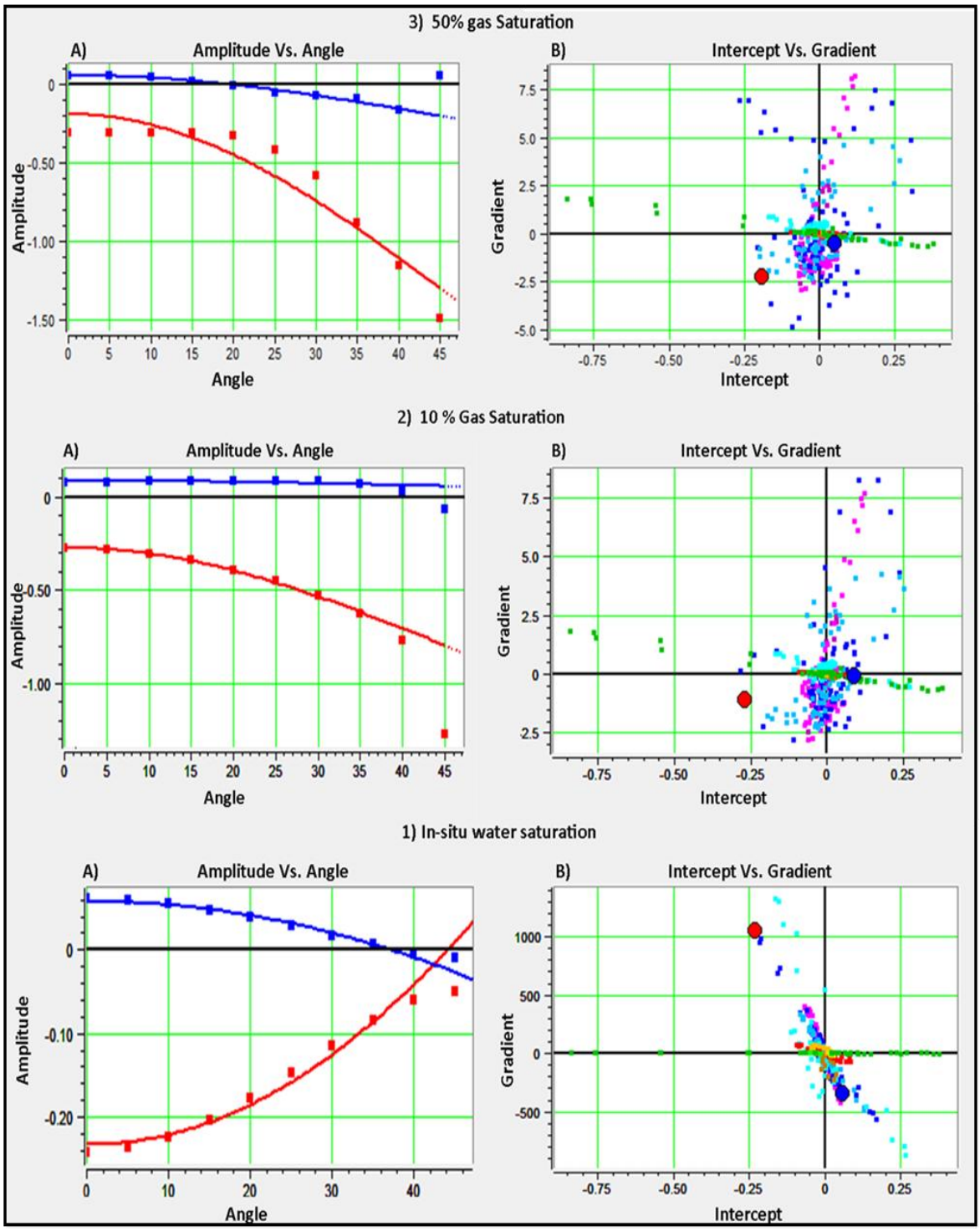


**Figure 6.3:** Amplitude versus angle and intercept versus gradient cross-plot for the in-situ water, 10% gas and 50% gas saturated Knurr reservoir top and bottom.

### Stø Formation

The Stø Formation shows a quite similar response for top and bottom before and after fluid replacement, as observed for the Knurr Formation. The AVO classes for top and bottom remain same and are falling in class IIa before and after fluid substitution (Table 6.7). Figure 6.4 shows for in-situ water case the amplitude is high for both top and bottom of

reservoir at zero-offset which becomes negative at angle $35^{o}$ and $42^{o}$ respectively. For 10% and 50% gas substitution the amplitude at zero-offset for the bottom of reservoir is closer to zero which becomes negative at an angle of $10^{o}$.

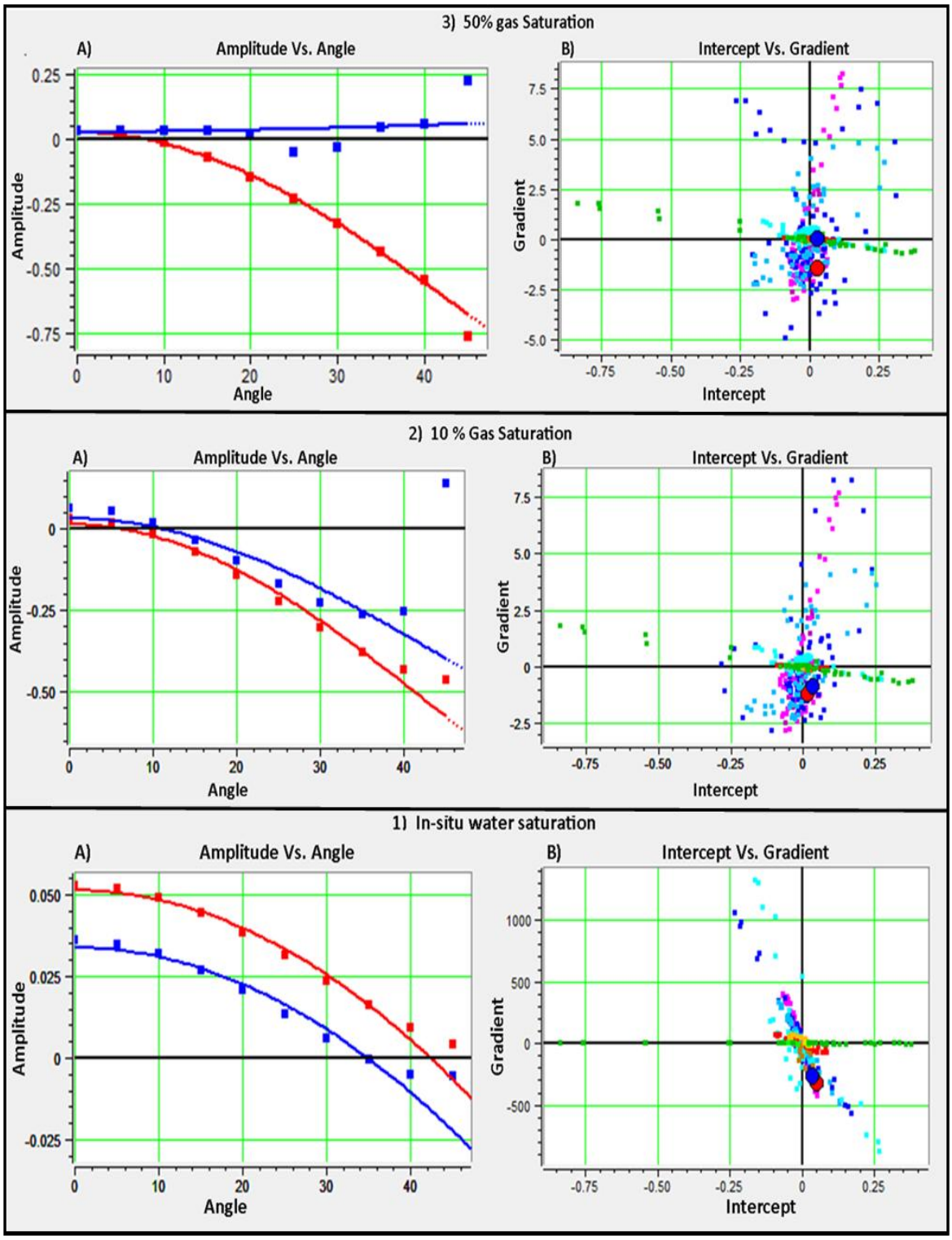


**Figure 6.4:** Amplitude versus angle and intercept versus gradient cross-plot for in-situ water, 10% gas and 50% gas saturated Stø reservoir top and bottom.

**Table 6.7:** AVO classes for top and bottom of the Stø Formation with respect to in-situ water, 10% and 50 % gas.

| Fluid Saturation (%) | AVO Class | |
|---|---|---|
| | Reservoir Top | Reservoir Bottom |
| In-situ water | II a | II a |
| 10% Gas | II a | II a |
| 50% Gas | II a | II a |

The intercept gradient cross-plot showed consistent results for the top and bottom of the reservoir. The intercept for all substitution cases for top and bottom of the reservoir remains positive whereas the gradient for top and bottom of reservoir remains negative. For all substitution cases reservoir sands are falling in fourth quadrant of intercept gradient cross-plot (Table 6.8).

**Table 6.8:** The intercept (A) and gradient (B) value of the Stø Formation top and bottom for in-situ water, 10 and 50% gas saturation.

| Fluid Saturation (%) | Quadrant | | Intercept (A) | | Gradient (B) | |
|---|---|---|---|---|---|---|
| | Res. Top | Res. Bottom | Res. Top | Res. Bottom | Res. Top | Res. Bottom |
| In-situ water | 4 | 4 | + | + | - | - |
| 10% Gas | 4 | 4 | + | + | - | - |
| 50% Gas | 4 | 4 | + | + | - | - |

# 6.2 Discussion

## 6.2.1 Knurr Formation reservoir section AVO response

The top of the reservoir zone, selected from the Knurr Formation, is not showing any strong reflection on synthetic seismogram in case of in-situ water saturation as shown (red trace) in the Figure 6.6. According to Avseth et al, (2008), the strength of the cap rock is precursor to the AVO response of the reservoir rock. The gamma ray log for that section tells the answer that the cap rock is thin band of claystone. The claystone is thin and there is no significant impedance contrast hence showing no significant wiggle on synthetic trace for the top of reservoir section. The bottom of reservoir section possesses a significant impedance contrast. The underlying Hekkingen Formation holds a thick deposit of shale which gives high negative reflectivity at the bottom.

When 10% gas introduced to the system, the density decreased (Fig. 6.5). Vp decreased sharply whereas Vs slightly increased. The fluid modulus also decreased and this ultimately dropped the effective modulus of the reservoir. The synthetic trace for 10% gas showed strong reflectivity at the top of the reservoir (Blue trace Fig. 6.6).

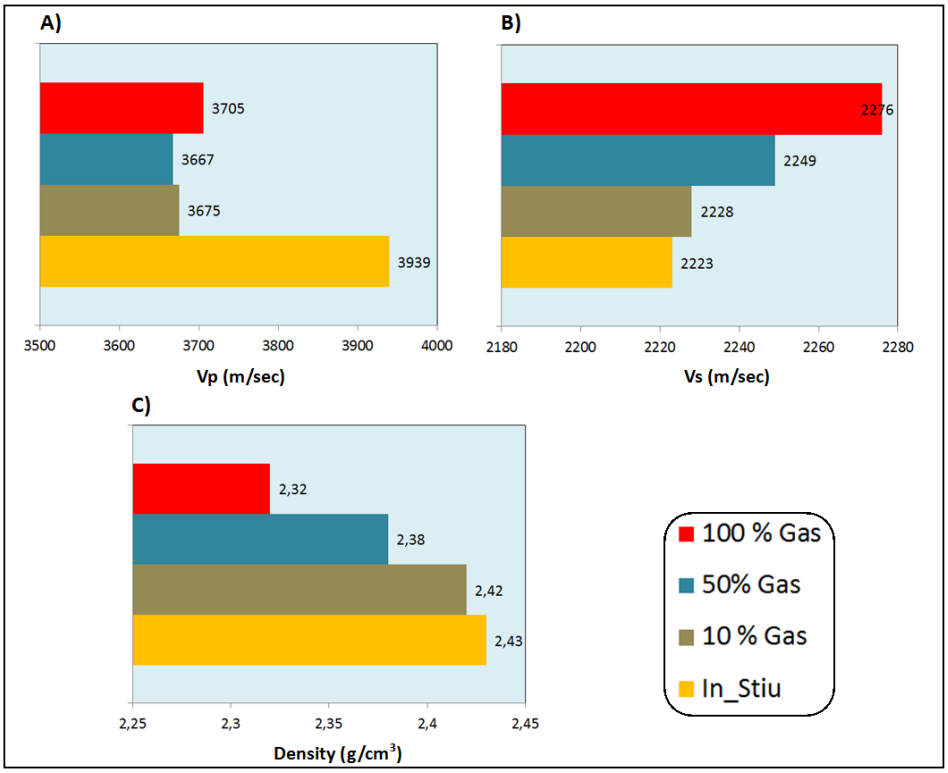


**Figure 6.5:** The Vp, Vs and the bulk density in the well 7120/1-2 with different saturation, for the Knurr Formation reservoir section.

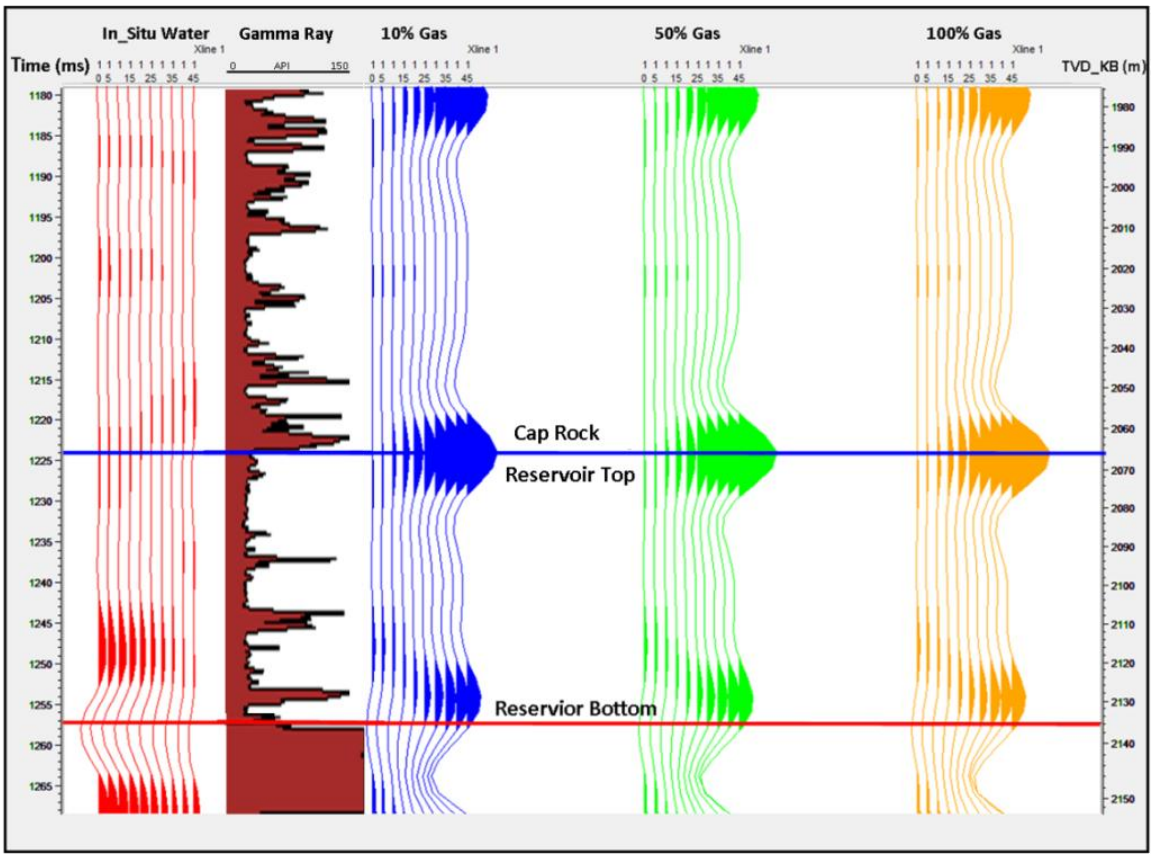


**Figure 6.6:** The synthetic seismogram of the Knur Formation reservoir section with different fluid substitution scenarios.

In second substitution phase 50% gas is introduced to the reservoir. The density decreases significantly with minor change in Vp and Vs. The reason behind minor change in Vp is that the bulk modulus is not that sensitive to changes in percentage of similar fluids. The sensitivity of fluid modulus is more robust when gas is introduced to the water bearing system. The later substitution does not affect the seismic velocities that significantly as observed in the case of first (10%) substitution.

### 6.2.2 Stø Formation AVO response

The Stø Formtion is underlain by thick cap rock of the Fuglen Formation. When 10% gas introduced to the system it reduced the density. Where a sharp decrease in Vp observed whereas Vs increased slightly (Fig. 6.7). This change in density and seismic wave produced a drastic effect on resulting synthetic seismogram and strong positive reflectivity produced a sharp wiggle over the top of the reservoir (Fig. 6.8). The later substitution (50% and 100% gas) has not produced any significant difference in Vp but Vs steadily increased. The decrease in bulk density observed at every substitution.

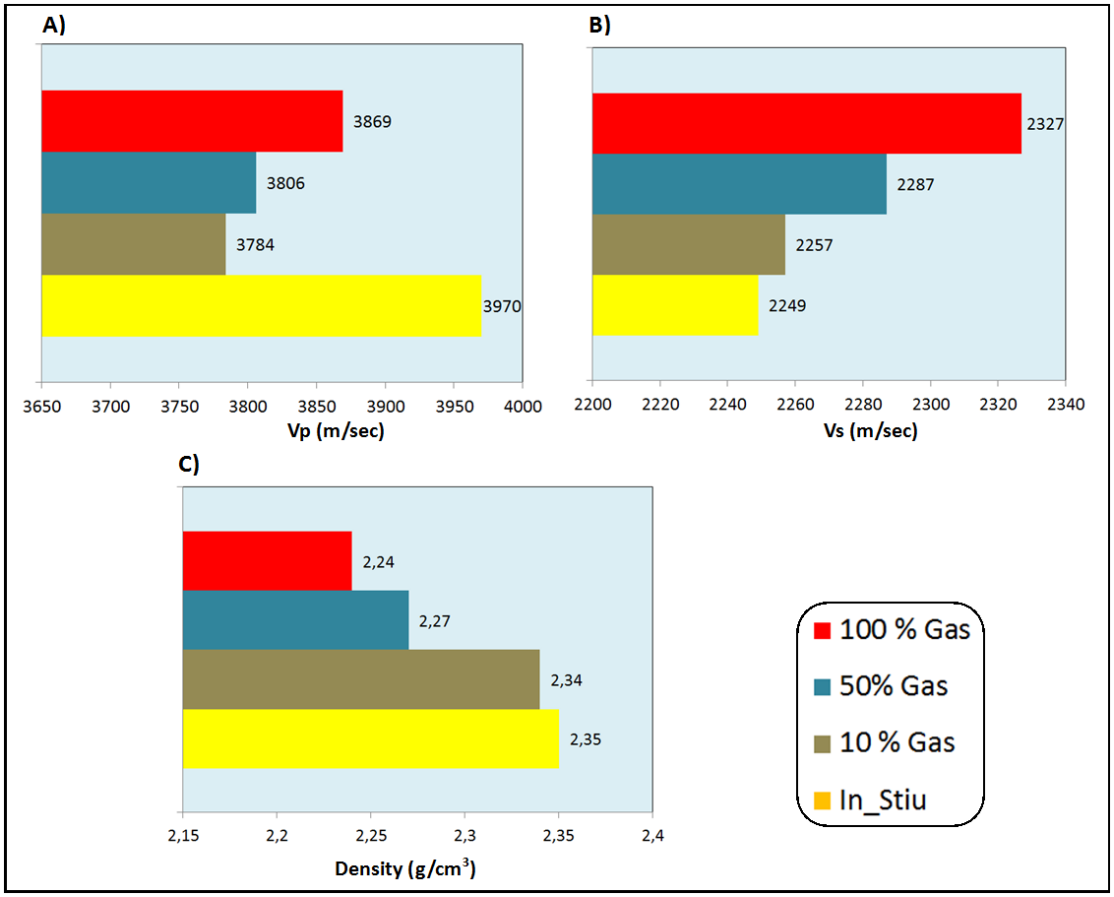


**Figure 6.7:** The Vp, Vs and the bulk density in the well 7120/1-2 with different saturation, for the Stø Formation.

The increase in amplitude with the substitution of different fluids is quite different in both reservoirs. Knurr reservoir shows change in amplitude around $30^{o}$ whereas the Stø Formation shows a sharp increase in amplitude at an angle of $10^{o}$. This difference has a simple reason as the Knurr reservoir is overlain by a thin cap rock whereas the Stø reservoir has a thick cap rock which sharply increased its amplitude at a small offset.

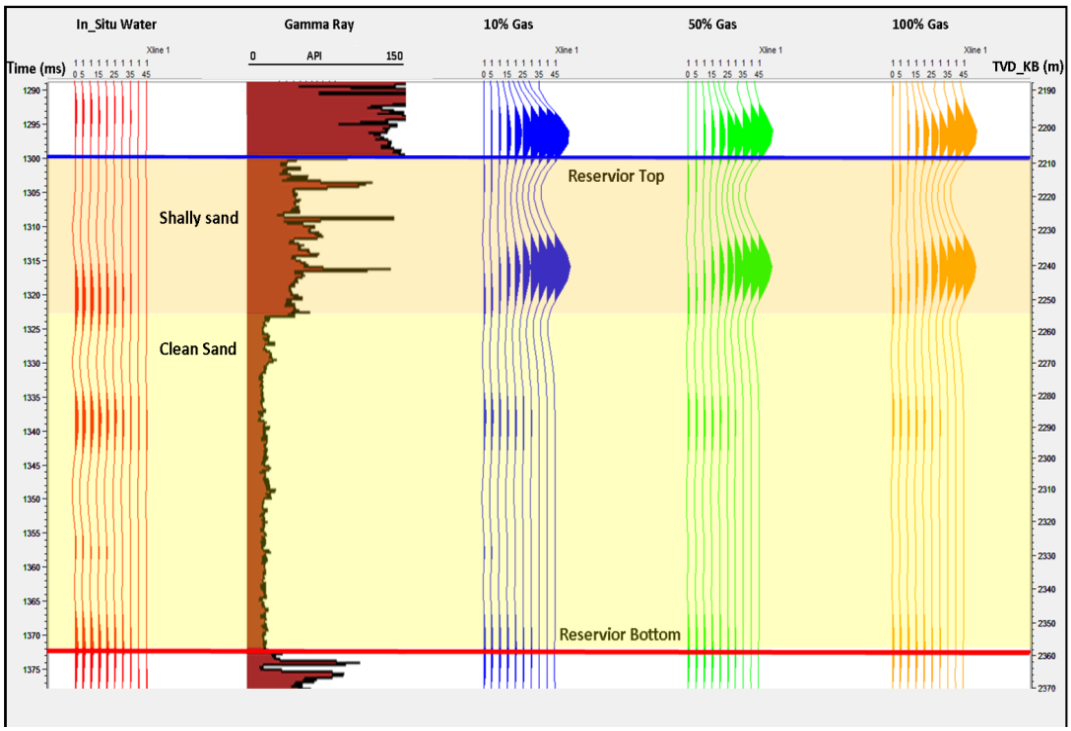


**Figure 6.8:** The synthetic seismogram of the Stø Formation with different fluid substitution scenarios.

Figures 6.3 and 6.4 show the amplitude versus angle cross-plot for Knurr and Stø reservoirs. The range of reflectivity for both reservoirs is close to zero which shows the effect of cementation. Figure 6.9 from Avseth et al. (2005) shows the effect of cementation on brine saturated and hydrocarbon saturated rocks. If in-situ water saturated amplitude versus gradient cross-plot is compared to the Figure 6.7. The Stø Formation shows higher cementation effect than the Knurr Formation. This also validates the high proportion of cement in the Stø Formation which is discussed in chapter 5.

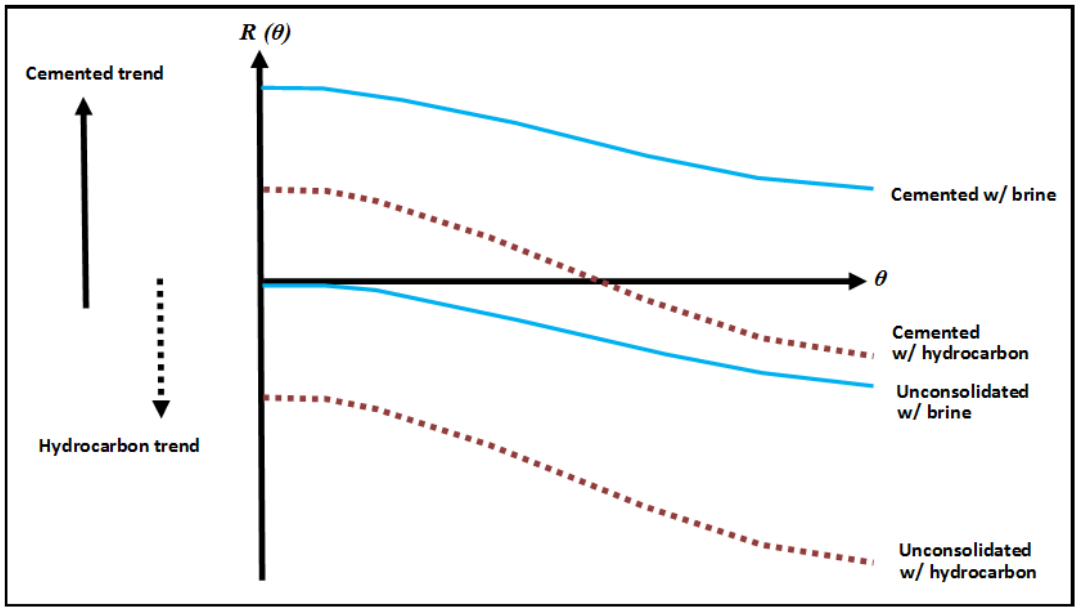


**Figure 6.9:** The AVO response for unconsolidated and cemented sand reservoirs with different fluid saturation capped by shale (modified from Avseth et al. 2005).

### 6.2.3 Uncertainties in FRM

The fluid replacement modeling is not absolute and carrying some uncertainties due to absence of core data. The value of porosity and net-to-gross are derived from geophysical well logs. Moreover the calculated Vs also contain uncertainties. Simmon and Bakus, (1994) stated that for gas sand at 20% porosity the Vp and Vs values are 3560 m/s and 2374 m/s respectively. But only 3 percent increase in porosity decreases the Vp and Vs values to 3350 m/s and 2231 m/s. In this case the input porosity is considered equal to the output porosity which does not account the effect of compaction. This can be the reason behind similarity in AVO response for shallow and deep reservoirs.

Similarly net-to-gross is an important factor too to add uncertainties in FRM. The gas substitution is applied by using Gassmann-Biot relationship. The Gassman theory is valid for the situation where all pores are connected. In heterogeneous reservoirs the presence of clay decreases pore connectivity. This can also affect the generated results especially the Knurr reservoir sandstone with net-to-gross 0.78. The upper part of the Stø Formation in this case is shaly which can mislead the results.

# Chapter 7: Summary and conclusion

The Loppa High (LH) is situated between the northern boundary of the Hammerfest Basin and the south-western vicinity of the Maud Basin. The complex evolution history of the LH started way back in Carboniferous. During Late Carboniferous carbonates deposited on the LH area, later on Permian clatics, shales and cherty limestone deposited on the area. The major clastic reservoir bodies are deposited during Mesozoic. Pre Triassic and Triassic sediments eroded due to uplift and deposited in Late Triassic (Snadd Formation). During Middle Jurassic sea level fall led to the deposition of reservoir rock (Stø Formation) deposited coastal marine environment. The rifting and continued fault activity in the Cretaceous led to the erosion and deposition of clastic wedge (Knurr Formation) towards the boundary between the Loppa High and Hammerfest Basin along the Asterias Fault complex. All these rocks carry good reservoir potential and are analyzed in detail during this study. A suite of five wells 7120/1-1, 7120/1-2, 71202-1, 7120/2-2 and 7121/1-1 is used to study Mesozoic reservoir rocks.

Triassic petroleum system is more operative in the LH area whereas Late Jurassic play is also effective in the south-western part of the high. Several stages of uplift have tilted and eroded the LH which destroyed the petroleum plays. The reactivation of faults has breached the seal which offered the remigration of hydrocarbon. This is evident in the residual hydrocarbon found in reservoir section. Uplift also decreased the burial temperature which retarded the hydrocarbon generation from the source rocks. The uplift has some positive impacts on the petroleum play; the erosion of sands related to uplift have deposited along the flanks of the LH which is one of the major focuses for hydrocarbon exploration these days.

Geological parameters (i.e. porosity, shale volume, diagenesis) have a direct link with the elastic rock properties. Petrophysical studies in the SW LH area proved different magnitude of variation in the reservoir properties between different reservoir rocks. The Lower Cretaceous clastic wedge in the well 7120/1-2 showed good porosity and high N/G but the same unit shows drastic change in the eastern well 7120/2-2. The N/G decreases significantly proving poor reservoir quality or the wedge (Knurr Fm) in the eastern well. The Stø Formation shows a different aspect of variation in reservoir parameter from west to east. The N/G in both wells remain almost constant but the porosity from west to east decreased from 17% to 10% respectively. The Snadd Formation in the studied Loppa High area has thick deposits (over 1100 m thick) hydrocarbon shales with sand deposited during regression. There is an ideal scenario of in-situ source, reservoir and cap rocks within the Snadd Formation. The net-to-gross is low (avg. 0.40) compared to the whole thickness of the rock including source rock intervals. The average porosity is 11% which is fair for a reservoir rock. The reservoir properties decrease from the eastern well 7121/1-1 to the western well 7120/1-1.

Rock physics templates are used to predict the lithology, cement and fluid contents in the reservoir intervals. Velocity porosity relationship is used over rock physics cement model. Effect of cementation is found all three reservoir rocks in different wells. The magnitude of cementation varied from well to well. The Stø Formation which shows low porosity value in the well 7120/2-2 found to be highly cemented. The Snadd Formation also shows high cementation effect though it is found at very shallow present day depth with low geothermal gradient. This validates the effect of exhumation probably higher than 1000 m. The cement

reduced the porosity from the eastern well 7121/1-1 to the western wells (7120/2-1 and 7120/1-1).

Rock physics templates (RPT's) for fluid discrimination and lithology perdition are applied using relationship between AI versus Vp/Vs and Lamda-Rho versus Mu-Rho. There is no clear deviation found in the reservoir rocks and all reservoir sections follow the brine sand line which shows seismic properties being insensitive to the cemented rocks. Lamda-Rho versus Mu-Rho also validated the presence of cement in the reservoir sections.

Finally 'in-situ' and 'what if' scenario is used for AVO modeling. The well 7120/1-2 is chosen carrying shallow relatively the less cemented Knurr Formation and the deeply buried and the relatively high cemented Stø Formation. Castagna et al. (1993) derived Vs, Ricker wavelet and Aki-Richard equation are used for the AVO modeling. The Cap rock of the Knurr Formation reservoir section is very thin whereas the Stø Formation has thick cap rock. The rock showed slight changes in density, Vp and Vs when 10% gas substituted to the reservoir rocks. The density decreases on substitution of 50% and 100% gas but the seismic velocities have not shown any significant change on latter substitution of gas. Similarly a significant increment in amplitude is observed on the synthetic seismogram only when reservoir rock is substituted by 10% gas. The latter substitution of gas showed no changes of amplitude on synthetic seismogram.

After careful integration of results and discussion of different techniques this study finally derived the following conclusions though several limitations stated clearly may add uncertainties in the outcomes:

- The L. Cretaceous clastic wedge reservoir (Knurr Fm) deposited along the south-western flank of the LH is tested for its reservoir quality. The fair hydrocarbon saturation also makes it a good hydrocarbon prospect. The study from two wells gives a clear message that the exhumation and burial diagenesis played significant role on the petroleum system by rock properties of reservoir sandstones, source rocks and seals. The most important issue is the heterogeneity in reservoir rocks within the clastic wedge system. The Knurr Formation in the well 7120/1-2 holds good reservoir properties whereas the same formation in the well 71/2-2 is not that good to act as hydrocarbon reservoir. There is high clay contents in the eastern well 7120/2-2 which has deteriorated reservoir properties. This purposes that the rock properties are not same in wedge reservoir throughout the area and require careful examination of this play in the adjacent areas for further exploration.

- The Stø Formation has good reservoir properties in the well 7120/1-2 than the well 7120/2-2. The reason behind change in reservoir quality found to be cementation. RPT's analysis proved that the Stø Formation in the well 7120/2-2 has high Vp and AI and low porosity which suggest that the rock has gone through chemical compaction (high cementation).

- In general it can be predicted from the above discussion that the well 7120/1-2 is situated in locality where geological conditions were much more promising for the deposition of reservoir sands compared to the well 7120/2-2. The reservoirs are deeply buried with the higher influence of clay contents or cementation due to high geothermal gradient.

- The sandy part of the Snadd Formation possesses good reservoir properties with fair hydrocarbon saturation. The reservoir property vanishes gradually as we move from the east (7121/1-1) to the west (7120/2-1) and the south-west (7120/1-1) of the LH.

- The most important issue is the variation of rock properties from well to well which is controlled by geological processes (fault activity, sedimentation rate and sea level changes). The careful study of geological parameters with the integration of exhumation in the area is also important to analyze reservoir. That is how these results can be applied to the adjacent areas with the same geological settings.

- RPT's are site specific and have limitations. Applying a specific RPT belonging to different geological settings can mislead the interpretation. For example by applying the Han's model to investigate reservoirs there is a clear mismatch between theoretical model and the dataset (see Figs. 5.1-5.3), suggesting that the Han's model may not be suitable to image reservoir quality of the cemented reservoir rocks deal in this study.

- Similarly the AI versus Vp/Vs cross-plot generated mostly for unconsolidated sandstones and may not be suitable to discriminate fluids in cemented sandstones. It shows some deviation in the probable hydrocarbon section which still not that significant as expected. The reason behind this anomaly is the basin specific nature of RPT. Since it is generated for unconsolidated rocks so it requires a modification to apply it to the uplifted and cemented reservoir rocks in the SW Loppa High, the Norwegian Barents Sea.

- The AVO modeling shows changes in density, Vp and Vs over minor substitution of gas in brine saturated reservoirs. But there is no significant difference observed when gas substitution changed from 10% to 100% (Figs. 6.3-6.4). So the model tells us about the presence of gas but not the quantity of gas which is the significant pitfall of AVO modeling for the cemented reservoirs.

# References

AKI, K. & RICHARDS, P. G. 1980. Quantitative seismology: theory and methods, San Francisco, Freeman.

ASQUITH, G. B., KRYGOWSKI, D. & GIBSON, C. R. 2004. *Basic well log analysis*, American Association of Petroleum Geologists.

AVSETH, P., DVORKIN, J., MAVKO, G. & RYKKJE, J. 2000. Rock physics diagnostic of North Sea sands: Link between microstructure and seismic properties. *Geophysical Research Letters,* 27**,** 2761-2764.

AVSETH, P., MUKERJI, T. & MAVKO, G. 2005. Quantitative seismic interpretation: Applying rock physics tools to reduce interpretation risk: Cambridge.

AVSETH, P., JØRSTAD, A., VAN WIJNGAARDEN, A.-J. & MAVKO, G. 2009. Rock physics estimation of cement volume, sorting, and net-to-gross in North Sea sandstones. *The Leading Edge,* 28**,** 98-108.

AVSETH, P., MUKERJI, T., MAVKO, G. & DVORKIN, J. 2010. Rock-physics diagnostics of depositional texture, diagenetic alterations, and reservoir heterogeneity in high-porosity siliciclastic sediments and rocks --- A review of selected models and suggested work flows. Geophysics, 75**,** 75A31-75A47.

BATZLE, M. & WANG, Z. 1992. Seismic properties of pore fluids. *Geophysics,* 57**,** 1396-1408.

BACHRACH, R. 2008. Rock physics modeling of unconsolidated sands: Accounting for nonuniform contacts and heterogeneous stress fields in the effective media approximation with applications to hydrocarbon exploration. *Geophysics,* 73**,** E197.

BERGLUND L. T., AUGUSTSON J., FÆRSETH R., GJELBERG J. and RAMBERG-MOE H. (1986). The evolution of the Hammerfest Basin. Norwegian Petroleum Society, p. 319-338.

CASTAGNA, J. P., BATZLE, M. L. & EASTWOOD, R. L. 1985. Relationships between compressional-wave and shear-wave velocities in clastic silicate rocks. *Geophysics,* 50**,** 571-581.

CASTAGNA, J. P. 1993. *Offset-dependent reflectivity: Theory and practice of AVO analysis,* SEG

CASTAGNA, J. P. 1997. Principles of AVO crossplotting. *Leading edge,* 16**,** 337.Books.

CHI, X. 2009. Lithology and fluid differentiation using a rock physics template. *Leading edge,* 28**,** 60.

DALLAND , A., WORSLEY, D. & OFSTAD, K. 1988. A lithostratigraphic scheme for the Mesozoic and Cenoizoic succession offshore mid- and northern Norway. NPD-Bulletin, 4**,** 65.

DONALDSON, E. C. & TIAB, D. 2004. *Petrophysics: Theory and Practice of measuring reservoir rock and fluid transport properties*, Gulf Professional Publishing.

DONALDSON, E. & SIDDIQUI, T. 1989. Relationship between the Archie saturation exponent and wettability. *SPE formation evaluation,* 4**,** 359-362.

DORÉ, A. G. 1996. The impact of late Cenozoic uplift and erosion on hydrocarbon exploration: offshore Norway and some other uplifted basins. *Global and planetary change,* 12**,** 415.

DVORKIN, J. & NUR, A. 1996. Elasticity of high-porosity sandstones: Theory for two North Sea data sets. *Geophysics,* 61**,** 1363-1370.

EHRENBERG, S. N. 2004. Factors controlling porosity in Upper Carboniferous–Lower Permian carbonate strata of the Barents Sea. *AAPG bulletin,* 88**,** 1653.

ELVEBAKK, G., HUNT, D. W. & STEMMERIK, L. 2002. From isolated buildups to buildup mosaics: 3D seismic sheds new light on upper Carboniferous–Permian fault controlled carbonate buildups, Norwegian Barents Sea. *Sedimentary Geology,* 152**,** 7-17.

ELVEBAKK, G., HUNT, D. W. & STEMMERIK, L. 2002. From isolated buildups to buildup mosaics: 3D seismic sheds new light on upper Carboniferous–Permian fault controlled carbonate buildups, Norwegian Barents Sea. *Sedimentary Geology,* 152**,** 7-17.

FALEIDE, J. I. 1984. Evolution of the western Barents Sea. *Marine and petroleum geology,* 1**,** 123.

FALEIDE, J. l., VAGNES, E. & GUDLAUGSSON, S. T., 1993a. Late Mesozoic-Cenozoic evolution of the south-western Barents Sea in a regional rift-shear tectonic setting. Marine and Petroleum Geology, 10, 186-214.

FALEIDE, J. l., VAGNES, E. & GUDLAUGSSON, S. T., 1993b, Late Mesozoic-Cenozoic evolution of the southwestern Barents Sea. In: J. R. Parker (Ed). Petroleum Geology of Northwest Europe: Proceedings of the 4th conference, The Geological Society London, p. 933- 950.

FALEIDE J. F., BJOØRLYKKE K. and GABRIELSEN R. H. (2010). Geology of the Norwegian
Continental Shelf in Bjorlykke K. (2010), Petroleum Geoscience: from Sedimentary Environments to Rock Physics, Berlin, Heidelberg, Springer-Verlag Berlin Heidelberg, p. 467–499.

GABRIELSEN, R. 1984. Long-lived fault zones and their influence on the tectonic development of the southwestern Barents Sea. *Journal of the Geological Society,* 141**,** 651-662.

GABRIELSEN, R. H., FÆRSETH, R. B., JENSEN, L. N., KALHEIM, J. E. & RIIS, F. 1990. Structural elements of the Norwegian Continental Shelf Part I : The Barents Sea Region. NPD-Bulletin, 6**,** 33.

GABRIELSEN, R. H., FALEIDE, J. I., PASCAL, C., BRAATHEN, A., NYSTUEN, J. P., ETZELMULLER, B. & O'DONNELL, S. 2010. Latest Caledonian to Present tectonomorphological development of southern Norway. *Marine and Petroleum Geology,* 27**,** 709-723.

GASSMANN, F. 1951. Über Die elastizitat poroser medien. Vier, der Natur Gesellschaft.

GALIUS L. J. and Johansen T. A. (2010). Petroleum Geophysics, Unigeo, Bergen.

GERNIGON, L. & BRÖNNER, M. 2012. Late Palaeozoic architecture and evolution of the southwestern Barents Sea: insights from a new generation of aeromagnetic data. *Journal of the Geological Society,* 169**,** 449-459.

GLOVER P. W. J. (2005). Petrophysics MSc course notes (GLG - 66565), Department of Geology, University Laval, Canada.

GOODWAY, B., CHEN, T. & DOWNTON, J. Improved AVO Fluid Detection And Lithology Discrimination Using Lamé Petrophysical Parameters;"λρ", μρ, λμ Fluid Stack", From P And S Inversions. 1997 SEG Annual Meeting, 1997.

GOLOSHUBIN, G. 2006. Reservoir imaging using low frequencies of seismic reflections. *Leading edge,* 25**,** 527.

GONZÁLEZ, E. F. 2008. Seismic inversion combining rock physics and multiple-point geostatistics. *Geophysics,* 73**,** R11.

GLØRSTAD-CLARK, E., FALEIDE, J. I., LUNDSCHIEN, B. A. & NYSTUEN, J. P. 2010. Triassic seismic sequence stratigraphy and paleogeography of the western Barents Sea area. Marine and Petroleum Geology, 27**,** 1448-1475.

GARAT, J., KRIEF, M., STELLINGWERFF, J. & VENTRE, J. 1990. A petrophysical interpretation using the velocities of P and S waves (full waveform sonic). *Log Analyst,* 31**,** 355-369.

GRAY, D., GOODWAY, B. & CHEN, T. 2005. Bridging the gap: Using AVO to detect changes in fundamental elastic constants.

GREENBERG, M. L. & CASTAGNA, J. P. 1992. SHEAR-WAVE VELOCITY ESTIMATION IN POROUS ROCKS: THEORETICAL FORMULATION, PRELIMINARY VERIFICATION AND APPLICATIONS1. *Geophysical Prospecting,* 40**,** 195-209.

GUDLAUGSSON, S., FALEIDE, J., JOHANSEN, S. & BREIVIK, A. 1998. Late Palaeozoic structural development of the south-western Barents Sea. *Marine and Petroleum Geology,* 15**,** 73-102.

HAN, D.-H., NUR, A. & MORGAN, D. 1986. Effects of porosity and clay content on wave velocities in sandstones. *Geophysics,* 51**,** 2093-2107.

HASSAN,S.2012. Development of the Late Paleozoic, Mesozoic and Cenozoic sedimentary succession in SW Barents Sea and their role in fluid leakage process. University of Tromso, Norway.

HASHIN, Z. & SHTRIKMAN, S. 1962. A variational approach to the theory of the elastic behaviour of polycrystals. *Journal of the Mechanics and Physics of Solids,* 10**,** 343-352.

HENRIKSEN, E. 2011. Uplift and erosion of the greater Barents Sea: impact on prospectivity and petroleum systems. *Memoirs of the Geological Society of London,* 35**,** 271.

HENRIKSEN, E. 2011. Tectonostratigraphy of the greater Barents Sea: implications for petroleum systems. *Memoirs of the Geological Society of London,* 35**,** 163.

KNUTSEN, S.-M., HARALD AUGUSTSON, J. & HAREMO, P. 2000. Exploring the Norwegian part of the Barents Sea—Norsk Hydro's lessons from nearly 20 years of experience. *In:* KARI OFSTAD, J. E. K. & ALEXANDER-MARRACK, P. (eds.) *Norwegian Petroleum Society Special Publications.* Elsevier.

LARSSEN, G. B. 2002. Upper Palaeozoic lithostratigraphy of the southern Norwegian Barents Sea, [S.l.], [s.n.].

LI, Y., DOWNTON, J. & XU, Y. 2007. Practical aspects of AVO modeling. *The Leading Edge,* 26**,** 295-311.

LØSETH, H., GADING, M. & WENSAAS, L. 2009. Hydrocarbon leakage interpreted on seismic data. *Marine and Petroleum Geology,* 26**,** 1304-1319.

MAVKO G., MUKERJI T. and DVORKIN J. (2009). The rock physics handbook: Tools for seismic analysis of porous media. Cambridge University Press, New York.

MAGOON, L. B., AND DOW, W.G., 1991. The petroleum system—From source to trap. *American Association of Petroleum Geologists Bulletin,* 75**,** 627.

MONDOL, N. H., AVSETH, P., FAWAD, M. & SMITH, T. 2010. Vs Prediction in Unconsolidated Sands - Physical and Geological Controls on Shear Wave Velocities. 72nd EAGE Conference & Exhibition incorporating SPE EUROPEC Barcelona, Spain.

OHM, S. E. 2008. Geochemically driven exploration models in uplifted areas: Examples from the Norwegian Barents Sea. *AAPG bulletin,* 92**,** 1191.

POLYAEVA E., Klarner S., Lowrey C. J. and Zabrodotskaya O. (2011). Depth dependent rock physics trends for Triassic reservoirs in the Norwegian Barents Sea. 73rd EAGE Conference and Exhibition incorporating SPE EUROPEC.

PETERS, K. E. & CASSA, M. R. 1994. Applied source rock geochemistry. *MEMOIRS-AMERICAN ASSOCIATION OF PETROLEUM GEOLOGISTS***,** 93-93.

PETERS, K. E., MOLDOWAN, J. M. & WALTERS, C. C. 2005. *Biomarkers and isotopes in the environment and human history,* Cambridge, UK [u.a.], Cambridge Univ. Press.

PELTONEN, C., MARCUSSEN, Ø., BJØRLYKKE, K. & JAHREN, J. 2009. Clay mineral diagenesis and quartz cementation in mudstones: The effects of smectite to illite reaction on rock properties. *Marine and Petroleum Geology,* 26**,** 887-898.

RUTHERFORD, S. R. 1989. Amplitude-versus-offset variations in gas sands. *Geophysics,* 54**,** 680.

SAYAGO, J. 2012. Characterization of a deeply buried paleokarst terrain in the Loppa High using core data and multiattribute seismic facies classification. *AAPG bulletin*, 96**,** 1843.

SAYERS, C. 2009. Introduction to this special section—Rock physics. *Leading edge,* 28**,** 15.

SELDAL, J. Lower Cretaceous: the next target for oil exploration in the Barents Sea? Geological Society, London, Petroleum Geology Conference series, 2005. Geological Society of London, 231-240

SELNES A., DVORKIN J., CARR M., HOFFMANN J. AND HUBERT L. 2004. Rock physics diagnostics, effective medium models and analysis of the Stø Formation, Hammerfest Basin, Norway. EAGE 66th Conference &Exhibition-Paris, France.

SIMMONS, J. & BACKUS, M. 1994. AVO modeling and the locally converted shear wave. *GEOPHYSICS,* 59**,** 1237-1248.

STEWART, D. J., BERGE, K. & BOWLIN, B. 1995. Exploration trends in the Southern Barents Sea. *In:* HANSLIEN, S. (ed.) *Norwegian Petroleum Society Special Publications.* Elsevier.

SUND, T. 1984. *Tectonic development and hydrocarbon potential offshore Troms, northern Norway*.

THYBERG, B., JAHREN, J., WINJE, T., BJØRLYKKE, K., FALEIDE, J. I. & MARCUSSEN, Ø. 2010. Quartz cementation in Late Cretaceous mudstones, northern North Sea: Changes in rock properties due to dissolution of smectite and precipitation of micro-quartz crystals. *Marine and Petroleum Geology,* 27**,** 1752-1764.

UJUANBI O, OKOLIE J, JEGEDE S. 2008, Lamda-mu-rho technique as a viable tool for litho-fluid discrimination - The Niger-Delta example: International Journal of Physical Sciences Vol. 2 (7), pp. 173-176.

VASCO, D. W. 2004. Seismic imaging of reservoir flow properties: Time-lapse amplitude changes. *Geophysics,* 69**,** 1425.

VERNIK, L. & LIU, X. Z. 1997. Velocity anisotropy in shales: A petrophysical study. Geophysics, 62**,** 521-532.

WOOD, R., EDRICH, S. & HUTCHISON, I. 1989. Influence of North Atlantic tectonics on the large scale uplift of the Stappen High and Loppa High, western Barents shelf. *Extensional tectonics and stratigraphy of the North Atlantic margins: AAPG Memoir,* 56**,** 559-566.

WORSLEY, D. 2008. The post-Caledonian development of Svalbard and the western Barents Sea. *Polar research,* 27**,** 298.

XU, S. & WHITE, R. E. 1996. A physical model for shear-wave velocity prediction1. *Geophysical Prospecting,* 44**,** 687-717.

YOUNG, R. A. & LOPICCOLO, R. D. 2008. Method of processing seismic data to extract and portray AVO information. Google Patents.